UiT
THE ARCTIC UNIVERSITY OF NORWAY

Faculty of Science and Technology

Department of Geosciences

Structural and Metamorphic Implications of the Final Emplacement of the Lyngen Nappe

—

William Joel Schiffer

Master's thesis in GEO-3900 - June 2017

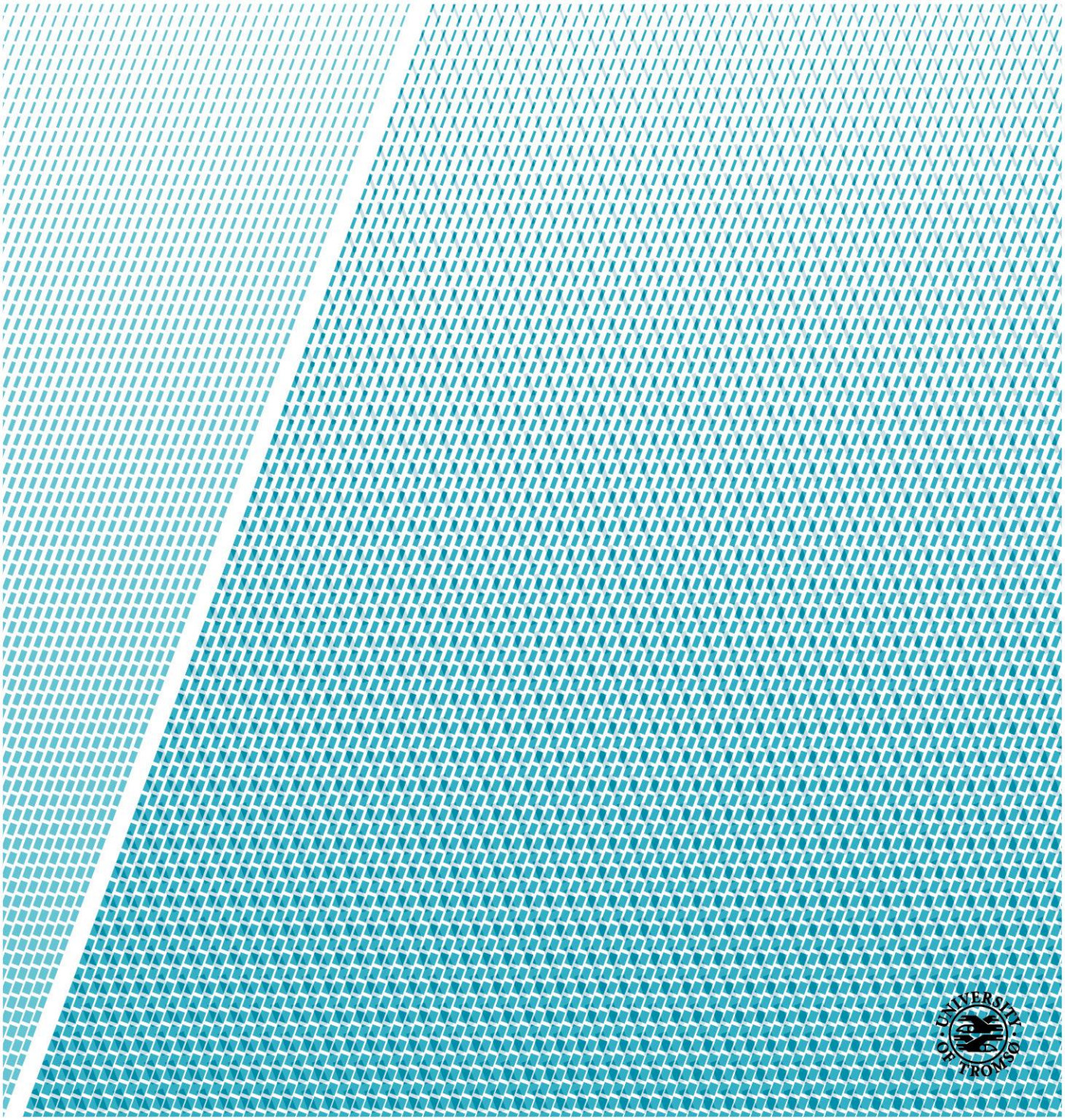

UiT The Arctic University of Norway

Faculty of Science and Technology

Department of Geosciences

GEO-3900

Master thesis in Hard Rock Geology

Structural and Metamorphic Implications of the Final Emplacement of the Lyngen Nappe

Submitted By: William Joel Schiffer

Primary Supervisor: Prof. Holger Stünitz

Co-supervisor: Prof. Jiří Konopásek

Tromsø, June 2017

ACKNOWLEDGEMENTS

Completion of this thesis would have been impossible without the help and support of those who have stuck with me throughout this adventure. I am forever grateful to you all, and will always look fondly on my time here in Tromsø.

To Holger Stünitz, danke schön for your guidance and supervision, and for giving me this opportunity with an interesting and exciting project. I am honored to have received your expertise and wisdom, and I feel my geologic knowledge has grown exponentially because of it. Thank you also for trusting me as your navigator in Tenerife and Lanzarote! To Jiří Konopásek, thank you also for your guidance and supervision, and answering all my questions. Your petrologic expertise was fundamental in this work. The modelling certainly could not have been done without your help. You have also spurred my growth as a geoscientist, and I am lucky to have worked with you.

To Erik Klæbo, takk skal du ha for being a great field and collaborative partner, as well as a good friend. I could not have completed the field work alone, and our glacier-chasing episodes made it all the more worthwhile. Thank you for putting up with me through this grand adventure.

To Trine Dahl, Karina Monsen, Melanie Forien, and Erling Ravna, thank you for your help in the lab with thin sections, sample preparation, SEM work, and XRF analysis. Thank you also for allowing me to have free reign to work when I wanted. Thanks to Martin Racek at Charles University in Prague for the SEM analyses of my samples, and to Thanusha Naidoo for the XRF analysis at the University of Oslo. Also to Carly Faber, thank you for your knowledge and insight to the Nordmannvik Nappe, and a better understanding of its history.

Til alle mine super norsk geologi venner, tusen takk for koselig vennskapet på Tromsø og universitetet. Jeg kan ikke si hva det betyr til meg på norsk, men jeg er glad i dere. Til Astrid Lemme, takk for skiturer og for din nordlige kos. Også til Jørgen Bolstad, Marte Festøy, Ane Finstad, Andreas Grumstad, Gaute Sandnes, og Tonje Strømø, skål! Til alle mine andre norsk venner (som skal ikke lese dette), tusen takk for vennskapet ditt, og for støtten din. Til Michael Malterud, takk for filmer og biljard spill. Også til Christoffer Lindskog, Torunn Birkenes, og Maria Nilssen, skål!

To my English-speaking geology friends, thank you for creating such a wonderful international community. Olga Agafonova, thanks for the long walks, the meals, and the short excursions. Elliot Broze, my fellow American, thanks for the opportunity and the adventure of Svalbard! Gustavo Martins, my favorite Brazilian, thanks for the great discussions (mostly musical) and honest opinions. Laura Swinkles, thanks for being a great office-mate.

To my friends back home, Kyle Hardy, Bill Bailey, Christina Muñoz, Chet Smith, Zach Wilder, Kelly Canchola, Llewelyn Joseph, Austin Parr, William Hays, Christy Muse, Curtis McConnell, Mike Eldredge, and Gary Howard, thank you for your outstanding support, and making me believe that this was a possibility. Finally (and most importantly), to my ever-loving and supportive family. Mom, Dad, Rebecca, Grandma, Kathy, Ben, Karen, John, Payton, Olivia, the Hinelines, and the Gelminis, I could not have set one foot out of Texas without y'all behind me. I hope I've done you guys proud.

This thesis is dedicated to my hero, William Charles Schiffer, for being the man I always aspire to be; and to the memory of Derek Main, who inspired me to go down this rocky path of geology many moons ago.

William Joel Schiffer **Tromsø, June 2017**

ABSTRACT

The Lyngen Nappe, an allochthonous unit of the Northern Norwegian Caledonides, consists of Greenschist-facies rocks overlying Amphibolite- to Granulite-facies rocks in the Nordmannvik Nappe. The lower-grade metamorphism seen in the Lyngen rocks juxtaposes higher-grade rocks both above and below. The nature and origin of this metamorphic break is investigated, specifically in the sheared rock units comprising the contact between the Lyngen and Nordmannvik nappes, to determine the kinematic and metamorphic conditions present during the final emplacement of the Lyngen Magmatic Complex. These mafic rocks primarily consist of the Lyngen Gabbro, part of an ophiolite sequence formed in the former Iapetus Ocean, and now overly the metasedimentary paragneisses of the Nordmannvik Nappe that formed the Baltican basement. These nappes were emplaced and deformed during the Scandian orogenic phase of the Caledonian Orogeny. Structures observed in the field strongly indicate a top-to-the-West shear sense at this contact, while petrologic modelling of the rocks in this shear zone provide evidence for prograde development. Estimated metamorphic conditions of the Nordmannvik Gneiss (625-675°C and 8.5-10 kB) represent minimum values during Scandian shearing for temperature and pressure when compared to previous estimates (680-710°C and 9.4-10.1 kB [Faber, pers. comm., 2017]). Above the Nordmannvik rocks, a trend of decreasing temperatures and pressures is observed, with conditions of 580-600°C and 10-10.5 kB, followed in the higher rocks by estimates of 540-550°C and 7.5-8.25 kB. Structural and mineralogical similarities between the Garnet Mica gneisses of the Nordmannvik Nappe and the overlying phyllites and schists, however, hint at a common origin through retrograde metamorphism. An extensional detachment for the Lyngen Nappe is proposed, within a few possible tectonic models.

Key Words: Scandinavian, Caledonian, Nordmannvik, Lyngen, shear sense, kinematics

CONTENTS

1 INTRODUCTION

1.1 GEOGRAPHY OF THE STUDY AREA

The Lyngen Peninsula is situated roughly 50 kilometers due east of Tromsø in Northern Norway. The peninsula itself has a north-south trend and is divided into northern and southern segments. The primary focus of this study concentrates on the eastern end of the peninsula, bordering on the Lyngenfjord. Our study area stretched from Koppangen in the north to the area around Nordkjosbotn in the south (Figure 1).

Figure 1 - Geographic overview of study area. Gridlines refer to WGS84 UTM-zone 34W.

1.2 ABBREVIATIONS

Minerals/Oxides		**Technical Abbreviations/Structural Units/Rock Types/Elements/Ions**	
Qtz	Quartz	NC	Nappe Complex
Act	Actinolite	Ma	Age/Time in Millions of Years
Kfs	Alkali Feldspar	ca	Circa/Approximately
Pl	Plagioclase	MORB	Mid Ocean Ridge Basalt
Bt	Biotite	T-MORB	Transitional MORB
Ms	Muscovite	kB	Kilobars (unit of Pressure)
Cal	Calcite	°C	Degrees Celsius
Dol	Dolomite	D_1	First major deformation event
Chl	Chlorite	D_2	Second major deformation event
Czo	Clinozoisite	D_3	Third major deformation event
Zo	Zoisite	F_2	Second-generation fold
Di	Diopside	F_3	Third-generation fold
Grt	Garnet	S_1	Foliation developed during D_1
Hbl	Hornblende	XRF	X-Ray Fluorescence
Ky	Kyanite	P-T	Pressure-Temperature
Sil	Sillimanite	CPO	Crystallographic Preferred Orientation
Opq	Opaque Mineral	SEM	Scanning Electron Microscope
Zrn	Zircon	EDS	Energy Dispersive (X-Ray) Spectroscopy
Ep	Epidote	EBSD	Electron Back-Scatter Diffraction
St	Staurolite	ROI	Region of Interest
Aln	Allanite	FM	Formation
Ap	Apatite	LOI	Loss on Ignition
Rt	Rutile	°	Degrees
Ilm	Ilmenite	cm	Centimeters
Ttn	Titanite	m	Meters
Po	Pyrrhotite	g	Grams
Ccp	Chalcopyrite	GBM	Grain Boundary Migration
Pa	Paragonite	SGR	Subgrain Rotation
Ctd	Chloritoid	BLG	Bulging
Ma	Margarite	PPL	Plain Polarized Light
Jd	Jadeite	XPL	Crossed Polarized Light
Law	Lawsonite	BSE	Backscattered Electron
Fath	Fe-Anthophyllite	%	Percent
Alm	Almandine	Wt.%	Weight Percent
Pyr	Pyrope	X_{Mg}	Molar percentage of Magnesium, Mg/(Mg+Fe)

Sps	Spessartine	X_{Fe}	Molar percentage of Iron, Fe/(Fe+Al)
Grs	Grossular	X_{An}	Molar percentage of Anorthosite, An/(Ab+An+Or)
Ab	Albite	LMC	Lyngen Magmatic Complex
An	Anorthite	GMG	Garnet Mica Gneiss
Or	Orthoclase	GMS	Garnet Mica Schist
Al_2O_3	Aluminium Oxide	CNG	Conglomerate Schist
MgO	Magnesium Oxide	FYL	Phyllite
CaO	Calcium Oxide	GRN	Greenschist
TiO_2	Titanium Dioxide	AMS	Amphibolite Schist
Cr_2O_3	Chromium (III) Oxide	GBR	Gabbro/LMC
FeO	Iron (II) Oxide	Cl	Chlorine
FeO_{TOT}	Total Iron Oxide	F	Fluorine
Fe_2O_3	Iron (III) Oxide	Br	Bromine
MnO	Manganese (II) Oxide	Au	Gold
SiO_2	Silicon Dioxide	Al	Aluminium
Na_2O	Sodium Oxide	Mg	Magnesium
K_2O	Potassium Oxide	Ca	Calcium
ZnO	Zinc Oxide	Ti	Titanium
P_2O_5	Phosphorus Pentoxide	Cr	Chromium
SO_3	Sulfur Trioxide	Fe^{2+}	Ferrous Iron
NiO	Nickel (II) Oxide	Mn	Manganese
CuO	Copper (II) Oxide	Si	Silicon
SrO	Strontium Oxide	Na	Sodium
Y_2O_3	Yttrium (III) Oxide	K	Potassium
ZrO_2	Zirconium Dioxide	Zn	Zinc
PtO_2	Platinum Dioxide	Fe^{3+}	Ferric Iron
BaO	Barium Oxide	H	Hydrogen
Bi_2O_3	Bismuth (III) Oxide		

Table 1 - Table of abbreviations used in this paper.

1.3 REGIONAL GEOLOGY

1.3.1 The Caledonian Orogeny

The Caledonian Orogeny was a long and extensive mountain-building event in Paleozoic times, caused by the collision of two primary paleocontinents, Baltica and Laurentia. A smaller microcontinent, Avalonia, was also involved. Baltica included present-day Scandinavia and most of Northern Europe. Most of what is now Norway is composed of accreted terranes from this orogenic episode. Laurentia contained most of present North America, including the US, Canada, and Greenland. This large craton has remained largely unchanged through Earth's history, and was situated near the equator for most of the Ordovician and Silurian (Cocks, 2001). The smaller continent of Avalonia was comprised of parts of the modern-day UK and New England. Occurring from the Late Pre-Cambrian/Early Cambrian to the Early/Middle Devonian, the Caledonian Orogeny included several spatially and temporally different events or phases all related to the closing of the former Iapetus Ocean.

1.3.1.1 Precambrian (pre-550 Ma) History

The origins of these events can be traced back to the opening of this paleo ocean, which rifted Laurentia and Baltica away from the Gondwanan supercontinent (Figure 2). Dolerite dikes of T-MORB (transitional mid-ocean ridge basalt) character in the Correvarre Nappe (upper part of the Kalak NC [Nappe Complex]) in Northern Norway dated at 582 Ma (Million Years) (Zwaan & van Roermund, 1990) are interpreted to have intruded just prior to the initiation of Iapetus sea-floor spreading (Roberts, 1990).

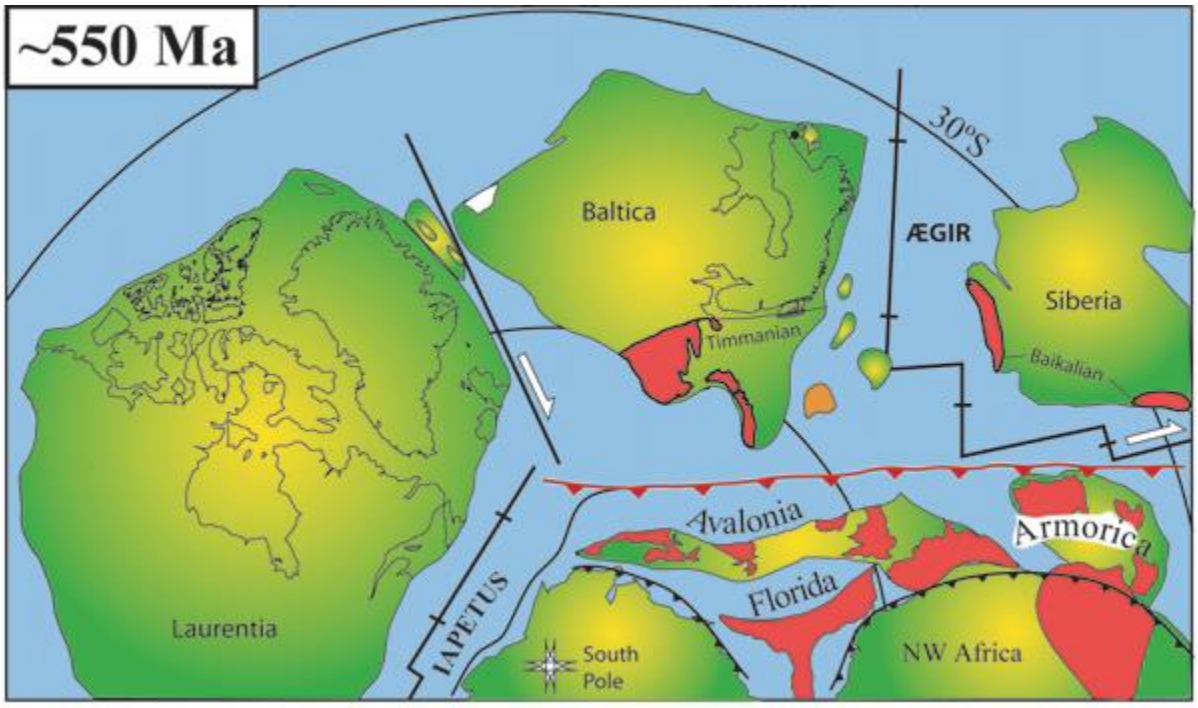

Figure 2 - Reconstruction of Late Precambrian (roughly 550 Ma), just after initiation of Iapetus rifting. From Torsvik and Cocks (2005).

1.3.1.2 Cambrian (ca 500 Ma) History

The Iapetus continued to spread throughout the Cambrian, while deep subduction beneath an arc or microcontinent (possibly the Kara Terrane) occurred on the Caledonide margin of Baltica (Cocks & Torsvik, 2002) (Figure 3). Near the end of the Cambrian, an arc polarity reversal in the Iapetus ceased sea-floor spreading and obduction, and began arc formation on the Laurentian and Gondwanan margins (Cocks, 2001).

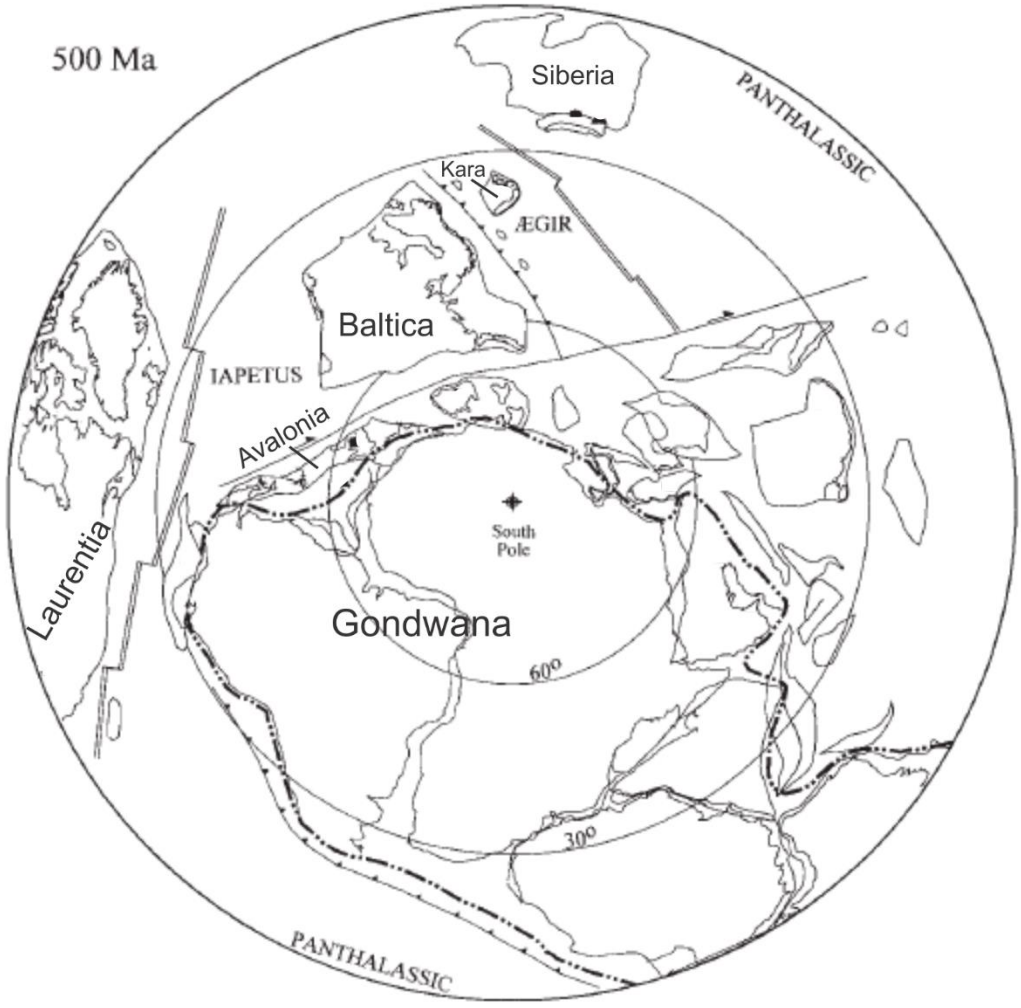

Figure 3 - Late Cambrian reconstruction (500 Ma). Note subduction zone between Baltica and Kara. Modified after Cocks and Torsvik (2002).

1.3.1.3 Ordovician (480-460 Ma) History

During the Ordovician, a collision with the Kara terrane caused Baltica to rotate more than 90 degrees rapidly in a counter-clockwise fashion (Torsvik et al., 2001; Fortey & Cocks, 2003) (Figure 4). This period was also marked by Iapetus arc collisions on both Baltican and Laurentian margins (Cocks, 2001).

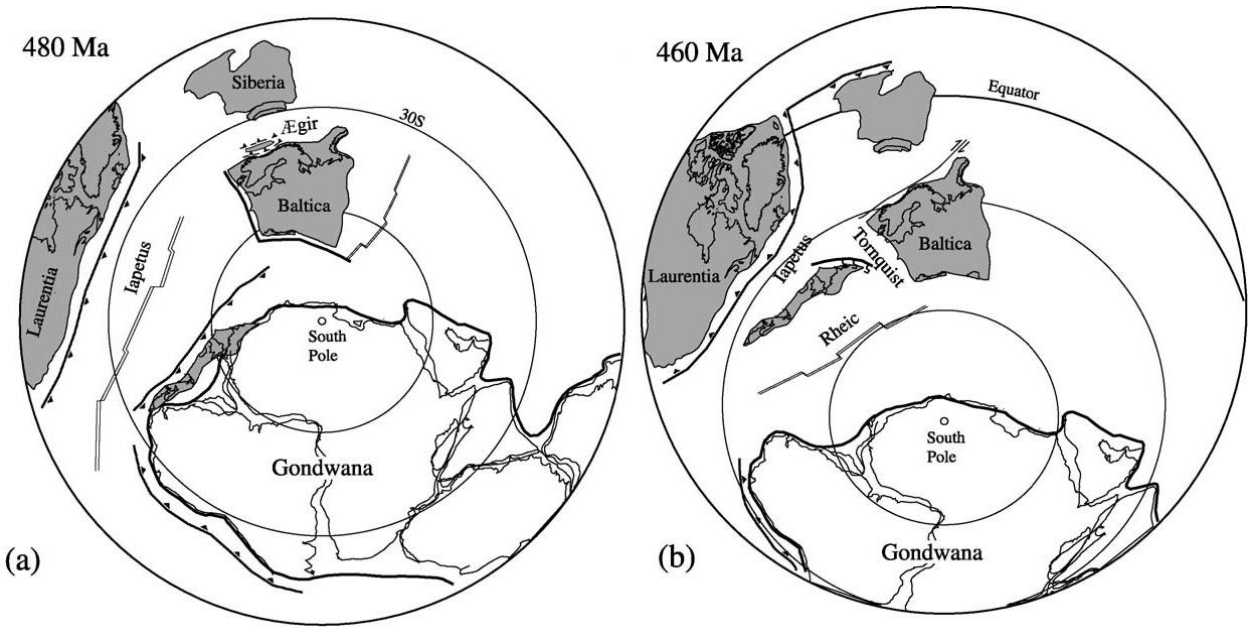

Figure 4 - Early Ordovician (a) (480 Ma) and Mid- to Late-Ordovician (b) (460 Ma) reconstructions. Note intense rotation of Baltica. From Roberts (2003).

1.3.1.4 Silurian (440-420 Ma) History

The shorter Silurian period saw both the collision of Avalonia and Baltica in the Early Silurian (440 Ma), and the main collision of those two with Laurentia and the end of the Silurian, approximately 425 Ma (Cocks & Torsvik, 2002) (Figure 5). However, the collision between Baltica and Laurentia actually began in the North prior to Avalonia's convergence with Laurentia, due to the fact that the Iapetus closed from north to south.

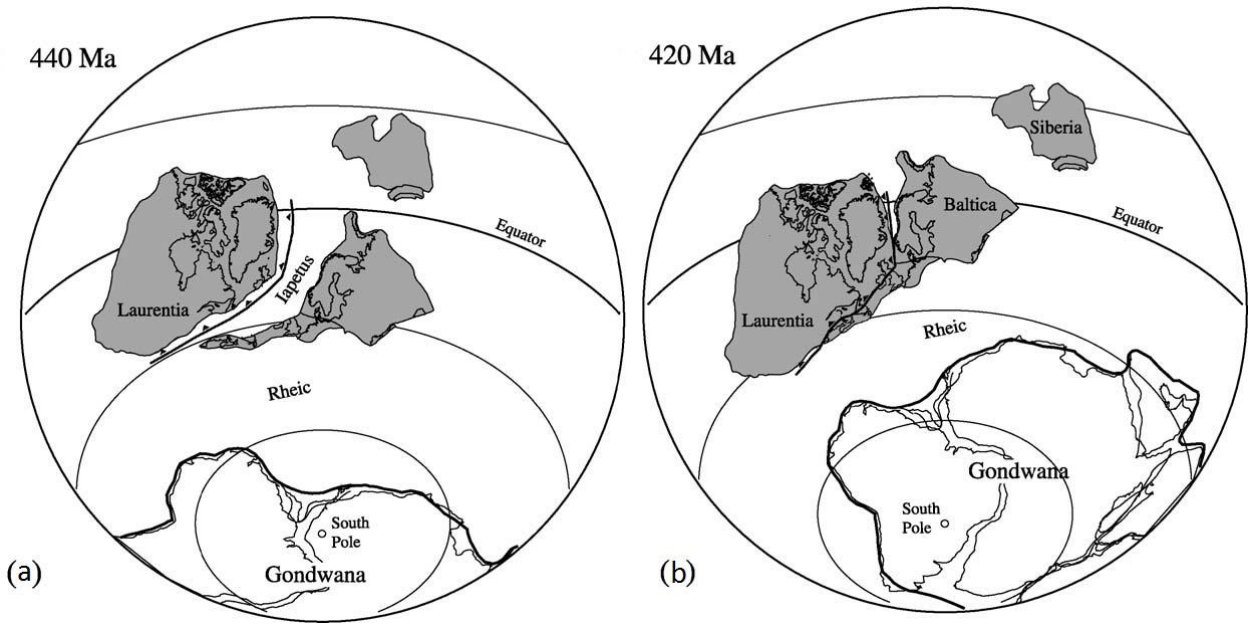

Figure 5 - Early Silurian (a) (440 Ma) and Late Silurian (b) (420 Ma) reconstructions. Note the convergence of Avalonia with Baltica at 440 Ma, and the primary Caledonian collision between Baltica and Laurentia at 420 Ma. From Roberts (2003).

1.3.1.5 Devonian (post-420 Ma) History

Subsequent extensional deformation of these landmasses continued into the Devonian, and manifested many of the nappe stacks we see today (as seen in the Western Gneiss Region of Southwestern Norway) as Baltica was subducted beneath Laurentia. This extensional event may also be responsible for the nature of the Lyngen-Nordmannvik nappe contact studied herein. It is interesting to note the similarity of fit between Baltica and Laurentia both pre- and post-Caledonian, especially given the independent drift and rotation of Baltica for nearly 200 Ma (Torsvik et al., 1996).

1.3.2 The Caledonides of Scandinavia

Throughout Norway and parts of Sweden, the effects of the Caledonian Orogeny are still present in the landscape and in the geologic record. Many prominent mountain range areas represent stacks of thrust sheets formed from this event due to arc and continental collision over the long Caledonian orogenic process. There is, however, a clear distinction between many of these groups of rocks in relation to the time of their deformation. Two primary phases of the Caledonian Orogeny in Scandinavia were originally described in these rocks, namely the Finnmarkian and the Scandian phase. The Finnmarkian phase has now been established to be a false interpretation, but the Scandian phase is well-known, and principally related to the main continental collision between Laurentia and Baltica, occurring in the Mid Silurian to the Early Devonian. The Scandian nappes represent an orogenic convolution of an Ordovician to Silurian sedimentation sequence (Ramsay et al., 1985). However, the history of metamorphism and nappe emplacement in Scandinavia is far too complex to easily fit into a one- or two-stage model, as in some previous literature (Andresen et al., 1985). Other phases have also been described, such as the Trondheim and Taconian events (Figure 6 a & b, respectively). The Trondheim event refers to an Early Ordovician subduction event between Baltica and Iapetan arcs or a microcontinent, while the Taconian also describes Mid to Late Ordovician arc accretion, but is limited to the margin of Laurentia (Roberts, 2003).

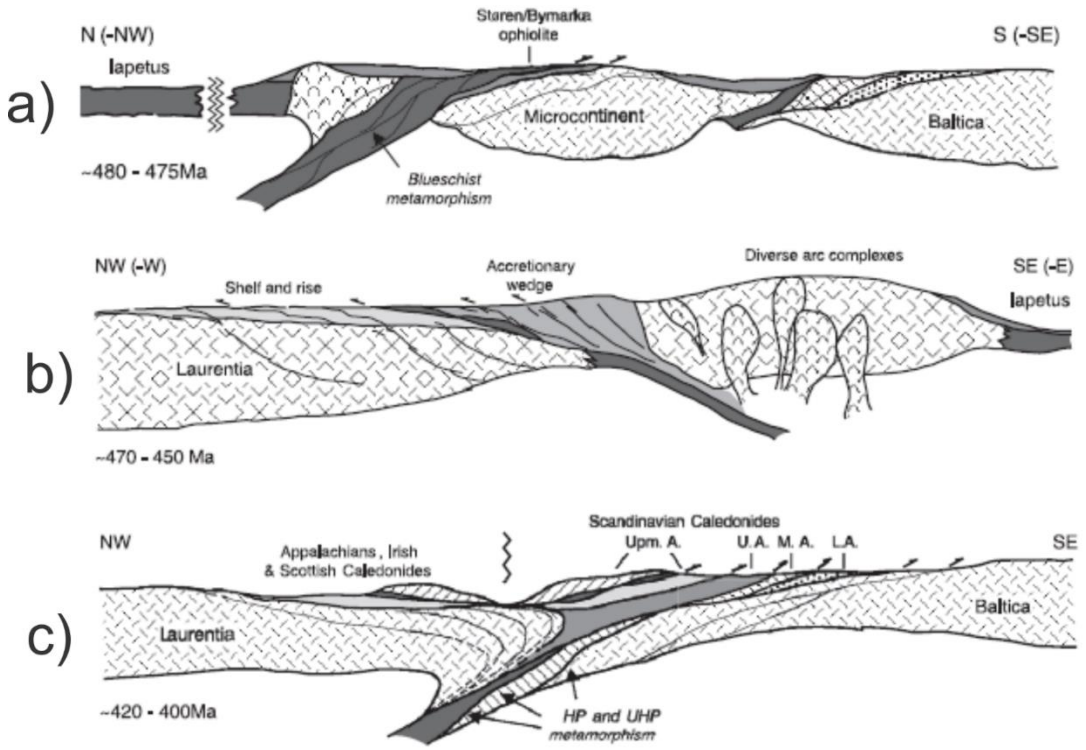

Figure 6 - Caledonian tectonometamorphic evolution of Baltican and Laurentian margins. (a) Baltican margin during the Trondheim Phase, Early Ordovician. Profile relates to Trondheim area of mid Norway. (b) Margin of Laurentia during the Taconian event, Mid/Late Ordovician. Parts of these sequences and terranes would later be emplaced onto Baltica during the Scandian Phase to form parts of the Uppermost allochthon. (c) Margins of Baltica and Laurentia during main Scandian continental collision, Late Silurian/Early Devonian. L.A., M.A., U.A., Upm.A. – Lower, Middle, Upper, and Uppermost allochthons, respectively. From Roberts (2003).

1.3.2.1 Scandian Phase

The Scandian Phase of the Caledonian Orogeny was characterized by oblique continental collision and deep subduction of Baltica beneath Laurentia (Andersen et al., 1991; Eide & Torsvik, 1996; Torsvik et al., 1996) (Figure 6c). The nappes structurally above the Kalak NC of Northern Norway are inferred to have been emplaced during this event (Sturt et al., 1978; Roberts & Gee, 1985). These new groups of nappes were thrust over an eroded Baltica basement, and also reactivated some thrusts in the lower sequences (Ramsay et al., 1985). However, some of these nappe units have elements of a pre-Scandian tectonometamorphic history (Lindstrom & Andresen, 1992), which is probably related to an earlier basement or rifting history. A regionally extensive dismembered ophiolite (LMC [Lyngen Magmatic Complex]/Gratangseidet Mafic Complex) emplaced structurally above the Narvik NC (Nordmannvik and lower nappes correlative) proposes a boundary between these two exotic terranes with differing pre-Scandian histories (Andresen & Steltenpohl, 1994). Peak metamorphism in this phase may have occurred at the beginning of the Devonian, around 417 Ma (Ramsay et al., 1985), shortly following the collision of Baltica and Laurentia in the Silurian at approximately 425 Ma. The Scandian nappe units contain plutonic intrusive rocks, and volcanic rocks are only seen in the Troms region (Gayer et al., 1985). This orogenic phase was followed by orogenic collapse and extension in the Devonian (Roberts, 2003), which involved low-angle ductile detachments relating to top to the west/southwest shear sense (Hossack, 1984; Norton, 1987; Seranne, 1992; Fossen & Dunlap, 1998; Osmundsen et al., 1998; Braathen et al., 2000; Osmundsen et al., 2003) (Figure 7).

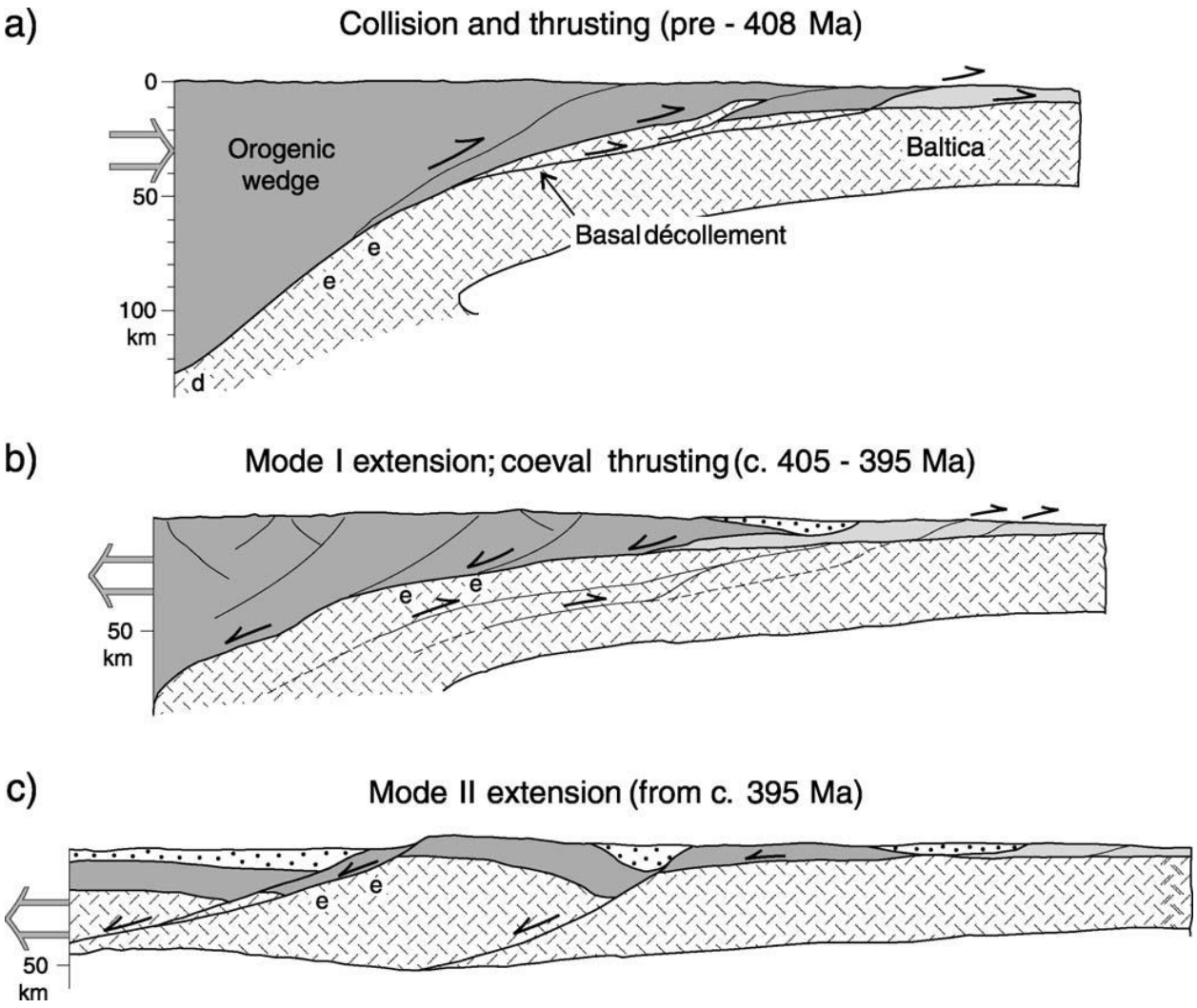

Figure 7 - Schematic WNW-ESE profiles depicting the Devonian post-orogenic history of the Scandinavian Caledonides, including late-stage extensional deformation and gravitational collapse. (a) Main Scandian continental collision. (b) Initial orogenic collapse and backsliding. (c) Crustal collapse with steep, top-West shear zones. e – eclogite formation; d – microdiamond formation. From Fossen and Dunlap (1998); Fossen (2000); Roberts (2003).

1.3.2.2 Allochthons of the Scandinavian Caledonides

The nappes of the Norwegian Caledonides are each categorized into separate allochthons, depending on the interpretation of their origin in relation to Baltica. These range from Lower, Middle, Upper, and Uppermost allochthons (Figure 8). The Lower and Middle allochthons are composed of shelf and continental rise sequences native to the Baltican margin, while the Upper allochthon is derived from oceanic, magmatic arc, and marginal basin rocks of the Iapetus Ocean (Gale & Roberts, 1974; Gee, 1975; Stephens & Gee, 1985; Pedersen et al., 1988; Stephens & Gee, 1989; Pedersen et al., 1991; Grenne et al., 1999). The Uppermost allochthon and the higher units of the Upper allochthon are generally exotic terranes derived from spreading ridges, island arcs, and marginal basins of the Iapetus Ocean (Gee, 1975; Stephens, 1988), and usually infers a Laurentian affinity of the rocks. There is evidence that some of these formations were not only derived from Laurentia, but that they were also initially deformed there during the Taconian Orogeny, before their emplacement onto Baltica during the Scandian event (Roberts et al., 2002).

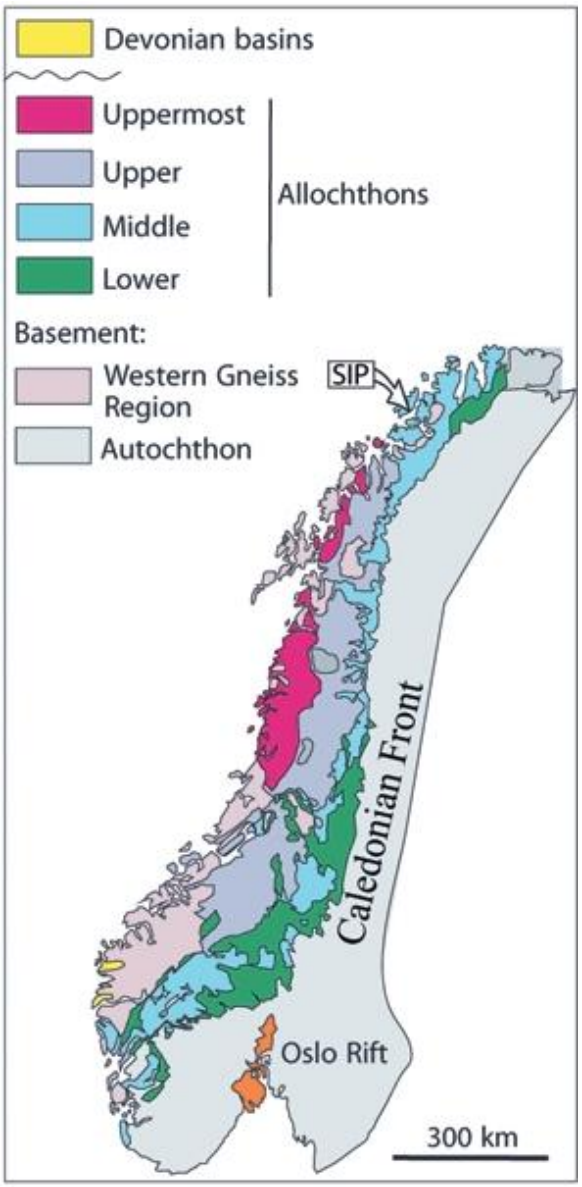

Figure 8 - Tectonostratigraphy of the Scandinavian Caledonides, showing spatial distribution of allochthonous units. From Roberts and Gee (1985); Corfu et al. (2004); Torsvik and Cocks (2005).

1.3.3 Scandinavian Caledonides in Troms/Lyngen

Within the Caledonian rocks of Scandinavia, those residing in the Lyngen and Troms areas are of extreme value and importance, for they can contain both pre-Scandian and Scandian structures and fabrics. This is in large part due to their location between rocks of predominant pre-orogenic character (to the North) and rocks with mostly Scandian heritage (to the South). These rocks are also, naturally, of supreme importance to this work. The Caledonian geology of this area is dominated by a gently westward-dipping stack of nappes that were thrust Southeastwards across the Precambrian Baltic shield (Chapman et al., 1985), each with specific lithologies, metamorphic grades, and ages (Andresen et al., 1985). The major lithotectonic units of this region are (from structurally lowest to highest): the autochthonous Dividal Group, and the Kalak, Vaddas, Kåfjord, Nordmannvik, Lyngen, Nakkedal, and Tromsø nappes (Andresen et al., 1985) (Figure 9 & Figure 10).

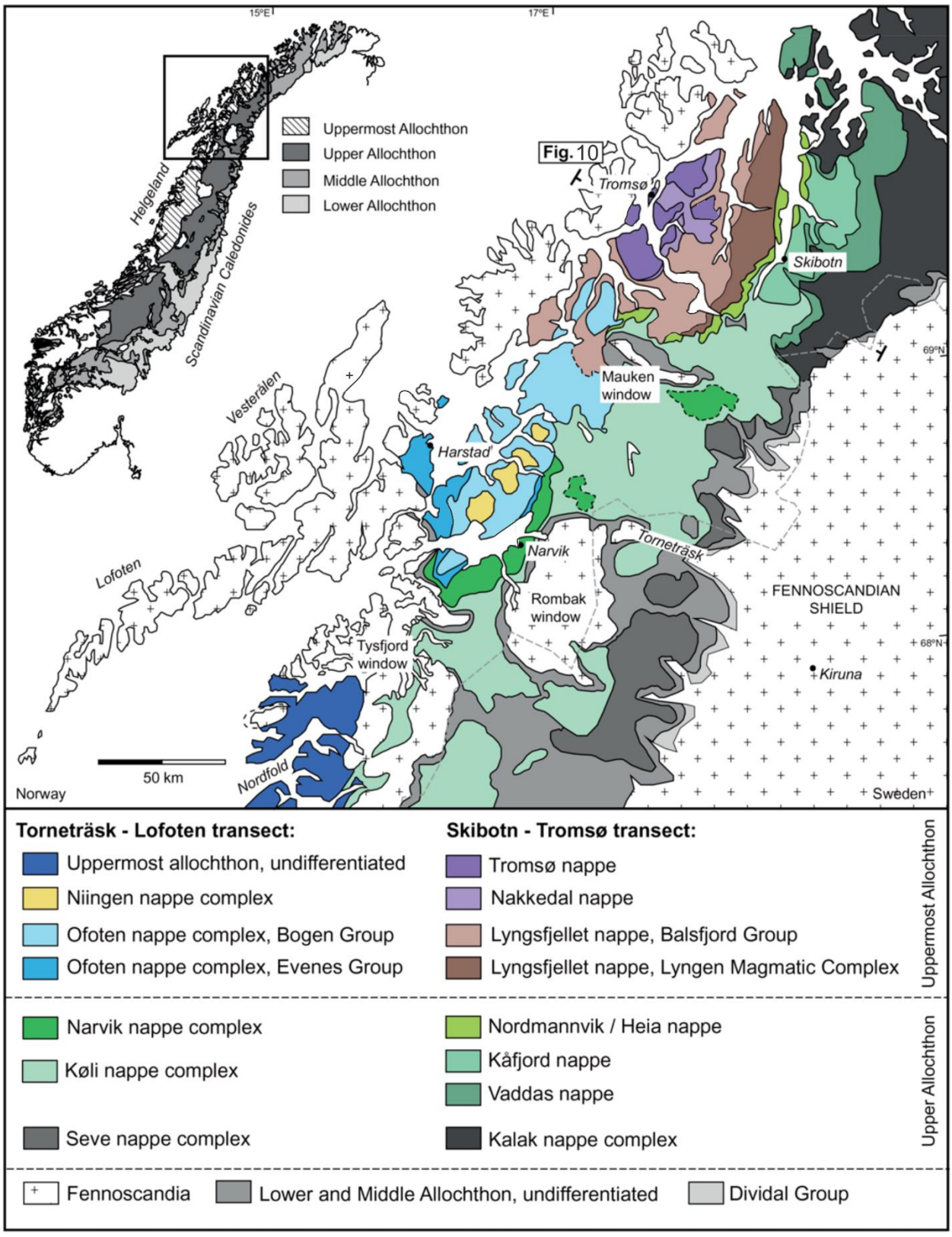

Figure 9 - Tectonostratigraphy of the Northern Scandinavian Caledonides. Modified after Augland et al. (2014).

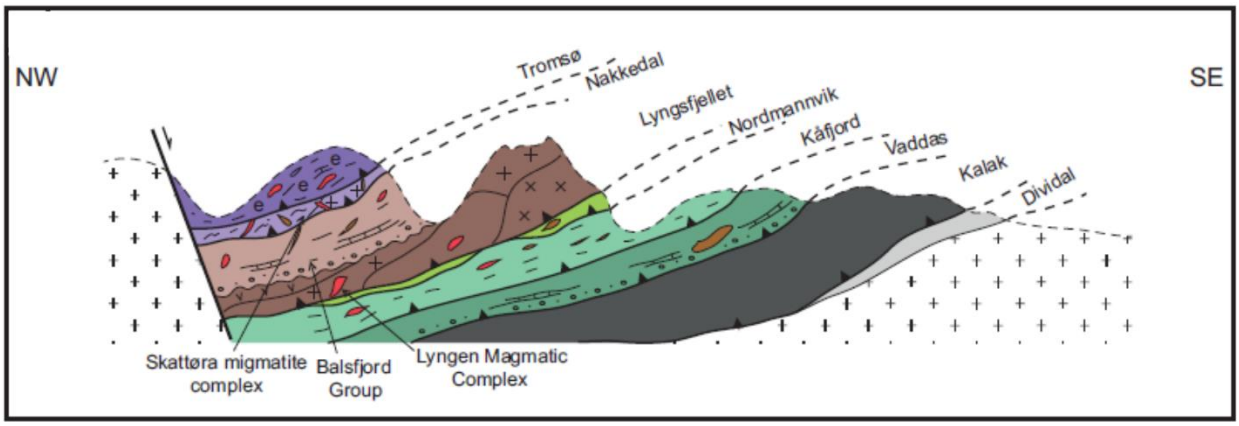

Figure 10 - Cross section from Figure 9 showing relative nappe relationships. From Augland et al. (2014).

1.3.3.1 Caledonian Allochthons in Troms/Lyngen

The Middle Allochthon, here represented by the Kalak NC, consists of pre-Caledonian Fennoscandian basement and unconformably overlying Late Neoproterozoic shelf and continental rise sediments (Roberts & Gee, 1985; Andréasson, 1994). The primary rocks observed in the Kalak NC are psammites and pelites, which underwent middle greenschist facies metamorphism (Andresen et al., 1985). The Vaddas Nappe represents the base of the Upper Allochthon, and is a sequence of mica-schist, marble, quartzite, and amphibolite (Andresen et al., 1985). The rest of the Upper Allochthon currently includes the Kåfjord and Nordmannvik nappes, and is composed of metamorphic rocks postulated to represent the Baltica-Iapetus continent-ocean transition (Stephens & Gee, 1985; Andréasson, 1994), ophiolites, and island-arc and volcanic rocks (Harland & Gayer, 1972). The Uppermost Allochthon currently consists of the Lyngen, Nakkedal, and Tromsø nappes, and contains Caledonian intrusive rocks interpreted to have originated near or within the continental margin of Laurentia (Stephens et al., 1985; Roberts et al., 2002; Barnes et al., 2007; Roberts et al., 2007; Augland et al., 2012). The Nakkedal Nappe is composed of quartzofeldspathic paragneisses and the Skattøra Migmatite Complex (Augland et al., 2014). Capping this nappe stack is the Tromsø NC, which is a complex suite of kyanite-mica-schists, amphibolites, anorthosites, calc-silicates, marbles, gneisses, and eclogites (Andresen et al., 1985). Besides the LMC of the Lyngen Nappe, other potential ophiolite fragments have been described in other nappes of the Upper Allochthon (Hodges, 1985; Barker, 1986), which could suggest the presence of multiple exotic terranes in the Upper and Uppermost allochthons (Andresen & Steltenpohl, 1994).

1.3.3.2 Nordmannvik Nappe

The Nordmannvik Nappe occurs on the easternmost parts of the Lyngen peninsula, and further East across the fjord. It thins to the Southwest, and appears discontinuously as the Heia Nappe (Andresen et al., 1985; Zwaan et al., 1998). The rocks of this unit are predominantly pelitic schists and paragneisses, and strain partitioning has been observed from East to West as the ductile deformation grades increase towards the contact with the overlying Lyngen Nappe (Hibelot, 2013). Two distinct metamorphic fabrics in the Nordmannvik Nappe indicate separate tectonothermal events: An early Amphibolite- to Granulite-facies melting and migmatization event related to a gabbroic intrusion around 440 Ma; and an overprinting mylonitic fabric formed from a subsequent Amphibolite- to Eclogite-facies nappe stacking and shearing event at the beginning of continental collision, around 430 (Kraus, 2016) (Faber, pers. comm., 2017).

1.3.3.3 Lyngen Nappe

The Lyngen Nappe is dominated by the Lyngen Gabbro, or LMC, which itself is subdivided into the Strupen (East) and Jiekkevarri (West) suites (Furnes & Pedersen, 1995). These two suites are usually separated by the oceanic, high-temperature, ductile Rypdalen Shear Zone (Slagstad, 1995; Augland et al., 2014). At the base of the LMC lies the Kjosen Unit, a mylonitic greenschist-amphibolite. This unit then transitions into the underlying Koppangen FM (Formation), composed predominantly of a crenulated phyllite, which then transitions through a greenschist-facies shear zone (Augland et al., 2014) into the schists and gneisses of the Nordmannvik Nappe below. Unconformably overlying the LMC is the Balsfjord Group, represented by metamorphosed Late Ordovician/Early Silurian sedimentary rocks (Bjørlykke & Olaussen, 1981) with an increasing metamorphic grade towards the overlying Nakkedal Nappe (Andresen & Bergh, 1985). All of these units have undergone low to middle greenschist-facies metamorphism, in contrast to the amphibolite to granulite grade rocks of the under- and overlying nappes (Andresen & Bergh, 1985; Andresen et al., 1985). A detailed geologic map of the Lyngen Nappe is presented in Figure 11.

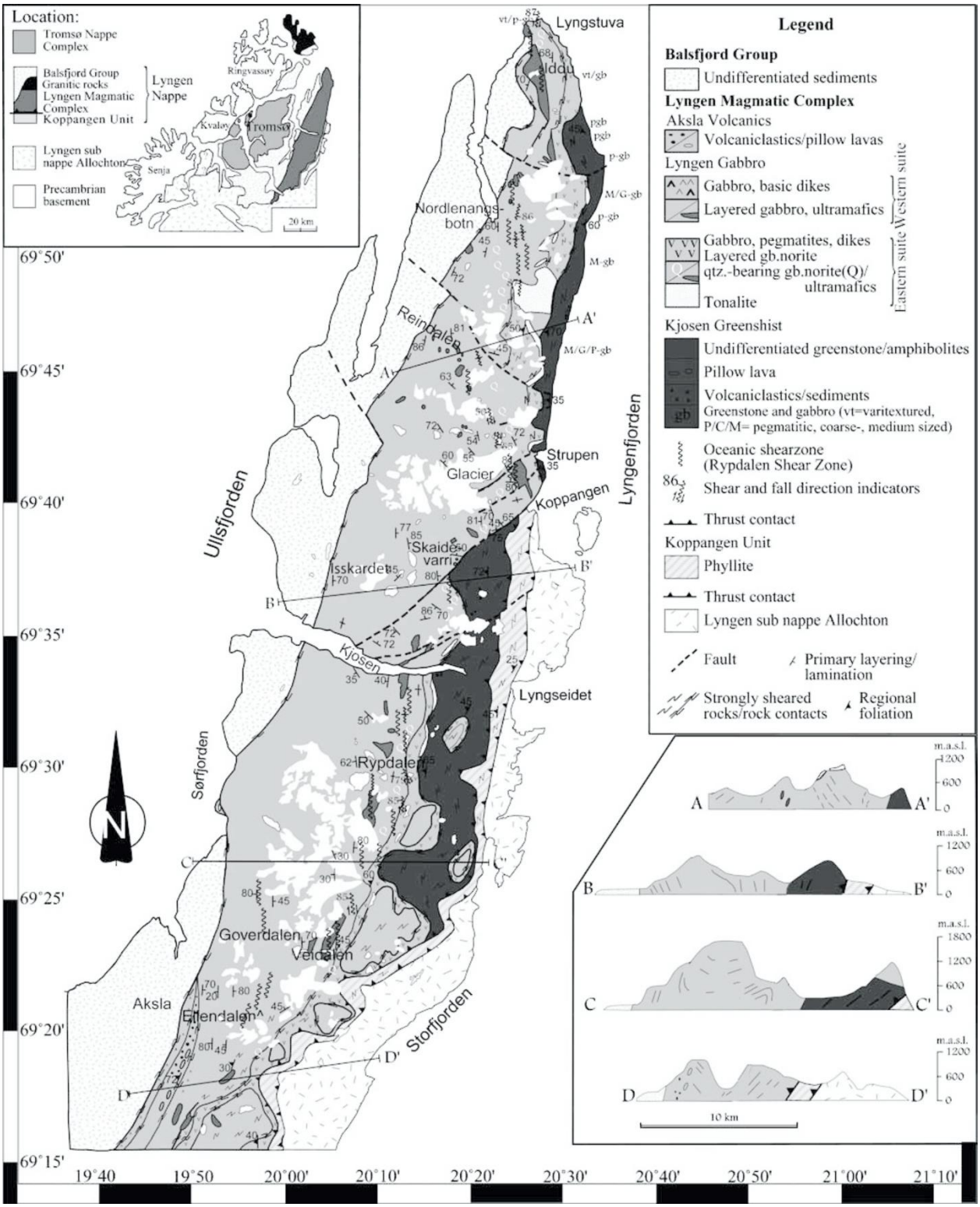

Figure 11 - Detailed geologic map of the Lyngen Peninsula including several cross-section profiles as indicated on the map. From Slagstad (1995); Kvassnes et al. (2004).

1.3.3.3.1 The Lyngen Gabbro as a dismembered ophiolite

The nature of the Lyngen Gabbro has long been recognized as part of an ophiolite, most likely the cumulate or layer 3 of an obducted sequence (Furnes et al., 1979; Minsaas & Sturt, 1985). The primitive nature of the gabbro is in agreement with an ophiolite interpretation (Minsaas & Sturt, 1985), where primary mantle melts rise to high lithospheric levels (Gayer et al., 1985). The occurrence of a thick MORB (mid-ocean ridge basalt) lava thrust slice and a thicker gabbro slice also adds support to the dismemberment of an ophiolite during Scandian terrane accretion (Anderson et al., 1992; Oliver & Krogh, 1995). However, a true MORB ophiolite is very difficult to emplace, and it may be more likely that the LMC was emplaced as a fore- or backarc ophiolite (Figure 12).

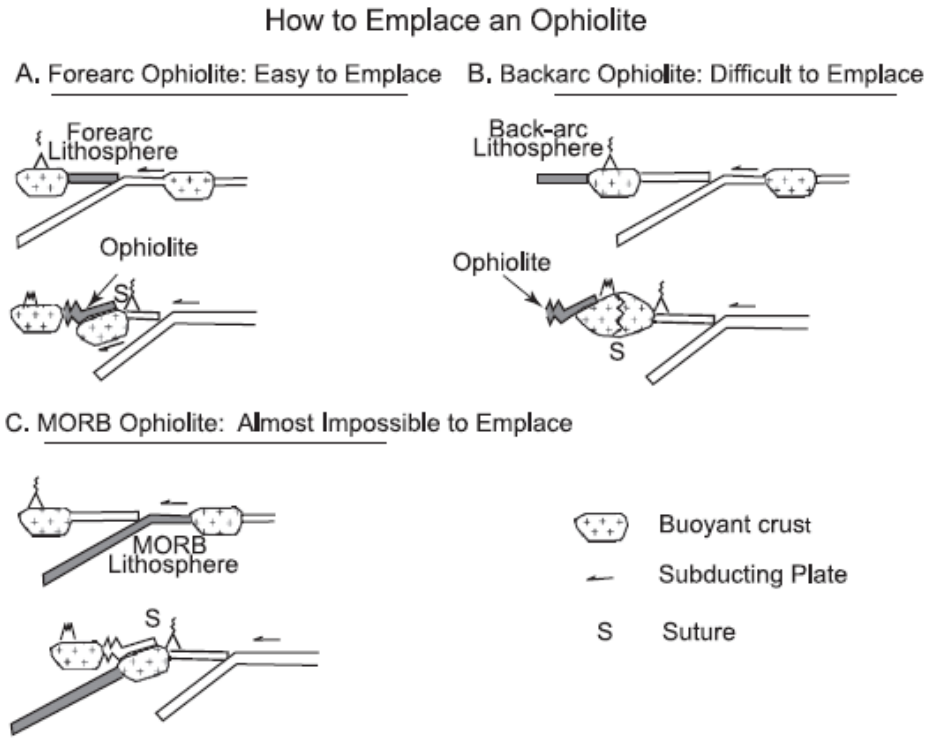

Figure 12 - Schematics of ophiolite emplacement and their relative feasibilities. (a) Subduction of buoyant material leading to subduction zone failure, followed by isostatic rebound of the buoyant crust beneath the ophiolite. (b) Compression and shortening of the arc leads to its uplift. (c) Sediments and seamount fragments may be scraped off the downgoing plate, but decollements do not cut deep into the subducting lithosphere. From Stern (2004).

1.4 Previous work in the Lyngen & Nordmannvik nappes

1.4.1 Lithological Descriptions

1.4.1.1 Rocks of the Nordmannvik Nappe

The Nordmannvik Nappe is dominated by a blastomylonitic kyanite-sillimanite bearing garnet-mica-gneiss with an upper amphibolite facies metamorphic history (Andresen et al., 1985). Pyroxene-bearing amphibolite lenses occur locally (Lindstrom & Andresen, 1992), as well as small bodies of Sagvandite and basic granulites (Andresen et al., 1985). Thin (200-500 m [meters]) layers and lenses of dolomite marble occur near the base and the top of the Nordmannvik Nappe (Augland et al., 2014).

1.4.1.2 Rocks of the Lyngen Nappe

1.4.1.2.1 Koppangen Formation Phyllites

Occurring in a wide shear zone which marks the contact between the Lyngen and Nordmannvik nappes is a fine-grained phyllite, commonly referred to as the Koppangen FM. This unit is typically a dark grey color, with occasional garnets and amphibolites (Andresen & Bergh, 1985; Andresen et al., 1985).

1.4.1.2.2 Kjosen Formation Greenschists

Lying over the Koppangen FM is the Kjosen FM, which forms a transition between the phyllites and the overlying LMC (Andresen et al., 1985). These rocks are primarily highly sheared greenschists and hornblende-bearing amphibolites (Munday, 1974), but also contains metabasalts of a MORB to calc-alkaline nature (Furnes & Pedersen, 1995). They are compositionally very similar to the overlying gabbro, and typically display a Northwesterly mineral lineation (Munday, 1974).

1.4.1.2.3 The Lyngen Gabbro

The Lyngen Gabbro dominates the vast majority of the Lyngen Peninsula, and nearly all the high peaks of the Lyngen Alps are composed of these rocks. The LMC is wedge-shaped with a maximum thickness on its Western margin (Chroston, 1972), is typically interpreted to be an ophiolite fragment (Andresen et al., 1985), and together with the underlying Kjosen FM represents a primitive, poorly fractionated magma (Munday, 1970; Gayer et al., 1985). These metagabbros generally indicate transitional features between continental and MORB or island arc tholeiite signatures (Gayer et al., 1985) (Figure 13), and could represent a lower crustal transition from MORB-like hydrous magmatism to high-calcium boninitic magma from a depleted source (Kvassnes et al., 2004). Fresh gabbros are primarily composed of augite, orthopyroxene, magnetite, and a calcic plagioclase (Munday, 1974). The rocks are also strongly saussuritized with clinozoisite set in albite (Munday, 1974), and have a well-preserved magmatic layering (Andresen & Bergh, 1985). The LMC is subdivided into two magmatic suites, named the Jiekkevarri and Strupen Units. The Eastern suite (Strupen) is characterized by an island-arc to boninitic composition (Furnes & Pedersen, 1995), while the Western suite (Jiekkevarri) shows a typical MORB affinity (Oliver & Krogh, 1995). Non-tectonic transitions between rocks of boninitic and island-arc composition indicate that this magmatism happened concurrently (Kvassnes et al., 2004).

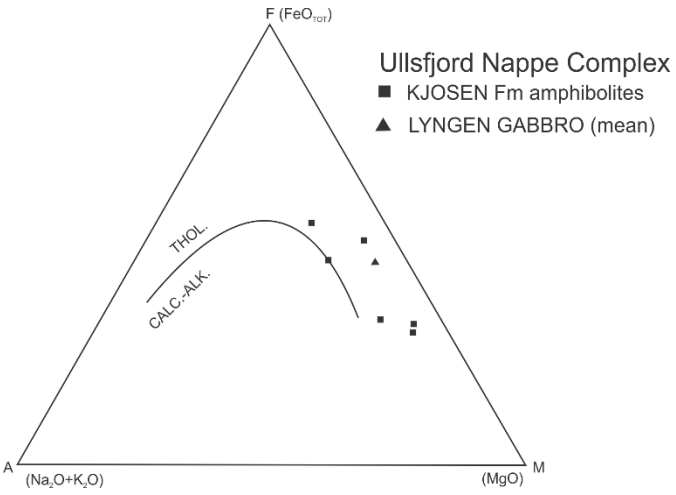

Figure 13 - AFM plot illustrating the tholeiitic composition of the Lyngen Gabbro and the Kjosen Greenschist. Boundary line after Irvine and Baragar (1971), diagram modified after Gayer et al. (1985).

1.4.1.2.4 The Balsfjord Group

Unconformably overlying the LMC is the Balsfjord Group, which contains metamorphosed Late Ordovician to Early Silurian fossiliferous sedimentary rocks (Andresen et al., 1985). This unit is lithologically diverse both along and across strike, and includes schists, conglomerates, and various carbonate rocks (Andresen & Bergh, 1985; Andresen et al., 1985). The Sagelvvatn Group, occurring Southeast of Balsfjord, includes some volcanic rocks as well as those mentioned just before (Bjørlykke & Olaussen, 1981).

1.4.2 Tectonometamorphic Evolution

The rocks of the Lyngen and Nordmannvik nappes each have their own long and complex evolutionary histories through multiple stages of deformation and metamorphism. Their generally proposed tectonometamorphic histories are provided herein.

1.4.2.1 Nordmannvik Nappe

At least two significant metamorphic events have occurred in the Nordmannvik Nappe, both pre- and syn-orogenic, relating to the Caledonian Orogeny. Metamorphic P-T (pressure-temperature) estimates of the pre-orogenic melting event indicate 8.2-10.5 kB (kilobars) and 800-850°C (degrees Celsius) (Faber, pers. comm., 2017). This amphibolite-facies prograde metamorphism is recognized as occurring pre-D_1 (first major deformation event), while development of the mylonitic fabric (with P-T estimates of 9.4-10.1 kB and 680-710°C [Faber, pers. comm., 2017]), S_1 (foliation developed during D_1), under upper amphibolite- to granulite-facies (locally) characterizes the D_1 event (Andresen & Bergh, 1985; Lindstrom & Andresen, 1992). It has been postulated that this mylonitic foliation was developed prior to the Scandian event, due to truncation of this foliation by the thrust fault separating the Nordmannvik and Kåfjord nappes (Lindstrom & Andresen, 1992). An age of 435 Ma for a gabbroic body in the Nordmannvik Nappe supports its intrusion post-dating a high-grade metamorphic event (Augland et al., 2014) (Figure 15). The origin of the Nordmannvik Nappe was previously interpreted as either: a tectonic fragment of a volcanic arc or microcontinent onto which the Lyngen gabbro was emplaced; or a fragment of the Seve Nappes that was tectonically emplaced by an out-of-sequence-thrust higher up in the tectonostratigraphy later in the Scandian Phase (Lindstrom & Andresen, 1992). However, it is now inferred to have derived from Baltican basement rocks (Stünitz, pers. comm., 2017).

1.4.2.2 Lyngen Nappe

Three primary deformational phases are recognized in the Lyngen Nappe, and are noted as D_1, D_2 (second major deformation event), and D_3 (third major deformation event), representing their order of occurrence. The LMC is generally interpreted as forming in a forearc setting, and it is also likely that it was accreted on to the continental margin of Laurentia and partially eroded during an early Caledonian event (Augland et al., 2014). During the D_1 event, the base of the gabbro became sheared and folded, yielding the Kjosen FM (Munday, 1974). During this period, dike intrusion occurred in these basal rocks, producing sheets of amphibolite seen in the Kjosen greenschists (Munday, 1974). One of these tonalitic intrusions has been dated at 481 Ma, giving an estimate on the formation of the ophiolitic suite (Augland et al., 2014) (Figure 15). The next deformational event, D_2, is when the tectonic emplacement of the LMC and the Kjosen rocks are believed to have occurred (Munday, 1974). The shear zone that separates the Lyngen and Nordmannvik nappes is deformed by F_2 (second-generation fold) folds, indicating that the nappe welding occurred after this folding event (Andresen & Bergh, 1985). Deformation during the D_3 event is responsible for the F_3 (third-generation fold) crenulation folds and lineations (Andresen & Bergh, 1985). The low-grade metamorphic rocks of the Sagelvvatn Group are indicative of regressive and transgressive sedimentation cycles and volcanism on a continental shelf during the Early Silurian (Bjørlykke & Olaussen, 1981). The Balsfjord Group also contains clastic deposits with boulders of up to a meter in diameter, plus rapid lateral facies changes, all indicating deposition in a tectonically active basin (Andresen & Bergh, 1981; Olsen, 1982). The occurrence of basic dikes in these rocks also implies crustal extension (Andresen et al., 1985). Metamorphic conditions for the Balsfjord Group have been estimated at 450°C and at pressures of 3.5 kB (Andresen & Bergh, 1985). An age of 425 Ma for a granite occurring in this unit supports syn- to post-orogenic magmatism (Augland et al., 2014) (Figure 15). D_2 deformation in the Balsfjord Group, however, appears to post-date the movement along the Lyngen-Nordmannvik boundary (Bergh, 1980). The rocks of the Lyngen Nappe are by no means inactive today. The Lyngen peninsula is still an active, fault-bounded region surrounded by areas of less uplift, and many paleosurfaces are preserved (Osmundsen et al., 2010). Several small recent earthquakes have occurred along major Caledonian faults, such as the Lyngen-Nordmannvik boundary (Osmundsen et al., 2010) (Figure 14).

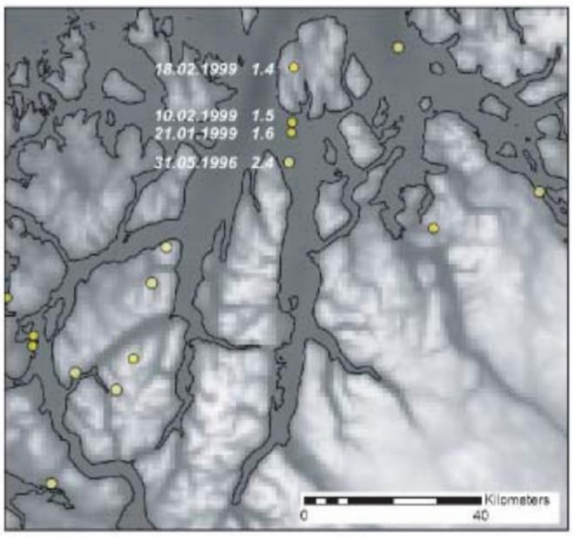

Figure 14 - Earthquake epicenters in Lyngen in the late 90's. Note the four epicenters lying on Northward projection of the Lyngen-Nordmannvik Boundary. From Osmundsen et al. (2010).

1.4.2.3 Dating of rocks within the Lyngen & Nordmannvik nappes

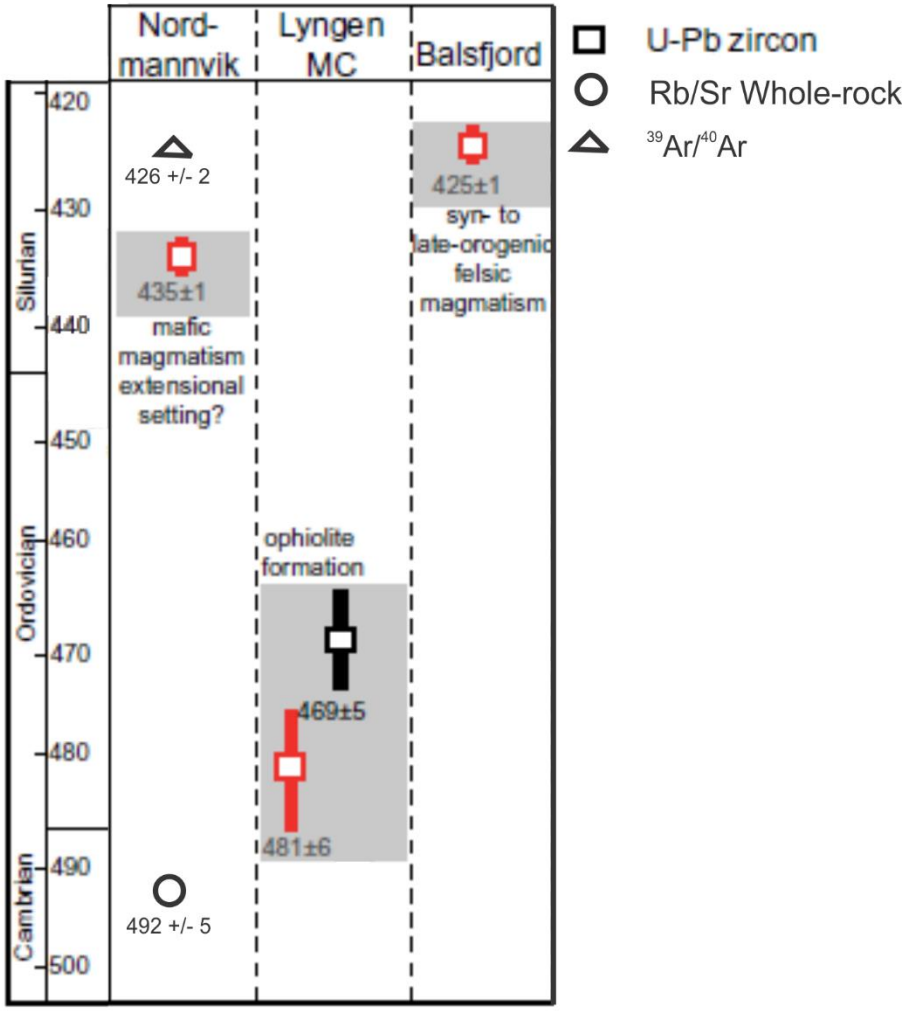

Figure 15 - Selected dates for rocks in the Lyngen & Nordmannvik nappes. Data points in red & modified figure from Augland et al. (2014); Black square from Oliver and Krogh (1995); Rb/Sr age from Lindstrom and Andresen (1992); $^{39}Ar/^{40}Ar$ age from Dallmeyer and Andresen (1992).

1.5 AIMS & GOALS

This project was designed to determine the structural and petrological nature of deformations associated with the final emplacement of the Lyngen Nappe over the underlying Nordmannvik Nappe. Estimation of peak metamorphic conditions as well as prograde and retrograde pathways can be obtained by studying the petrology and quartz microstructures of the different rock units along the contact zone. This, combined with both macro- and microscopic structural kinematic data, can provide an important part of the tectonic history for these rocks.

1.5.1 Petrology & Metamorphism

A keystone trait of this nappe contact is the significant jump in metamorphic grade from Upper Amphibolite to Granulite facies rocks in the Nordmannvik Nappe to the Greenschist facies rocks of the overlying Lyngen Nappe. Studying the petrology and metamorphic history of these units can help unravel some of the characteristics of the relationship between these two nappes, such as the origin of the sheared phyllitic rocks at the contact zone. This task can be carried out by petrological analyses of mineral assemblages and their phases, and by whole-rock composition analyses of samples collected in the field.

1.5.1.1 Origin of Phyllites & Greenschists

In the area between Koppangen and Lyngseidet, two distinct rock units occur between the gneisses and schists of the Nordmannvik Nappe and the magmatic rocks of the LMC. Together, these two units make up a wide shear zone acting as a contact between the two nappes. These are the phyllites of the Koppangen FM, directly overlying the Nordmannvik rocks, and the greenschists and amphibolitic rocks of the Kjosen FM, directly below the Lyngen Gabbro (Figure 11). The origin and derivation of these rocks have been little discussed in previous works, but the answer is of some importance to this project. These rocks will be discussed further, and in greater detail, in another section of this thesis.

1.5.1.1.1 Kjosen Greenschist

The rocks of the Kjosen FM are most likely derived from the Lyngen Gabbro itself, as they bound the whole of the gabbro on its eastern side (Chroston, 1972), and are very similar in chemical composition (Munday, 1970; Randall, 1971; Munday, 1974) (Figure 13). It is thus inferred that the Kjosen greenschists represent a sheared and folded basal unit of the Lyngen Gabbro (Munday, 1974).

1.5.1.1.2 Koppangen Formation

The unit of phyllitic rocks, commonly referred to as the Koppangen FM, is more ambiguous as to its origin. At their base, they form a gradational contact with the high-grade schists of the Nordmannvik Nappe. The upper limit of this unit also grades into the greenschists of the Kjosen FM, providing a particular challenge in field identification of these three rocks. They are commonly considered to be metasediments related to the LMC, possibly as metamorphosed deep-water shales (Oliver & Krogh, 1995). In a previous study of the Nordmannvik Nappe, it was postulated that the phyllites and the underlying gneisses and schists evolved from a common protolith, due to similarities in mineralogy and structure, and could have formed during a retrograde metamorphic event (Hibelot, 2013).

1.5.2 Kinematics

One of the main keys to unlocking the secrets of this nappe contact is the use of kinematic indicators, both in the field and in thin section. Determination of how this nappe was emplaced depends heavily on the identification of these shear sense indicators. Identification of possible indicators in the field can be later compared with, and possibly verified by, certain indicators in microstructural studies.

1.5.2.1 Out-Of-Sequence Thrusting vs. Low-Angle Normal Faulting

The Lyngen Nappe lies in a geologic setting dominated by thrust sheets. The contact between the Lyngen and Nordmannvik nappes is largely assumed to be a thrust fault. This is partly due to a significant lack of concrete structural evidence. However, the nature of this contact is still a legitimate inquiry, and thus, is the main topic of this thesis. Analysis and interpretation of structures seen in the field and in thin section will be discussed in greater detail later in this report.

1.5.2.1.1 Out-Of-Sequence Thrust

Support of a thrust contact is prevalent in previous literature, however structural arguments are few and far between. A keystone of this contact is the obvious jump in metamorphic grade from Amphibolite and Granulite facies in the Nordmannvik Nappe to the Greenschist grade rocks of the Lyngen Nappe, which can be attributed to a thrust fault between the two (Andresen & Bergh, 1985). However, thrust emplacement of low grade rocks over higher grade units would indicate that this thrust occurred as an out-of-sequence thrust (Andresen & Steltenpohl, 1994), and data indicates that the movement along this contact postdates the metamorphic peak in the underlying Nordmannvik Nappe (Bergh, 1980). In a correlative nappe stack to the southwest of our study area, the Narvik NC was found to have earlier cooling ages than the overlying Ofoten NC, indicating an out-of-sequence thrust between the two nappes (Coker et al., 1995).

1.5.2.1.2 Low-Angle Normal Fault

While not often argued for in previous literature, there is significant reason to consider that the deformation between these two nappes could be associated with normal faulting and/or extensional regimes. A wide greenschist-facies shear zone occurs between the Lyngen and Nordmannvik rocks, overprinting both units, and could be attributed to deformation by low-angle normal faulting. The possibility exists for late orogenic collapse, which in turn could create low-angle extensional faulting (Rykkelid & Andresen, 1991).

1.5.3 Allochthon Designation

There appears to be some discrepancy as to which allochthon the Lyngen Nappe belongs to. In most early literature, it was considered to belong to the upper allochthon. In later publications, especially after the recognition of a tectonostratigraphically higher form, the Lyngen Nappe is considered to belong to the uppermost allochthon. The uppermost allochthon designation usually indicates nappe units containing sediments and fossils with a Laurentian Margin affinity, while the upper allochthon is reserved for island arc and ophiolite sequences. The Lyngen Nappe contains the LMC, composed of arc and ophiolitic rocks, as well as the overlying Balsfjord Group, composed of fossil-bearing metasedimentary rocks. This, understandably, is the primary source of confusion regarding the designation of the Lyngen Nappe. The underlying Nordmannvik Nappe is regarded as belonging to the upper allochthon. However, it has been recently proposed that these rocks more likely fit with the upper part of the middle allochthon, as they contain metasediments of Baltican affinity (Gee et al., 2008; Hibelot, 2013). If this assertion is correct, then a case could be made that the Lyngen Nappe, or at least the LMC, belongs to the oceanic rocks included in the upper allochthon.

2 METHODS

2.1 FIELD WORK

Field work was carried out over the course of several months in the Summer of 2016, between June and October, in collaboration with Erik Klæbo. The area covered included the Eastern Lyngen peninsula from Koppangen to Nordkjosbotn, with the majority of data for this paper between Koppangen and Lyngseidet. There was an emphasis on locating key structural data for kinematic indicators, as well as detailed rock descriptions for petrological study. Oriented samples were taken for both purposes. Structural data taken includes: strike and dip measurements of foliation planes, crenulations, and axial fold planes; and trend and plunge measurements for lineations, fractures, and fold axes. Potential macroscopic shear-sense indicators were well documented, including photographs and sketches, as well as their measured orientations in relation to the metamorphic fabric. Several dominant rock types were described in detail, including an estimation of mineral assemblages and descriptions of the metamorphic fabrics. Oriented hand samples were taken such that the foliation and lineation could be accurately marked on the rock, to be cut later for thin section preparation. As the rocks of each nappe have previously been mapped, an emphasis was not made to map each unit in a strict sense, but instead traverse the contact between the nappes in several profiles to determine the nature of the contact zone and its effects on the local lithologies.

2.2 LAB WORK

Sample	Rock	Thin Section	SSI	XRF/SEM
27.10.3	GMG	1.1	X	X
27.10.2	Qtz	1.2		
20.07.2	GMG	2.1	X	
20.07.1	Qtz	2.2		
15.09.1	GMS	3.1	X	X
15.09.2	Qtz	3.2		
15.09.3	FYL	4	X	
16.09.4	CNG	5		
16.09.3	FYL	6	X	
04.10.1	GRN	7	X	X
3.12.08	AMS	14e	X	X
14.09.2	GBR	8		
27.10.4	GBR	9		

Table 2 - Table of samples collected in the field, showing which samples were used for thin sections, and thereafter shear-sense indicators (SSI) and XRF (X-Ray Fluorescence) & SEM (Scanning Electron Microscope) analysis. GMG: Garnet Mica Gneiss; GMS: Garnet Mica Schist; CNG: Conglomerate Schist; FYL: Phyllite; GRN: Greenschist; AMS: Amphibolite Schist; GBR: Gabbro/LMC; Qtz: Quartz.

2.2.1 Thin Section Preparation

Several hand samples were chosen for thin section analysis. From these selected samples, small 'chips' were made with a MK Tile Saw, cutting the rocks perpendicular to the foliation and parallel to the lineation. These chips were then submitted to the Geology Laboratory, where they were mounted to glass slides, ground with a Knuth Rotor, and polished with a Struers Tegramin 30.

2.2.2 Polarizing Microscopy

Analysis of the prepared thin sections began with detailed observations with a polarizing microscope. Through this instrument, the mineral assemblages could be estimated, and microstructures in the rocks could be accurately described and interpreted for fabrics and kinematic indicators. Most of this work was carried out on a Leitz Orthoplan polarizing microscope. Photographs were taken using a Leica Z16 APO microscope, with a mounted Leica DFC 450 camera. With these microscopes, the thin sections could be viewed in either plain- or crossed-polarized light. An accessory gypsum plate could also be utilized.

2.2.3 X-Ray Fluorescence

Once the thin sections had been observed in detail, samples 1.1, 3.1, 7, and 14e were selected for further petrological analysis. In particular, these samples were chosen in an attempt to provide a resolution to the origin of the phyllitic Koppangen FM. This was done using the X-Ray Fluorescence (XRF) technique, in order to create petrologic and metamorphic pseudosections and P-T diagrams. The first step in this process was to crush and mill each sample into a fine powder. A Retsch BB2/A Jaw Crusher and a Retsch PM100 Milling Machine were used for this purpose. Next, a portion of each sample was weighed before performing the Loss on Ignition (LOI). This was done by placing each weighed sample into a small crucible, then baking the crucibles in an oven at 1000°C for approximately two hours. Each sample was then carefully weighed again to record its post-LOI weight. The next step was to create fused beads to be analyzed. 0.6 g (grams) of rock powder was mixed with 6 g of Flux (a homogeneous, anhydrous mix of 66% [Percent] Lithium Tetraborate and 34% Lithium Metaborate, with 0.2% Lithium Bromide added), for a 1:10 rock to flux ratio, which was then loaded into a XRF Scientific xrFuse 2 fusion machine (an initial set of beads was produced with a 1:14 rock to flux ratio [0.8 g of rock powder and 5.6 g of Flux], and was later analyzed with a Bruker S8 Tiger at the geology lab at UiT). The samples were first melted for five minutes at 1125°C, then shaken for five minutes. After letting the samples stand for 20 seconds, they were poured into holders to cool for eight minutes. The fusion beads produced from this process were then sent to Thanusha Naidoo at the geological laboratories at the University of Oslo for analysis.

2.2.4 SEM, EDS, & EBSD

Further work to constrain mineral phases and compositions, as well as to determine any crystallographic preferred orientation (CPO), was carried out through the use of a scanning electron microscope (SEM). Two important detectors were used for this purpose: the Energy Dispersive X-ray Spectroscopy (EDS) method, and the Electron Back-Scatter Diffraction (EBSD) method. The EDS detector provides a spectrum of chemical composition, and a quantification can be carried out based on selected regions of interest (ROI). This method can be implemented to constrain mineral compositions, create phase maps, and to create compositional profiles, such as across a garnet. The EBSD method determines the crystallographic orientation of the grains in a sample, and is primarily used to determine Quartz CPOs.

2.2.5 Petrologic Modelling

Thin sections 1.1, 3.1, 7, and 14e were sent to Charles University in Prague for detailed SEM/EDS analysis of selected mineral phases, carried out by Martin Racek. This data, along with the whole-rock compositions obtained from the XRF analysis, formed the basis of the petrologic modelling carried out by the software Perple_X, version 6.7.2 (Connolly, 2009). One Garnet profile for each sample was obtained, as well as compositional data from Biotite, Muscovite, Plagioclase, Epidote, Chlorite, and Staurolite. Compositional data was received in the form of weight percent of certain oxides and elements, listed in Table 3 below. Recalculations into molar proportions, end members (for Garnet and Plagioclase), plus X_{Mg} (molar ratio of Magnesium:Iron) and X_{Fe} (molar ratio of Iron:Aluminium) values (for Biotite, Chlorite, Staurolite, and Epidote) were done in an Excel spreadsheet. Compositional data from the whole-rock XRF analysis was acquired in weight percents of oxides and elements, also listed in Table 3 below. The data could then be entered into the Perple_X software to create P-T pseudosections for the interpretation of the metamorphic history of the selected samples. Perple_X was run using the hp04ver thermodynamic data file (Holland & Powell, 1998), the perplex_option computational option file, and the X(CO2) fluid equation of state from Holland and Powell (1991); Holland and Powell (1998). All pseudosections were calculated with SiO_2 in excess, and in the system of TiO_2, Al_2O_3, FeO, MnO, MgO, CaO, Na_2O, and K_2O. Depending on the section, H_2O was either calculated in excess, or with the LOI component as H_2O. Two solution model files were used, solution_model and solution_model_671. Mixing models utilized include Gt(WPH), Ctd(HP), hCrd, and Ilm(WPH) from White et al. (2000), Bio(TCC) (Tajcmanová et al., 2009), TiBio(WPH) (White et al., 2007), Gt(HP) (Holland & Powell, 1998), Amph(DPW) (Dale et al., 2005), Chl(HP) (Holland et al., 1998), Chl(W) (White et al., 2014), melt(HP) (Holland & Powell, 2001; White et al., 2001), Pheng(HP) (Holland et al., 1996), St(HP) (Xu et al., 2008), and feldspar (Fuhrman & Lindsley, 1988).

Oxides and Elements from SEM/EDS Data		Oxides used in XRF analysis		Oxides and Elements not used in XRF analysis	
SiO2	Silicon Dioxide	SiO2	Silicon Dioxide	P2O5	Phosphorus Pentoxide
TiO2	Titanium Dioxide	TiO2	Titanium Dioxide	SO3	Sulfur Trioxide
Al2O3	Aluminium Oxide	Al2O3	Aluminium Oxide	ZrO2	Zirconium Dioxide
Cr2O3	Chromium (III) Oxide	Fe2O3	Iron (III) Oxide	PtO2	Platinum Dioxide
MgO	Magnesium Oxide	MnO	Manganese (II) Oxide	Cr2O3	Chromium (III) Oxide
CaO	Calcium Oxide	MgO	Magnesium Oxide	Y2O3	Yttrium (III) Oxide
MnO	Manganese (II) Oxide	CaO	Calcium Oxide	Bi2O3	Bismuth (III) Oxide
FeO	Iron (II) Oxide	Na2O	Sodium Oxide	NiO	Nickel (II) Oxide
ZnO	Zinc Oxide	K2O	Potassium Oxide	CuO	Copper (II) Oxide
Na2O	Sodium Oxide			ZnO	Zinc Oxide
K2O	Potassium Oxide			SrO	Strontium Oxide
F	Fluorine			BaO	Barium Oxide
Cl	Chlorine			Br	Bromine
				Au	Gold

Table 3 – Table listing received forms of compositional data from SEM/EDS & XRF analyses. FeO was received as FeO_{TOT} (Total Iron Oxide).

3 DATA & RESULTS

3.1 FIELD DATA

3.1.1 Geologic Map

Based on data and observations in the field, a generalized geologic map was created, seen in Figure 16. The contacts bounding the phyllites, the garnet mica schists, and the locations of the conglomerate lenses were drawn primarily from data acquired in the field. The boundaries for the LMC, the Nordmannvik Marble, and the Sagvandite bodies were derived from maps published by NGU.

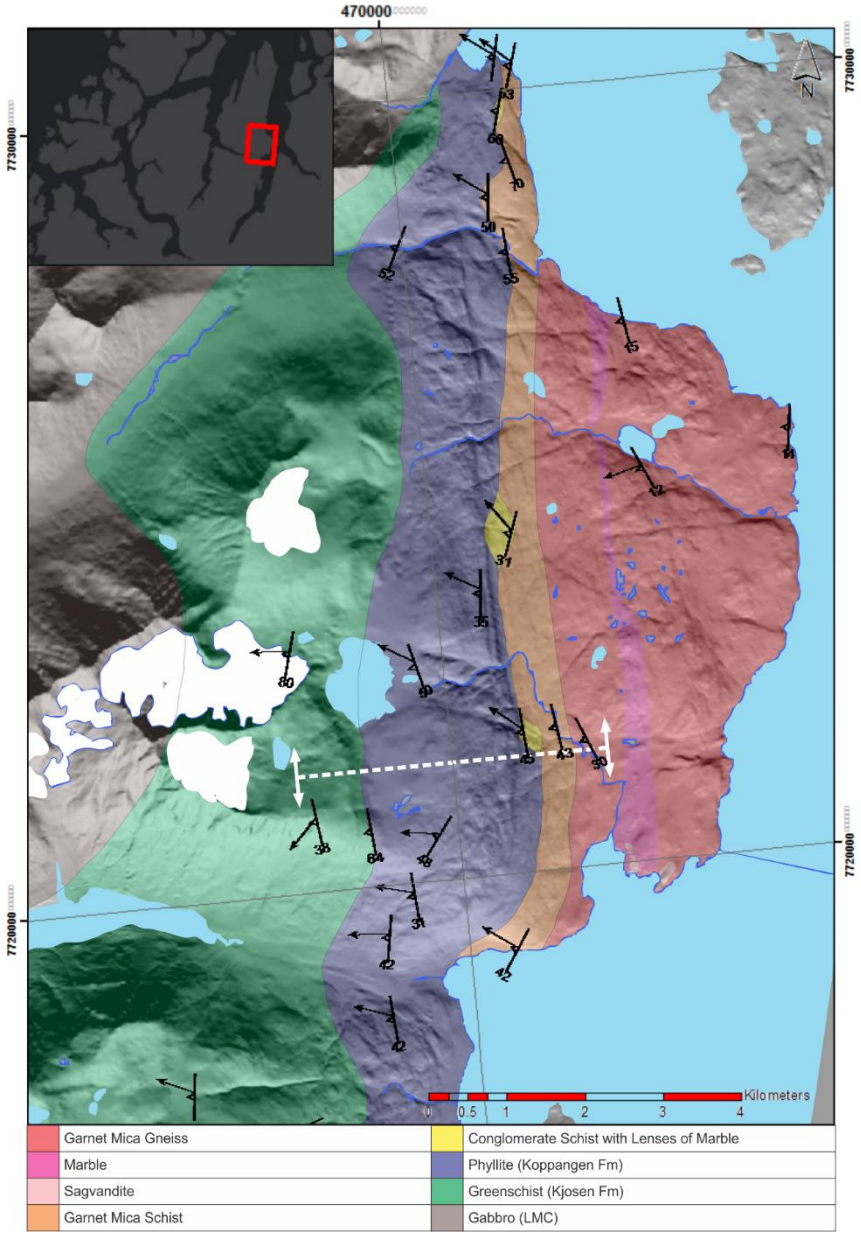

Figure 16 - Geologic map of the study area, including key foliation and lineation measurements, and location of the profile described below. Boundaries drawn from field data and from NGU data.

3.1.2 Rottenvik Profile

A significant amount of time in the field was spent in the Rottenvik area, as a nearly continuous East-West cross-section of these rocks was exposed. This area was therefore a suitable case for the construction of a geologic cross-section. Its location can be seen in Figure 16, and is illustrated by Figure 17.

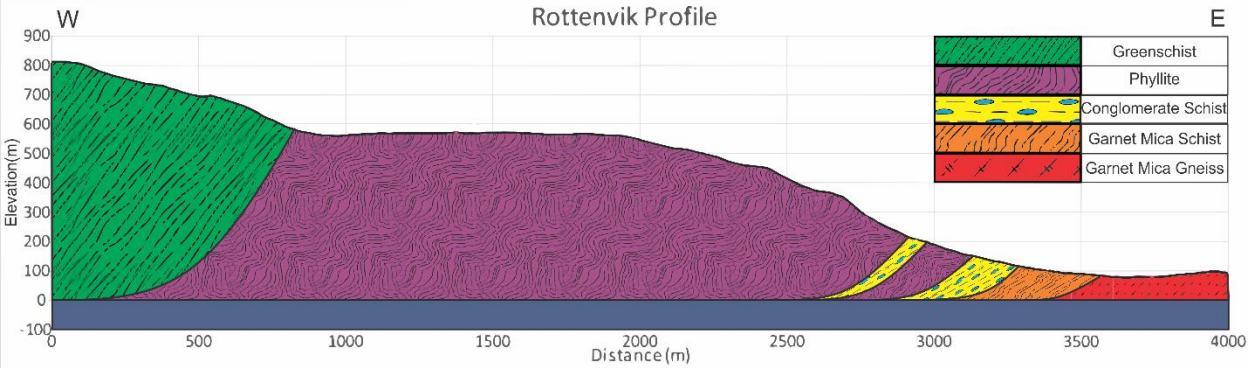

Figure 17 - Cross-section of Rottenvik Profile as indicated in Figure 16. Unit contacts drawn from field data within a 1 kilometer width from the profile line.

3.1.3 Stratigraphic Column

A stratigraphic column was also produced from the Rottenvik Profile to show the relative thicknesses of each unit. The profile was extended to include the LMC to the West, and remainder of the Nordmannvik Nappe on the Western side of the Lyngenfjord. The column is presented in Figure 18.

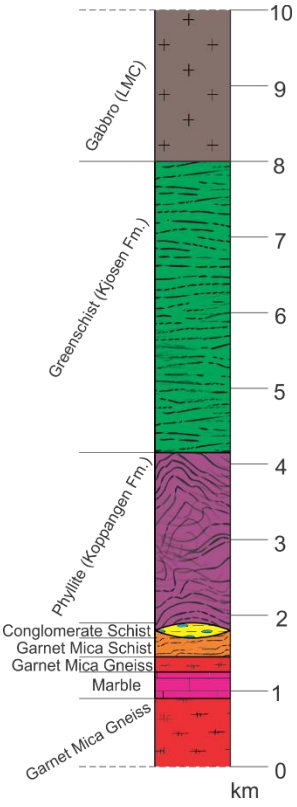

Figure 18 - Stratigraphic column based on Rottenvik Profile illustrated in Figure 16 & Figure 17.

3.1.4 Lithologic Descriptions from Field Observations

3.1.4.1 Garnet Mica Gneiss

The low-lying areas between Koppangen and Lyngseidet are dominated by the mylonitic Garnet Mica Gneiss of the Nordmannvik Nappe. These are primarily meta-pelitic paragneisses, however zones of granitoid migmatites occur in some areas. Marbles and calc-silicates are also seen, mostly in a North-South oriented zone of the peninsula. Small bodies of ultramafic Sagvandite are observed in the Southeast, near Lyngseidet. The foliation of these rocks ranges from vague to clearly defined by light-colored bands of Quartz and Plagioclase, with augens of Garnet and Feldspar. The foliation planes generally strike 189° (degrees), and their Westward dip averages 19°. Lineations observed are generally oriented 279° and plunge 16°. The gneisses range in color from a light grey closer to the overlying phyllites, to a very dark grey farther East from the contact. Minerals observed include Garnet, Quartz, micas, feldspars, and amphiboles. Garnets occur as large (0.5-1 cm [centimeters]) reddish subhedral grains, and decrease in abundance towards the overlying unit. Quartz occurs as veins and clasts, and is commonly associated with Plagioclase. Micas are clearly observed along the foliation, with a dominance of Biotite to the East, and primarily Muscovite to the West. Plagioclase is frequently observed in association with Quartz, and helps to create the white mylonitic banding. Amphiboles are occasionally seen as single grains, but are primarily observed in large (up to 2 m) amphibolitic lenses, which also include Garnet and Biotite. This unit forms the lowest part of the structural section.

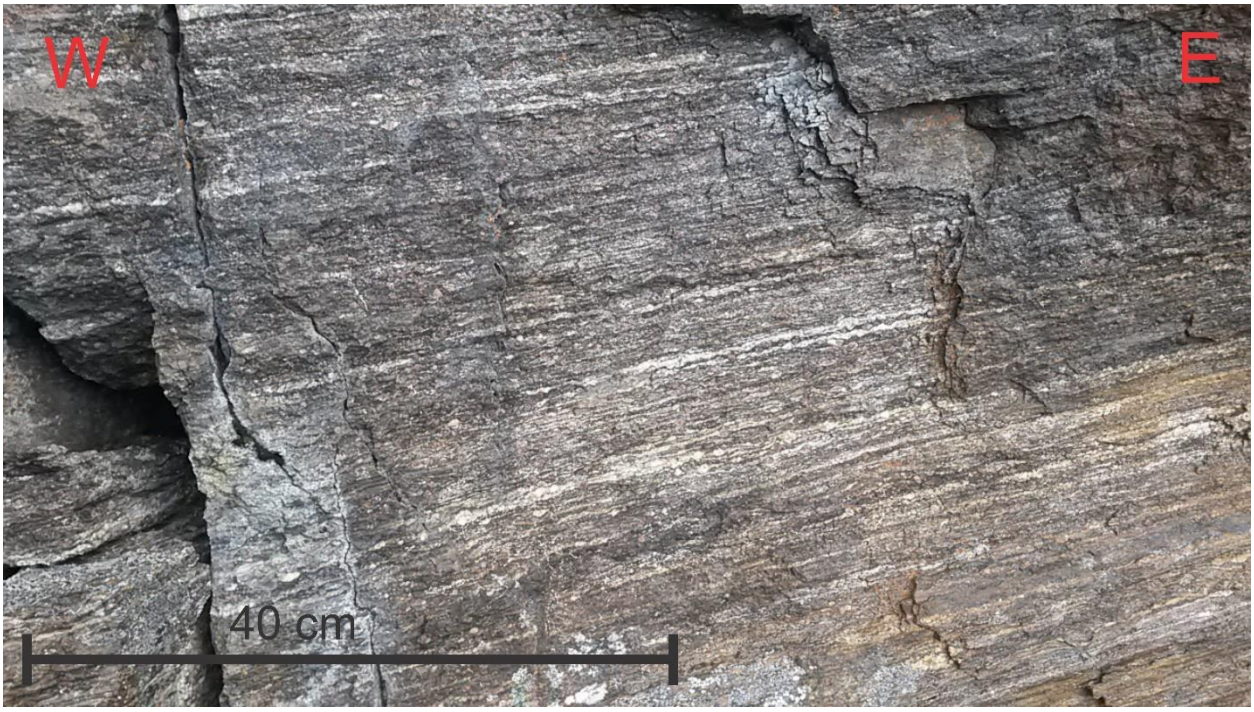

Figure 19 - Outcrop showing typical Garnet Mica Gneiss appearance.

3.1.4.2 Garnet Mica Schist

Above the Garnet Mica Gneiss, closer to the contact with the overlying phyllites, the mylonitic gneisses grade into a more schistose rock with a similar assemblage of minerals. This unit runs North-South, and is roughly 200-300 m wide. The foliation, still well-defined, generally strikes 180° and dips 48° to the west. It occurs as light grey/silver rock with a light brown weathering. Garnets are reduced in abundance from the gneisses, but retain the same relative size (up to 5 mm). Thin (1-3 mm), brittle layers alternate between Quartz and Plagioclase rich to Mica-rich with equal amounts of Biotite and Muscovite. Needle-shaped amphiboles are commonly observed in alignment with the lineation, which trends 302° and plunges 45°.

Figure 20 - Outcrop showing typical Garnet Mica Gneiss appearance.

3.1.4.3 Conglomerate Schist

In the contact zone between the Garnet Mica Schists and the Koppangen FM, several zones or megalenses were observed of what is here termed a Conglomerate Schist. This unit is discontinuous in extent and is characterized by a schistose foliation similar to that of the mica schists, but contains clasts of marble. These clasts occur as small (3-5 cm up to 10-15 cm) bodies elongated in the foliation planes, or as large (up to 100 square meters) zones of carbonate-rich rock. The lithologies surrounding these clasts and zones were identical to either the Phyllite or the Garnet Mica Schist, varying with each occurrence. These rocks are blue-grey in color, and are composed almost entirely of Quartz and carbonates. The foliation plane strikes 174°, dipping 44° to the West. Observed Lineations trend 311°, plunging 30°.

Figure 21 - Typical appearance of Conglomerate Schist. a) Mica Schist host rock with lenses of marble, red ovals showing marble clasts. b) Blue-grey appearance of carbonate zones.

3.1.4.4 Phyllite (Koppangen FM)

At the base of the Koppangen FM is a gradational contact zone between the Garnet Mica Schist of the Nordmannvik Nappe and the overlying phyllites. These rocks are very fine grained (most often individual grains are not discernable), and range from light grey to black in color. The black phyllites commonly have a graphite feel and appearance. In some areas, weathering of sulphide minerals have given the rocks a yellow to purple appearance. The thinly laminated foliation, which strikes 179° and dips 42° to the West, is generally schistose, with varying degrees of crenulation. This crenulation can be non-existent to very pronounced. Farther West, away from the contact, the Phyllites exhibit a significant increase in hardness and competence, while the fine-grained matrix is maintained. Veins and boudins of Quartz are common, and small-scale asymmetric folding of these veins frequently occurs. One outcrop displayed a strong interlayering between Quartz and phyllitic bands. Some observed grains that could be seen include Garnet, Pyrite, micas, and amphiboles. Garnets were roughly 5 mm subhedral grains, and occurred as rare and isolated grains. Pyrite crystals were more common, and were generally isolated euhedral grains. One vein of Pyrite was also observed in the Phyllite. Biotite and Muscovite were common micas, when the grains were large enough to be identified. Needles of Amphibole were observed on a few occasions. Lineations recorded averaged a trend of 283° and plunged 38°.

Figure 22 - Outcrop showing typical Phyllite characteristics close to the contact with the Garnet Mica Schist, including variance in color & brittle nature.

Figure 23 - Mineral appearances in Phyllite. a) Grains of garnet & pyrite in a typically crenulated phyllite. b) Euhedral pyrite crystal. c) Coarse pyrite vein.

Figure 24 - Outcrop showing Phyllite appearance away from the contact zone. Note the vastly differing outcrop appearance. White box corresponds to shear sense indicators shown in Figure 34.

3.1.4.5 Greenschist (Kjosen FM)

On its Western edge, the Koppangen FM forms a gradational contact zone with the overlying greenschists of the Kjosen FM. This zone is roughly 30-40 m wide, and is characterized by a change in color from dark grey to a deep green hue. The foliation strikes 177° and dips Westward 55°, while lineations observed averaged a trend of 255° with a plunge of 35°. This unit is also very fine-grained, however noted minerals include a nearly homogenous mix of Quartz and Chlorite. Crystals of Garnet, Pyrite and Amphibole were also occasionally noted. While generally very similar to the Phyllite in structure and appearance, a few zones of undifferentiated migmatitic greenstone were observed, which were similar in mineralogy, but usually lacking in a metamorphic fabric. These zones were generally highly fractured with leucosomes of Quartz, dark melanosomes of Amphibolite, and small (20 cm wide) brecciated zones.

Figure 25 - Outcrop showing typical Greenschist appearance. Note the characteristic green color.

Figure 26 – a) Outcrop in zone of undifferentiated greenstone. b) Close-up view of small breccia zone.

3.1.4.6 Amphibolite Schist

This unit occurs in the vicinity of Nordkjosbotn, lying above the Nordmannvik Gneiss, and is overlain by the LMC. The sample taken from this unit (14e) occurred just North of Nordkjosbotn, in a thin layer between the Phyllite and a thin overlying layer of metabasalt, which is then overlain by the LMC. This unit is very similar to the Garnet Mica Schist described above, but with a few minor differences. One sample location was investigated, where the schistose foliation was measured to strike 228°, and dip 14° to the Northwest. The observed lineation had a trend of 322°, plunging 14°. The rock is medium-grey in color, and visible minerals include Garnet, micas, Quartz, and amphiboles. The garnets are relatively abundant, compared to the Garnet Mica Schist, but generally smaller (up to 2 mm). Despite its similarities to the rocks of the Nordmannvik Nappe, this unit is mapped as a member of the Lyngen Nappe.

Figure 27 - Outcrop of Amphibolite Schist in the field.

3.1.4.7 Gabbro (LMC)

Overlying the Kjosen FM is the gabbroic LMC. This unit dominates the higher peaks and elevations in this area, which generally makes field investigations of these rocks particularly challenging. However, it can be easily reached in a few places, including near Koppangen and along the E91 road that travels Westward from Lyngseidet. From these two areas, the gabbros observed showed no metamorphic structural features. They occurred as massive, highly fractured, coarse-grained rocks with a medium to dark green color. Fibrous mineral lineations were seen on many fracture surfaces. Large (1-2 mm) subhedral epidote crystals in a dark matrix give the rock its distinctive greenish color. In an outcrop near Koppangen, Quartz and Plagioclase were observed in a fine-grained greenish groundmass.

Figure 28 - Outcrop of Gabbro near Koppangen.

3.1.5 Structural & Kinematic Data

Structural and kinematic data obtained in the field is here presented into coherent formats. This allows for better understanding and interpretation of this data.

3.1.5.1 Structural Projections

Presented below in Figure 29 is the compilation of foliation and lineation data gathered in the field for each rock unit, as well as one for all lithologies combined. From these projections, it is clear that all of the investigated units are similar in the strike and trend of their respective foliations and lineations. Dip and plunge angles, however, show a marked increase from the Garnet Mica Gneiss to the rest of the overlying units.

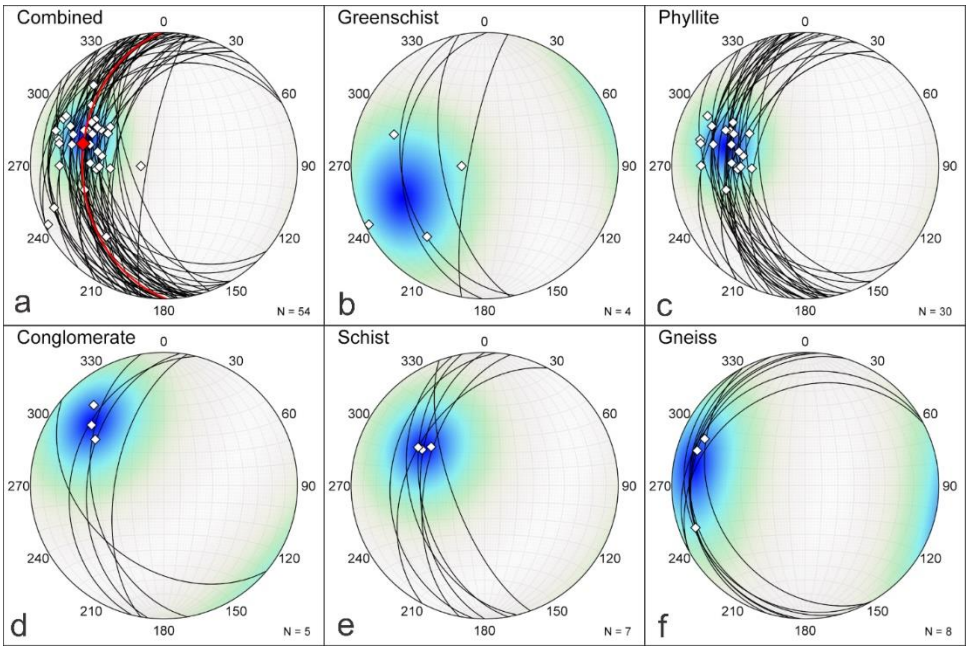

Figure 29 - Stereographic projections of field data in lower hemisphere Schmid net projections. Black lines represent foliation planes, white points indicate lineations. Red line and point on (a) are averages of foliations and lineations, respectively.

3.1.5.2 Macroscopic Shear Sense Indicators

Several macro-scale shear-sense indicators were observed in the field, and are organized in Table 4 below. Shear bands and sigma clasts were the dominant shear sense indicators observed. Shear bands are a ductile deformation mechanism that produces zones of localized shear strain, whereby the preexisting foliation is cut, and a new cleavage domain is defined within these bands (Twiss & Moores, 1992). Sigma clasts are porphyritic grains with asymmetric tails of material recrystallized from the porphyritic clasts, and the asymmetry of these tails define the sense of shear (Twiss & Moores, 1992).

Station	Rock	Shear Band	Sigma Clast	Fold	Shear Sense/ Thin Section	Hanging Wall Movement
12.07a	CNG	X			Dextral	NW; 319
12.07b1	CNG	X			Sinistral	SE; 139
12.07b2	CNG		X		Dextral	NW; 319
14.08a	GMG		X		Dextral	ESE; 108
14.08b	GMG		X		Dextral	ESE; 108
30.08	GMS	X			Sinistral	ESE; 120
02.09	FYL	X			Dextral	WNW; 291
03.09	FYL	X			Dextral	West; 270
10.09	FYL	X			Sinistral	NW; 295
15.09	GMS	X	X		Dextral/3.1	NW; 310
16.09	FYL		X		Dextral	WNW; 294
17.09-1	FYL			X	Dextral	West; 269
17.09-2	FYL	X	X		Dextral	West; 279
17.09-3	FYL		X		Dextral	WNW; 294

Table 4 - Table listing kinematic indicators observed in the field. Bold and italicized stations are depicted in the figures below.

a

Figure 30 - Amphibolite clasts in Garnet Mica Gneiss showing a dextral, top-to-the-East shear sense. Corresponding to Stations 14.08a & 14.08b from Table 4.

Figure 31 – Shear band & sigma clast in Garnet Mica Schist showing dextral, top-West shear sense. Corresponds to Station 15.09 in Table 4.

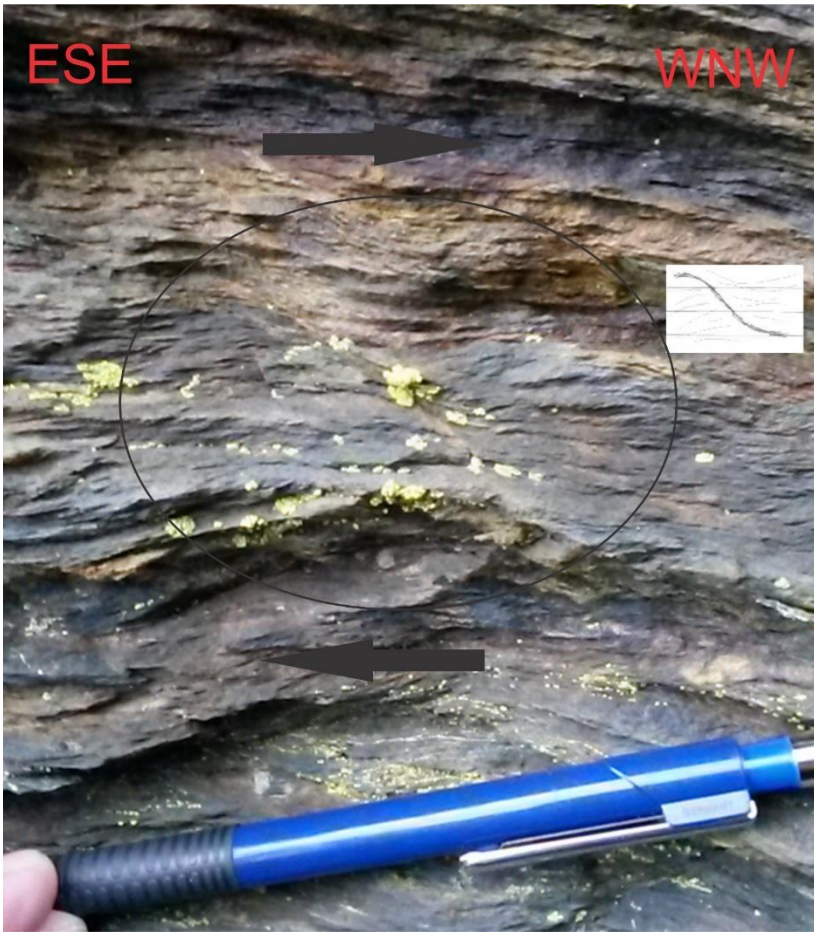

Figure 32- Shear band in Phyllite showing a dextral, top-West shear sense. Corresponding to Station 02.09 in Table 4.

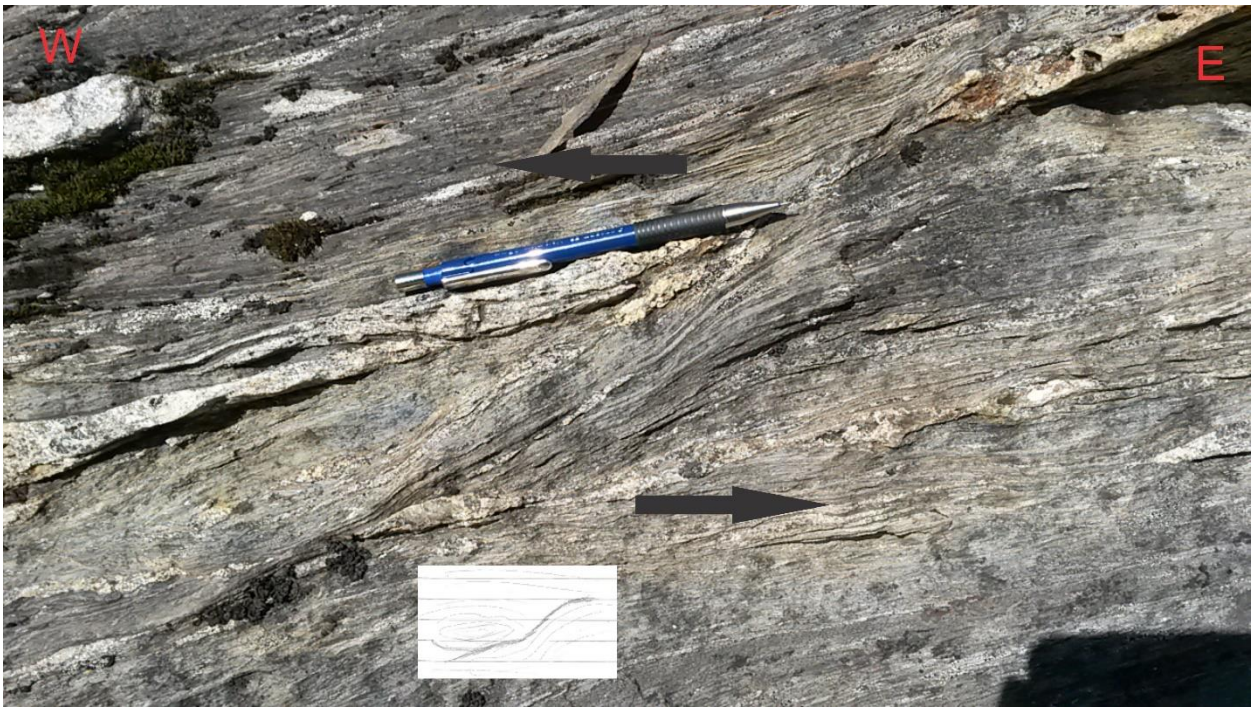

Figure 33 - Shear band in Phyllite showing a sinistral, top-West shear sense. Corresponds to Station 10.09 in Table 4.

Figure 34 - Sigma clast & shear band in Phyllite showing a dextral, top-West shear sense. Corresponds to Station 17.09-2 in Table 4. Close up from Figure 24.

3.1.5.3 Strain Partitioning

From our field observations, it is apparent that the shearing associated with the emplacement of the Lyngen Nappe is heterogenous and partitioned, both along and across strike. The general trend from East to West is one of increasing mylonitization and decreasing grain size. In the Nordmannvik rocks at the Eastern edge of the peninsula, a few locations were observed with pronounced levels of migmatization. Meanwhile, several zones in the Phyllites showed a sharp increase in crenulation and asymmetric folding of quartz veins.

3.2 LAB DATA

3.2.1 Mineralogy from Thin Sections

3.2.1.1 Garnet Mica Gneiss

Two sample locations for this unit produced prepared thin sections (numbers 1.1 and 2.1), each one with a corresponding Quartz sample (numbers 1.2 and 2.2).

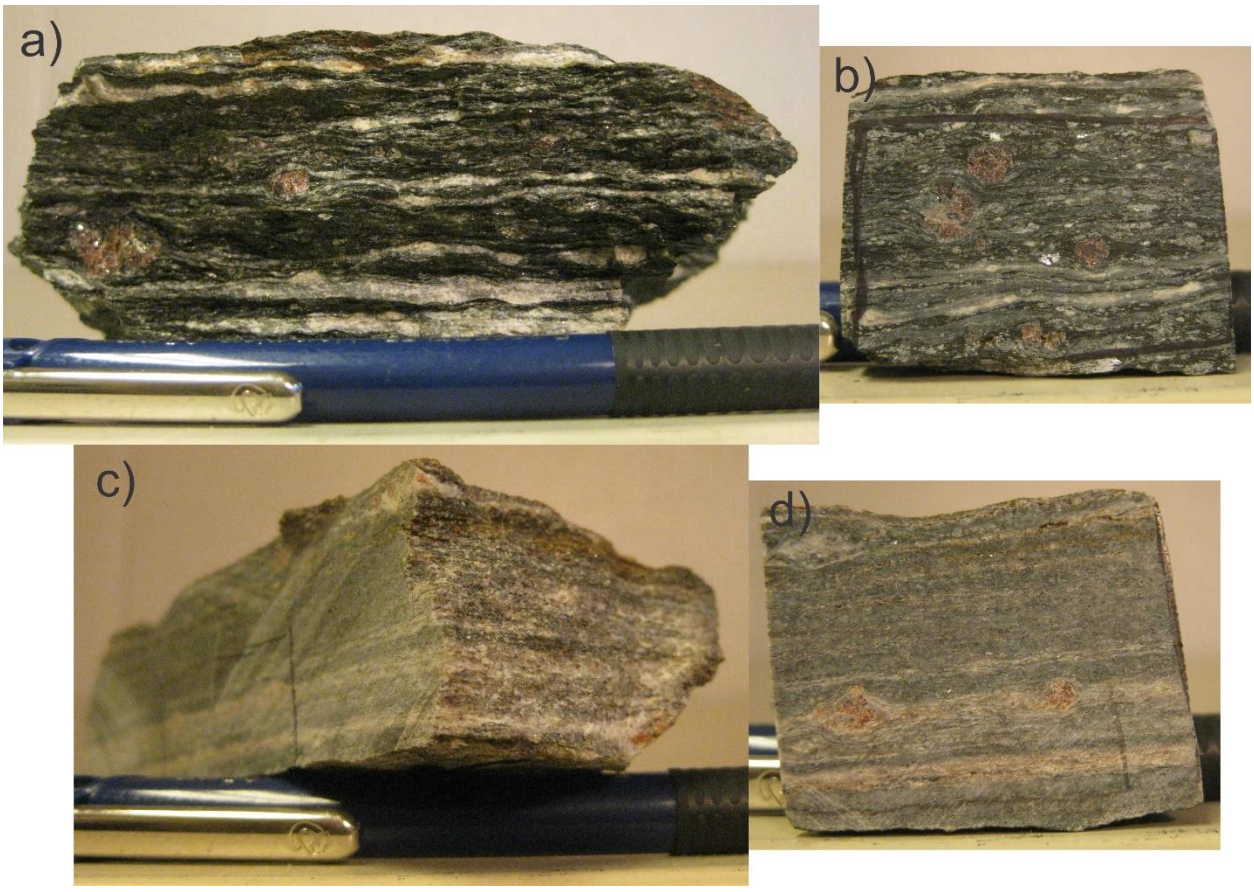

Figure 35 - Hand specimen view of Garnet Mica Gneiss. a) Sample 1.1 fresh surface, showing characteristic mylonitic foliation and large Garnet porphyroclasts in a dark, mica-rich matrix, with bands of Quartz and Plagioclase. b) Cut view of sample 1.1, from thin section preparation. c) Sample 2.1 fresh and cut surfaces, displaying a lighter and more homogeneous appearance compared to sample 1.1. d) Cut view of sample 2.1, from thin section preparation.

3.2.1.1.1 Quartz (50-70%)

The Quartz in these samples, generally occurring in ribbons, is characterized by lobate grain boundaries (Figure 36) (sometimes poorly defined) indicative of GBM (Grain Boundary Migration) recrystallization. Some grains also show undulose extinction, and some appearance of SGR (Subgrain Rotation) recrystallization. Grains ranged in sizes less than 1.0 mm. A closer investigation through the thin sections prepared from Quartz veins in these rocks showed clear core-mantle structures, with grains in the core domains ranging in size from 0.5-2.0 mm. In thin section 2.2, a slight blue tendency was observed through the Gypsum plate, indicating a possible dextral shear sense, which would represent top-to-the-West movement.

3.2.1.1.2 Feldspars (10-20%)

Porphyritic Feldspar grains were observed in both samples. Anhedral to subhedral in form, sizes ranged from 0.5-2.0 mm, with Alkali Feldspars generally larger than the Plagioclase grains. In thin section 1.1, Plagioclase occurred primarily in Quartz ribbons, with rare lamellar twinning. However, in sample 2.1, twins for both species were common, with lamellar twins in Plagioclase, and Tartan twinning in Alkali Feldspars.

3.2.1.1.3 Muscovite (5-20%)

Muscovite was present in both samples, but was the dominant mica in thin section 2.1. Observed grains were subhedral, and ranged in size from 0.5-2.0 mm. Commonly showing a high birefringence, these grains also occasionally formed mica fish microstructure. Some Muscovite grains were observed being crossed by zones containing Quartz, Ilmenite, and Aluminium silicate minerals in thin section 1.1.

3.2.1.1.4 Biotite (15%/<1%)

A marked difference in the abundance of Biotite was noted between the two samples. Nearly ubiquitous in sample 1.1, Biotite was noted as only a minor constituent in thin section 2.1. In both samples, however, crystals were strongly pleochroic, and dark brown in color. Sizes ranged anywhere below 1.0 mm. While almost absent in section 2.1, it was noted to generally form around Feldspar clasts.

3.2.1.1.5 Garnet (15%/<1%)

Large (up to 4 mm) euhedral garnets were observed in thin section 1.1, with inclusions of Quartz, Feldspar, and Biotite. In contrast, only one major Garnet crystal was observed in section 2.1, and was smaller (1.4 mm), subhedral, and partially replaced by Quartz and Feldspar.

3.2.1.1.6 Kyanite (10%/0%)

Kyanite was observed in thin section 1.1 only, and in relatively high abundance. Grains were subhedral, elongate, and with a very distinct cleavage pattern. Grain size was generally 2-3 mm in length, and some crystals showed undulose extinction patterns.

3.2.1.1.7 Sillimanite (5%)

Sillimanite occurs as thin needle-like grains, often forming groups or aggregates. These clusters were often observed in association with Kyanite or Muscovite.

3.2.1.1.8 Apatite (5%)

Small (roughly 0.1 mm) grains of Apatite were noted in both thin sections, occurring with a very low (dark grey) birefringence.

3.2.1.1.9 Calcite (0%/5-10%)

Calcite was observed only in thin section 2.1, and generally with two domains: a very fine-grained (<<0.1 mm) domain of anhedral crystals; and subhedral grains no larger than 0.1 mm.

3.2.1.1.10 Zoisite (0%/5%)

Straight-extinction Zoisite was noted in thin section 2.1, but not in 1.1. These were generally subhedral grains roughly 1.0 mm in size.

3.2.1.1.11 Clinozoisite (<5%)

Small (0.5 mm or smaller) subhedral grains of Clinozoisite were observed in both samples.

3.2.1.1.12 Diopside (<5%/0%)

Minor amounts of the Clinopyroxene Diopside were observed in thin section 1.1. 1.0 mm subhedral grains exhibited two 90° cleavages.

3.2.1.1.13 Staurolite (1%)

One Staurolite grain measuring 0.1 mm was observed in the matrix of thin section 1.1. A weak yellow pleochroism was noted. The crystal occurred between Quartz ribbons and adjacent to a Biotite-rich domain. Inclusions of Quartz and Muscovite were observed.

3.2.1.1.14 Opaque Minerals (<1%)

Opaque grains were small (<0.1 mm), anhedral in thin section 1.1, and euhedral in section 2.1. Ilmenite was identified via SEM in thin section 1.1.

3.2.1.1.15 Zircon (<1%/0%)

Zircons observed in thin section 1.1 occurred in Biotite, and were identified by pleochroic halos. Larger zircons measured up to 0.2 mm in size.

3.2.1.1.16 Hornblende (<1%)

One Hornblende crystal was observed in Quartz sample 1.2. It exhibited a strong blue-green pleochroism, and measured approximately 0.2 mm in size.

3.2.1.1.17 Metamorphism

A clear mineralogical difference is noted between the two samples of Nordmannvik Gneiss. Thin section 1.1 contains a clearly high-temperature assemblage of Qtz+Ms (Muscovite) +Bt (Biotite) +Grt (Garnet) +Pl (Plagioclase) +Kfs (Alkali Feldspar) +Ky (Kyanite) +Sil (Sillimanite) +Ilm (Ilmenite), indicating an Upper Amphibolite to Lower Granulite facies metamorphism. Section 2.1, however, is absent of Staurolite, Kyanite, and Sillimanite. Alkali Feldspars are abundantly perthitic, and a significant decrease in the presence of Biotite is noted. In addition, the appearance of Epidote group minerals may suggest a retrograde pathway to Upper Greenschist/Lower Amphibolite facies.

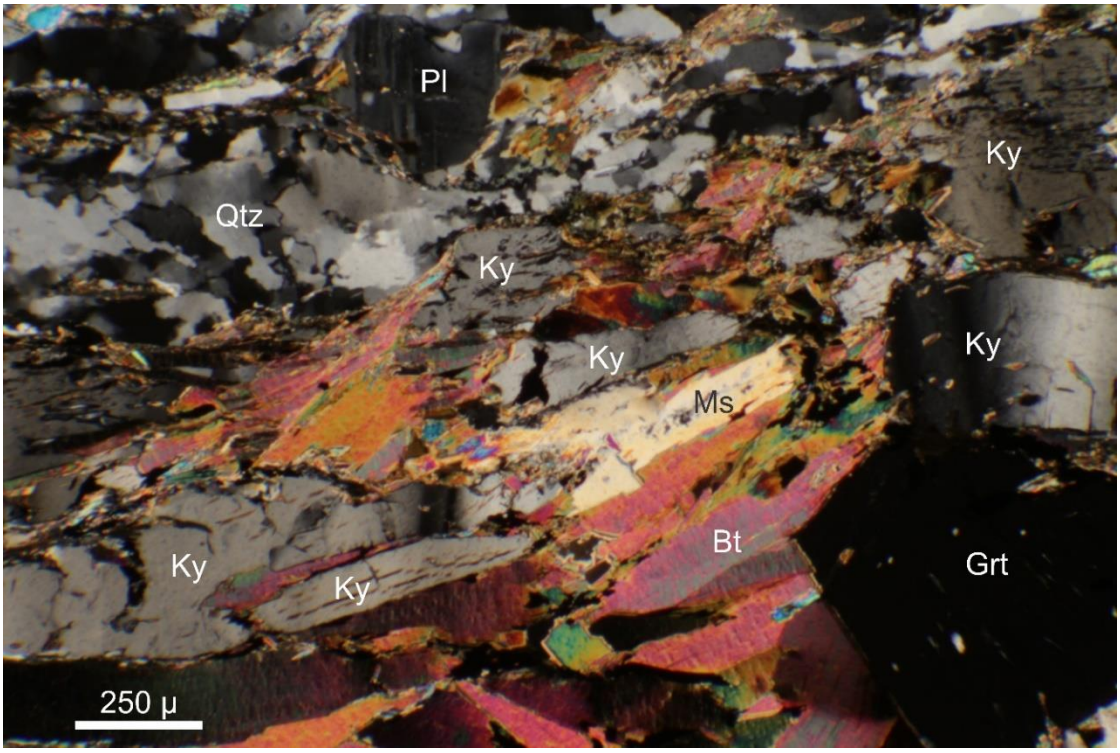

Figure 36 - Microphotograph of thin section 1.1, viewed under XPL (Crossed Polarized Light). Several large Kyanite grains (one showing undulose extinction, middle right), along with Plagioclase and a large euhedral Garnet, in a matrix dominated by micas and Quartz.

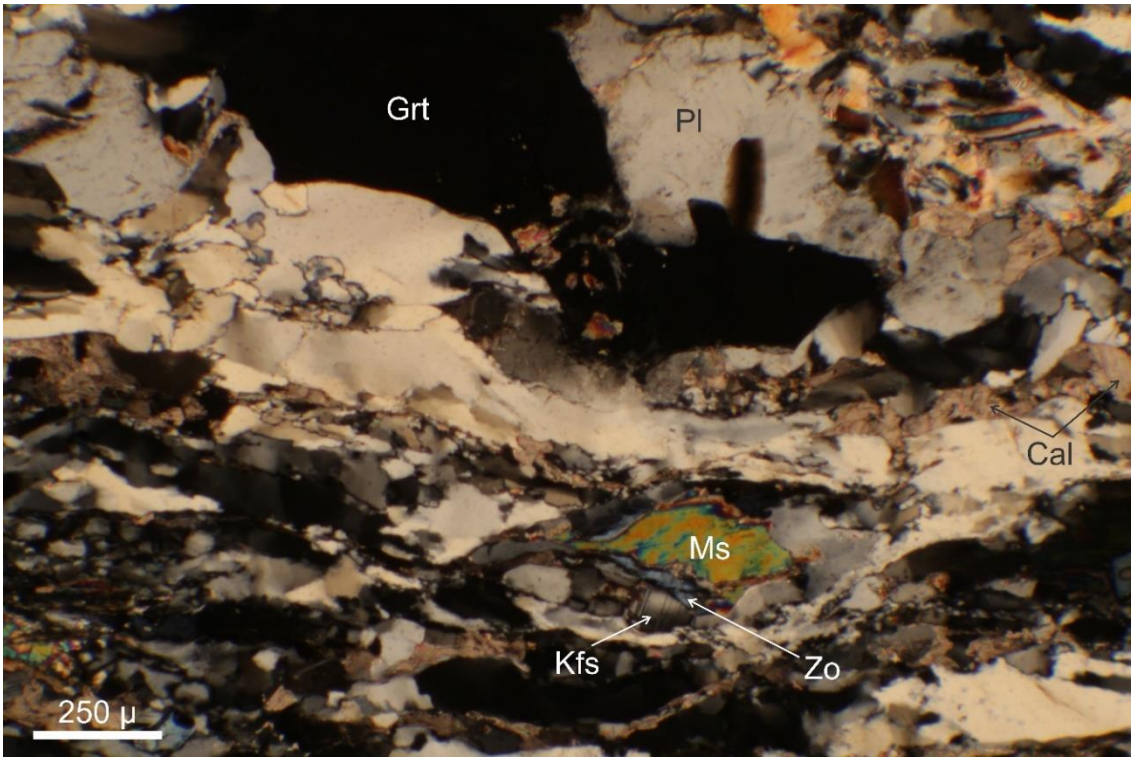

Figure 37 - Microphotograph of thin section 2.1, viewed under XPL. Large subhedral Garnet, replaced and surrounded by Plagioclase and Quartz. Smaller grains of Calcite (Cal), Alkali Feldspar, Zoisite, and Muscovite are also present.

3.2.1.2 Garnet Mica Schist

One prepared thin section, number 3.1 (along with its corresponding Quartz sample, section 3.2), represent this unit. In the field, these rocks appear to be transitional between the Nordmannvik gneisses and the Koppangen FM

Figure 38 - Hand specimen of sample 3.1. a) Garnet Mica Schist displaying prominent Quartz bands, with thinner fine-grained bands rich in micas. Foliation is more schistose compared to the underlying gneiss. b) Cut view of sample 3.1, from thin section preparation.

3.2.1.2.1 Quartz (70-80%)

As the dominant mineral constituent in this sample, Quartz occurs mainly in ribbons trending along the foliation plane. Grains are up to 3.0 mm in size, and show characteristics of GBM and SGR. Many grains also show undulose extinction. In the Quartz sample 3.2, crystals tend to show more traits of SGR, but some lobate grain boundaries do occur. Undulose extinction is still common. Larger grains range from 2-5 mm in size, while finer grained domains average 0.2-0.3 mm.

3.2.1.2.2 Biotite (20-30%)

Biotite is significantly present in this section, and occurs as medium brown, strongly pleochroic grains.

3.2.1.2.3 Muscovite (20%)

Muscovite is also prevalent, and occurs as very small (up to 1.0 mm in length) needle-like grains.

3.2.1.2.4 Garnet (10%)

Garnets in this thin section are strongly sheared and deformed. They can be easily described as poikilitic, with inclusions of Quartz and Plagioclase. Average grains size is roughly 4 mm.

3.2.1.2.5 Feldspar (10%)

Plagioclase and Alkali feldspars were both seen in this sample, with grain sizes up to 1.0 mm. Twinning in Plagioclase was commonly observed.

3.2.1.2.6 Zoisite (10%)

Poikilitic crystals of Zoisite were observed, with grain sizes ranging from 0.5-2.0 mm. Zoisite was commonly seen in association with Garnet.

3.2.1.2.7 Opaque Minerals (<5%)

Subhedral opaque minerals were observed, commonly occurring with micas. Identified minerals include Pyrrhotite, Chalcopyrite, and Ilmenite.

3.2.1.2.8 Chlorite (<1%)

Rare grains of Chlorite, roughly 1.0 mm in size, were seen as light green, weakly pleochroic crystals.

3.2.1.2.9 Zircon (<1%)

Zircon was observed as a minor constituent, identified by pleochroic halos in Biotite.

3.2.1.2.10 Apatite (<1%)

Small (0.1 mm) grains of Apatite were observed in thin section, and identified by SEM analysis.

3.2.1.2.11 Rutile (<1%)

Small (up to 0.2 mm) grains of Rutile were observed in thin section, commonly in association with Ilmenite.

3.2.1.2.12 Metamorphism

The sampled Nordmannvik Schist (thin section 3.1) contains a very similar assemblage to sample 2.1 of the Garnet Mica Gneiss. However, a small amount of Chlorite was noted, as well as the presence of Rutile in association with Ilmenite. The latter could possibly represent relict grains of a Granulite facies event, with the Chlorite and Epidote resulting from a Greenschist facies overprint.

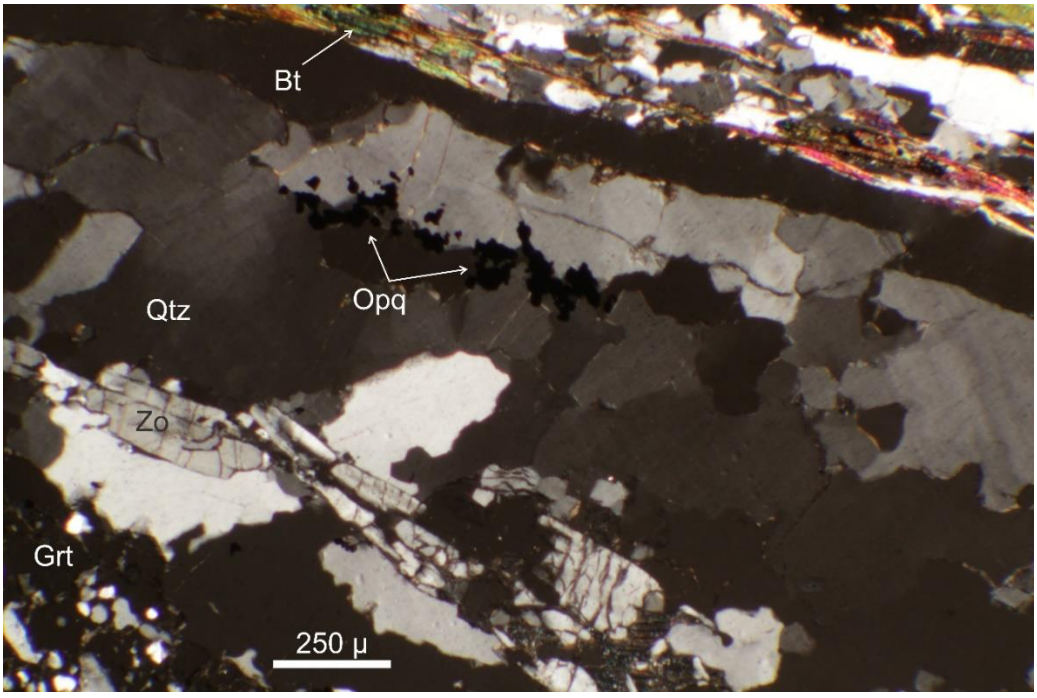

Figure 39 - Microphotograph of thin section 3.1, viewed under XPL. Quartz-rich band with large Zoisite grains, and poikilitic Garnet (lower left) with inclusions of Quartz.

3.2.1.3 Conglomerate Schist

For this unit, a lens of the carbonate material in the host rock was sampled, and is represented by thin section number 5.

3.2.1.3.1 Calcite (70-80%)

This sample is dominated by Calcite grains, both as a fine-grained (<0.1 mm) matrix, and as coarse-grained (up to 2.0 mm) aggregates. These grains exhibit an extremely high birefringence, with iridescent twin lamellae occurring ubiquitously. Calcite dominates the fine-grained groundmass (roughly 90% in these areas).

3.2.1.3.2 Quartz (30-40%)

Quartz is also a prominent constituent in this sample, and occurs primarily in wide (2-5 mm) quartz rich (40-60%) veins. Average grain size in these veins are roughly 0.5 mm. Many grains exhibit undulose extinction, and most grain boundaries show BLG (Bulging) and/or SGR recrystallization mechanisms.

3.2.1.3.3 Muscovite (<1%)

One coarse (0.5 mm) grain of Muscovite was observed, which implies that finer grained crystals might be a minor constituent in this sample.

3.2.1.3.4 Metamorphism

The metamorphic history of this unit is difficult to constrain, as this sample only consists of a carbonate lens. However, given that the Quartz appears to have been recrystallized through both BLG and SGR mechanisms, a lower-temperature regime (lower Greenschist facies) is inferred.

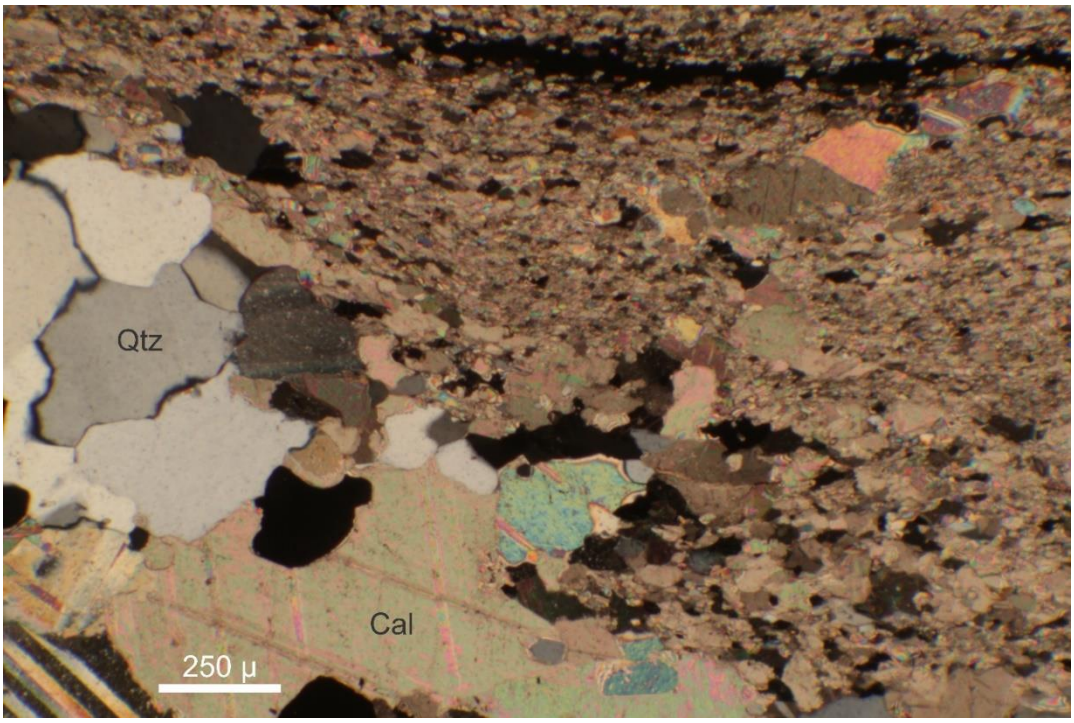

Figure 40 - Microphotograph of thin section 5, viewed under XPL. Large Quartz grains occurring with equally coarse-grained calcite (lower left), with a groundmass of fine-grained calcite.

3.2.1.4 Phyllite (Koppangen FM)

Two thin sections, numbers 4 and 6, represent the phyllitic Koppangen FM

Figure 41 - Hand specimens of Phyllite. a) Fresh surface view of sample 4, showing slightly crenulated schistose foliation, with the foliation defined by thin bands of very fine-grained material. Bands of Quartz are also present. b) Cut view of sample 4, from thin section preparation. c) Fresh surface view of sample 6, displaying typical phyllitic graphite color. d) Cut view of sample 6, from thin section preparation. A dark, fine-grained matrix dominates, with lenses and clasts of Quartz also present.

3.2.1.4.1 Quartz (60-70%)

Both samples are dominated by quartz, which occurs primarily in ribbons. The quartz domains display the effects of both SGR and BLG recrystallization mechanisms. The quartz grains can be very fine grained (less than 0.1 mm), or up to 0.5 mm in the coarser domains. In thin section 6, two very distinct domains occur: coarse-grained ribbons and veins, and a very fine-grained matrix.

3.2.1.4.2 Muscovite (20-40%)

Both Phyllite samples are also abundant in Muscovite. These grains occur as slender, needle-like crystals, no wider than 0.1 mm. Muscovite in thin section number 6 is concentrated in the fine-grained groundmass.

3.2.1.4.3 Calcite (30-50%/0%)

While not observed in thin section 6, Calcite occurs in abundance in thin section 4. Grain sizes vary from less than 0.1 mm up to 1.0 mm, and generally occur as either fine- or coarse-grained aggregates.

3.2.1.4.4 Plagioclase (5-10%)

Feldspar grains, most likely Plagioclase, were observed exclusively in thin section 4. These grains are usually distinguished from quartz by their dusty appearance, as observed twins were rare. Measured grains ranged from 0.2-0.5 mm is size.

3.2.1.4.5 Chlorite (1-5%)

Again observed only in thin section 4, Chlorite grains were occasionally encountered. In PPL (Plain Polarized Light), they showed a weak faint green pleochroism. Crystals were small, only up to 0.2 mm in size.

3.2.1.4.6 Opaque Minerals (<1-5%)

Opaque grains were observed in both samples, with a much higher abundance in thin section 4. In this section, subhedral grains were measured up to 0.2 mm in size, and many exhibited a tabular shape. In thin section number 6, opaque grains were anhedral, and very fine-grained (<0.1 mm).

3.2.1.4.7 Clinozoisite (<1%)

Few grains of Clinozoisite were observed, with a low yellow birefringence. These crystals were roughly 0.2 mm in length.

3.2.1.4.8 Metamorphism

The two Phyllite samples (thin sections 4 and 6) are dominated by Quartz and Muscovite. Chlorite and Plagioclase were also noted in sample 4, with Epidote minerals in both sections. This assemblage, together with the appearance of some carbonates, clearly suggest a Greenschist facies metamorphic history.

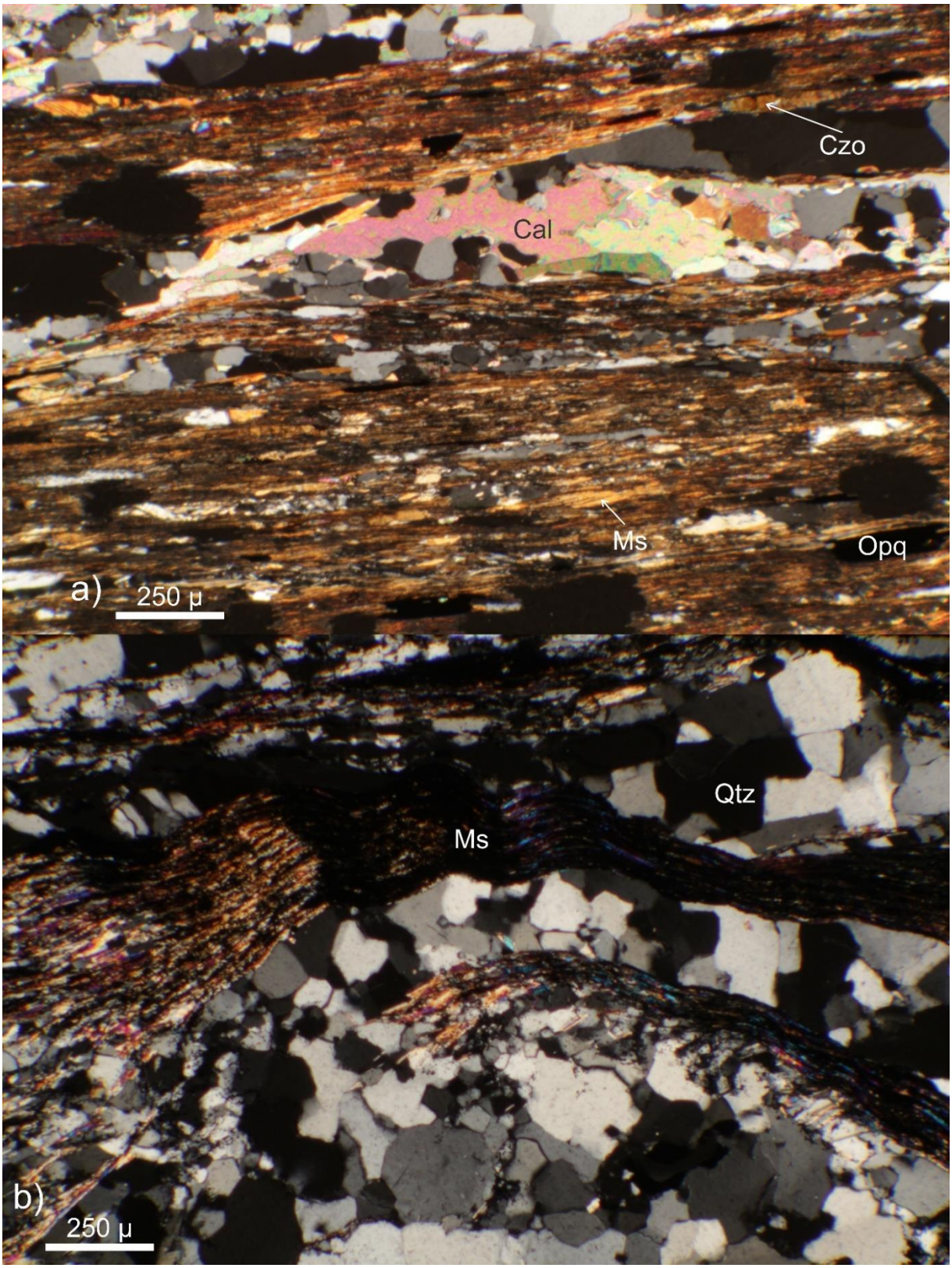

Figure 42 - Microphotographs of thin sections 4 (a) & 6 (b), viewed under XPL. a) Typical Phyllite texture, with ribbons of Quartz, and domains of fine-grained Muscovite. Tabular opaque grains and Calcite are also present. b) Crenulated mica ribbon between Quartz layers.

3.2.1.5 Chlorite Schist

One thin section (number 7) was prepared from this unit, occurring in the field as part of the mapped Kjosen FM greenschists. The mineralogy described below (specifically the lack of amphiboles), however, requires a more appropriate classification, and Chlorite Schist is adopted.

Figure 43 - Hand specimen view of Chlorite Schist. a) Partially fresh surface visible of sample 7, showing characteristic green color and homogeneous appearance. b) Cut view of sample 7, from thin section preparation. Visible in this view are sheared garnets, which are rarely seen in outcrops.

3.2.1.5.1 Quartz (60-70%)

Quartz in this section occurs mostly as a fine-grained (<0.1 mm) groundmass, but several clasts, aggregations, and veins occur with larger grain sizes (up to 0.5 mm). SGR is the dominant interpreted recrystallization mechanism, while some grains also exhibit characteristics of BLG.

3.2.1.5.2 Chlorite (20-30%)

The other major constituent in this sample is Chlorite. These crystals are up to 0.5 mm in size, are dark green in PPL, and show a strong pleochroism. They were observed to concentrate around porphyroclasts and Garnet tails, possibly in pressure shadows.

3.2.1.5.3 Garnet (5-10%)

The garnets observed in this sample are strongly poikilitic, with inclusions of Quartz, Chlorite, Feldspars, and opaque minerals. They range in size from 3-8 mm, and appear to have been strongly sheared.

3.2.1.5.4 Plagioclase (5%)

Several porphyroclasts of Plagioclase were observed, commonly with twins exhibited. These clasts were generally 0.5-1.0 mm in size, and subhedral in form.

3.2.1.5.5 Opaque Minerals (1-5%)

Many subhedral opaque minerals were observed, with an average size of 0.1 mm. Ilmenite was identified by SEM.

3.2.1.5.6 Epidote (1%)

Epidote was noted as very fine grained (<<0.1 mm) crystals, commonly in association with Ilmenite and Titanite. Cores were identified in the SEM as containing Allanite, or being enrichment in Rare Earth Elements.

3.2.1.5.7 Titanite (1%)

Titanite was observed in thin section, commonly surrounding or associated with Ilmenite.

3.2.1.5.8 Alkali Feldspar (<1%)

Few grains of Alkali Feldspar were seen in the thin section, but were noted to be similar in size and shape to the Plagioclase crystals.

3.2.1.5.9 Zircon (<1%)

Rare Zircons were observed in thin section, identified by pleochroic halos in Chlorite.

3.2.1.5.10 Metamorphism

The single Chlorite Schist sample (thin section 7) yielded a metamorphic assemblage of Qtz+Chl (Chlorite) +Grt+Pl+Kfs, with minor amounts of Epidote minerals, having Ilmenite and Titanite in association. Epidotes were noted as containing cores of Allanite. The garnets were partially replaced by Quartz and Chlorite, indicating a possible Greenschist facies overprint. This rock defines an obvious Greenschist facies metamorphism, however the absence of any white mica is an interesting note.

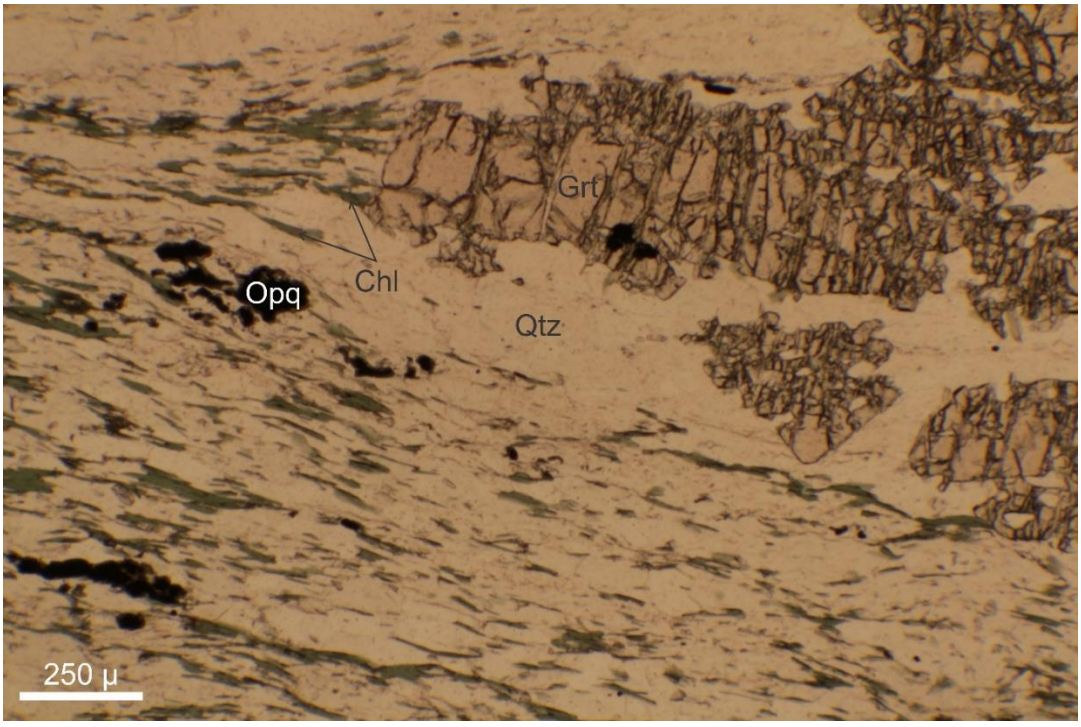

Figure 44 - Microphotograph of thin section 7, viewed under PPL. Deformed Garnet with interstitial Chlorite, in a matrix dominated by Quartz and Chlorite.

3.2.1.6 Amphibolite Schist

Thin Section 14e represents the Amphibolite Schist occurring North of Nordkjosbotn.

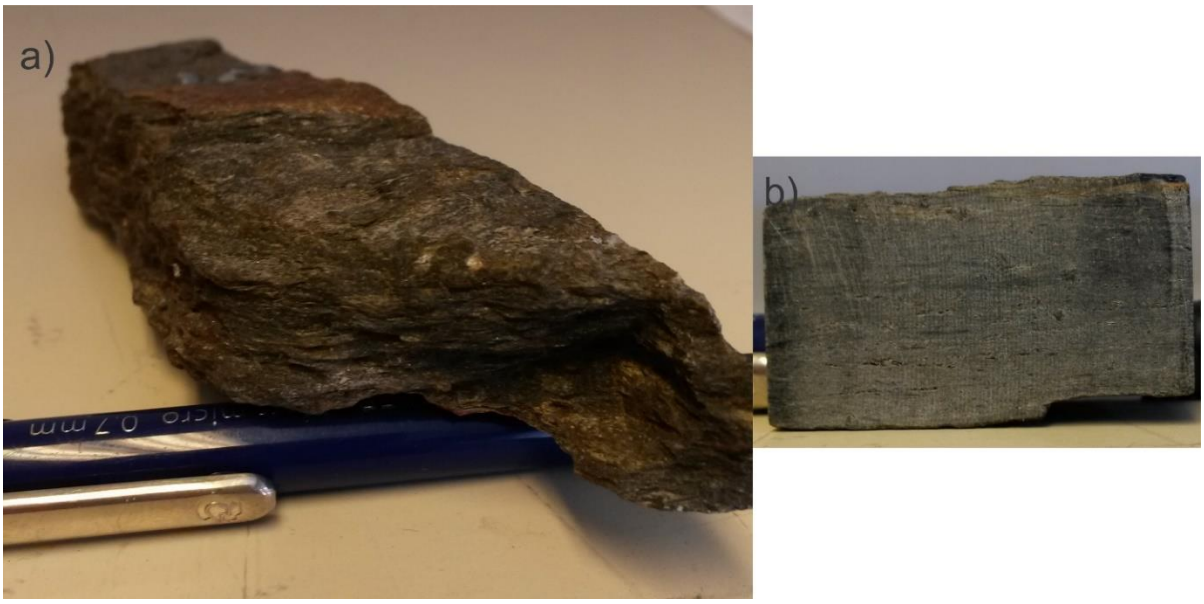

Figure 45 - Hand specimen view of Amphibolite Schist. a) Fresh surface view of sample 14e, displaying similar appearance and structure to the Garnet Mica Gneiss and Schist. b) Cut view of sample 14e, from thin section preparation. Garnets are very small rounded dark grains.

3.2.1.6.1 Quartz (50-70%)

The Quartz observed in this sample occurs primarily as ribbons, with grain sizes ranging from 0.1-1.0 mm. Many grains show undulose extinction, and the Quartz in this section is interpreted to have experienced SGR and BLG recrystallization.

3.2.1.6.2 Muscovite (30%)

Muscovite is a major constituent in this section, with grain sizes ranging from 0.5-1.0 mm. A spaced schistose foliation is defined by Muscovite, while both Quartz-rich and mica-rich domains occur.

3.2.1.6.3 Biotite (20-30%)

Biotite in this sample viewed in PPL occurred in medium to dark brown in color, and is strongly pleochroic. Anhedral grains were mostly present, with some subhedral crystals. Sizes ranged from 0.5-1.0 mm. While preferentially lying parallel to the foliation, some grains were observed oriented perpendicular to the foliation.

3.2.1.6.4 Garnet (10-15%)

Subhedral garnets, averaging 2 mm in size, were observed with inclusions of Quartz and opaque minerals. They also appeared to be strongly deformed, with subhelical inclusion trains indicating rotation of these porphyroblasts. Inclusions of Epidote were observed in some grains.

3.2.1.6.5 Opaque Minerals (5-10%)

Numerous large (up to 1.0 mm) subhedral opaque grains were observed in this section. Identified minerals include Ilmenite and Pyrrhotite. Ilmenite was observed as subhedral grains, with a general width of 0.1 mm. They were oriented parallel to the lineation when seen in the matrix.

3.2.1.6.6 Alkali Feldspar (5%)

Large (1.0 mm) poikilitic grains of Alkali Feldspar were observed in this sample, with opaque mineral inclusions.

3.2.1.6.7 Clinozoisite (5%)

Many coarse (1.0 mm) grains of Clinozoisite were observed in section. These occurred as subhedral, with a weak green pleochroism in PPL, and a low yellow birefringence under XPL (Crossed Polarized Light).

3.2.1.6.8 Plagioclase (5%)

Plagioclase grains occurred as 1.0 mm wide crystals, with a poikilitic texture.

3.2.1.6.9 Chlorite (1-5%)

Weakly green pleochroic Chlorite was observed in PPL, with grains roughly 0.5 mm in size.

3.2.1.6.10 Hornblende (1-5%)

Subhedral Hornblende grains were observed, averaging 0.25 mm in size.

3.2.1.6.11 Carbonate Minerals (1%)

Calcite was observed as a minor constituent in this sample, with grains up to 0.5 mm in size. Thin carbonate veins of Dolomite contained high amounts of Iron.

3.2.1.6.12 Zircon (<1%)

Several zircons were observed in section, identified by pleochroic halos in Biotite. These grains were less than 0.1 mm in size.

3.2.1.6.13 Apatite (<1%)

Small (0.1 mm) lens-shaped grains of Apatite were observed in thin section.

3.2.1.6.14 Epidote (<1%)

Epidote with Allanite cores were identified and analyzed by SEM.

3.2.1.6.15 Metamorphism

Sample 14e represents this unit, and contains the assemblage Qtz+Ms+Bt+Chl+Grt+Pl+Kfs. Epidote and Hornblende are also present. The presence of Hornblende, together with Chlorite and Epidote, indicate an Upper Greenschist to Lower Amphibolite facies assemblage. As in the Epidotes of sample 7, the cores were enriched in Rare Earth Elements, indicating Allanite. Chlorite was observed in some reaction tails of the garnets, indicating a metamorphic overprint.

Figure 46 – Microphotographs of thin section 14e. a) XPL view of alternating mica-rich and Quartz-rich bands, with interstitial Clinozoisite and opaques. Black circle indicates view of Figure 46b. b) PPL view of mica- and Quartz-rich bands, with interstitial Hornblende and Clinozoisite.

3.2.1.7 Gabbro (LMC)

Two Gabbro samples were collected, resulting in thin sections 8 and 9. While appearing similar in the field, inspection under the microscope proved to show large mineralogical differences between the samples.

3.2.1.7.1 Clinozoisite (40-60%)

A dominating abundance of Clinozoisite was observed in both samples. The crystals in thin section 8 were much coarser (1-3 mm) than the grains in sample 9 (up to 0.3 mm). Crystals were predominantly subhedral, exhibited a good single cleavage, and contained fine grained (<0.1 mm) inclusions of Chlorite and Plagioclase.

3.2.1.7.2 Chlorite (15-25%)

Chlorite was strongly represented in both Gabbro samples. Grain sizes ranged from 0.1-1.0 mm, with a much higher concentration of crystals smaller than 0.5 mm. Pleochroism was weak in both sections. In thin section 8, Chlorite displayed a tendency to form massive aggregations around grains of Clinozoisite. In thin section number 9, masses of very fine (<0.1 mm) needles were observed.

3.2.1.7.3 Actinolite (10-15%)

In PPL, Actinolite and Chlorite exhibit a similar green color. However, Actinolite displays a stronger pleochroism and a blue-green color shift, along with a higher birefringence.

3.2.1.7.4 Plagioclase (1%/40-50%)

A major difference in the occurrence of Plagioclase was noted between the two samples. Grains in thin section 8 were rare, usually occurring as fine-grained (<0.1 mm) inclusions of Clinozoisite, however isolated grains up to 0.5 mm were observed. In thin section 9, Plagioclase was very abundant, and grain sizes ranged from 0.2-0.5 mm. Their most striking feature is a strong saussuritization, with partial replacement by Clinozoisite, and commonly exhibit a low yellow birefringence. Twinning was also observed in many grains.

3.2.1.7.5 Quartz (30-40%/1-5%)

The second major difference between the two samples is the abundance of Quartz. Thin section 8 contained a relatively high concentration of Quartz, and together with a wide variety of other minerals observed, might be better classified as a calc-silicate skarn rather than a Gabbro. Nonetheless, Quartz in this sample exhibited characteristics of GBM and SGR, with many large grains showing undulose extinction. Core-mantle structures were common, with the large grains (core domains) 1-3 mm in size, surrounded by fine-grained (<0.1 mm) domains (mantle). In comparison, Quartz in thin section 9 was observed only in minor amounts, occurring in small pockets or zones, appearing sometimes to be a replacement to Plagioclase. These zones were fine-grained (<0.1 mm) domains, no more than 2 mm in size.

3.2.1.7.6 Opaque Minerals (1-5%)

Opaque minerals observed in both Gabbro samples were generally subhedral, occurring as fine-grained (<0.1 mm) in thin section 8, and more coarse-grained (0.2-1.0 mm) in thin section 9. Crystals were commonly observed as long and slender rod-shaped grains.

3.2.1.7.7 Calcite (1-5%/0%)

Calcite was observed in thin section number 8 only, and was only seen in a couple veins or fractures. These grains, anywhere from 0.1-1.0 mm in size, might be a secondary constituent, as the host rock was highly fractured.

3.2.1.7.8 Metamorphism

The general mineralogic assemblage from the two Gabbro samples (thin sections 8 and 9) is Qtz+Chl+Pl+Ep (Epidote) +Act (Actinolite). Especially given the association of Chlorite, Actinolite, Epidote, and Plagioclase, these rocks suggest a Greenschist facies metamorphism of the LMC. Sample 8, as a calc-silicate rock, could possibly indicate some metamorphic interaction between the Gabbro and the metapelites of the Nordmannvik Nappe.

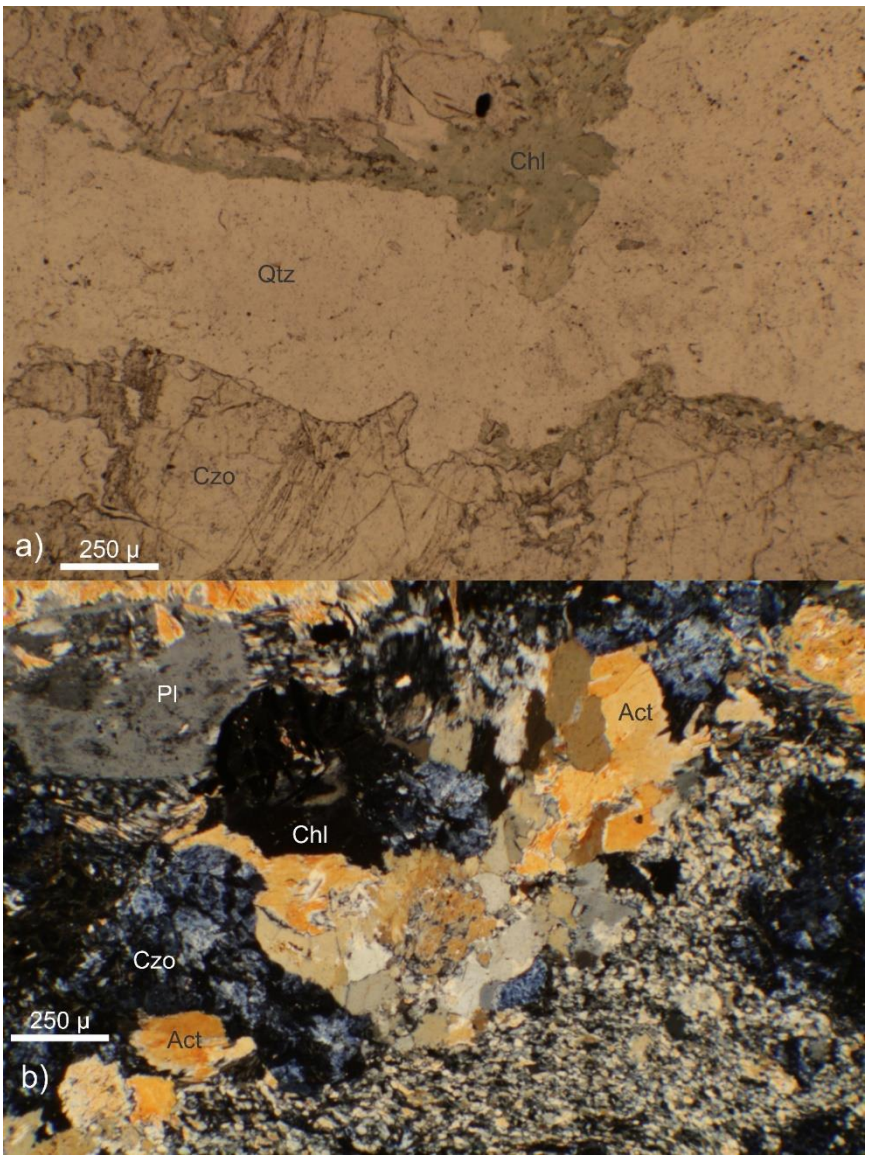

Figure 47 - Microphotographs of thin sections 8 (a, under PPL) & 9 (b, under XPL). a) Large Clinozoisite grains surrounding a Quartz vein, with Chlorite masses occurring at some edges of the Clinozoisite. b) Typical Gabbro texture, with blue birefringent Clinozoisite, yellow birefringent Actinolite (green to blue in PPL), Chlorite, and Plagioclase. Chlorite also dominates the fine-grained domain in the lower left area of the image.

3.2.2 X-Ray, Petrology, & Pseudosection Analysis

In order to gain a better understanding of the history and origin of some of the rock units studied in the field, four samples were selected for detailed petrologic analysis. The samples selected were: 1.1, a mylonitic Garnet Mica Gneiss from the Nordmannvik Nappe; 3.1, a Garnet Mica Schist from the Nordmannvik Nappe, but near (or within) the contact zone with the overlying phyllites; 7, a mylonitized Chlorite Schist between the Koppangen FM phyllites and the LMC; and 14e, an Amphibole-bearing Schist sampled from a profile further South, but occurring structurally between a thin slice of Phyllite and overlying mafic rocks associated with the LMC. Whole-rock compositional data was obtained from the XRF analysis of each sample, and detailed compositional data for various mineral phases was obtained by SEM and EDS analysis.

Sample	Pre-LOI weight (g)	Post-LOI weight (g)	Volatiles Lost (g)	% of Original Sample
1.1	5.807	5.751	0.055	0.954
3.1	5.073	5.041	0.032	0.633
7	4.527	4.466	0.062	1.361
14e	5.924	5.825	0.099	1.671

Table 5 - Table of pre- and post-LOI weights, indicating amount of volatiles lost during the process.

Sample	GMG 1.1	GMS 3.1	GRN 7	AMS 14e
SiO_2	57.23	88.10	72.14	69.59
TiO_2	1.13	0.23	0.44	0.83
Al_2O_3	21.13	5.05	12.18	14.13
Fe_2O_3	10.23	2.52	7.89	5.72
MnO	0.08	0.05	0.15	0.09
MgO	3.38	0.86	1.69	2.42
CaO	0.41	0.38	0.40	1.29
Na_2O	0.57	0.61	5.18	1.12
K_2O	4.28	0.96	0.04	3.21
Total Wt.%	98.42	98.76	100.13	98.39

Table 6 - Table of whole-rock compositional data for investigated samples. For the samples 1.1, 3.1, & 14e, values from the XRF analysis in Oslo were used. For sample 7, XRF values from analysis in Tromsø were utilized. Wt.%: Weight Percent.

	Main Minerals								
Sample	Qtz	Grt	Bt	Ms	Chl	Pl	Kfs	Ky/Sil	Ep/Czo/Zo/Aln
1.1	X	X	X	X		X	X	X	X
3.1	X	X	X	X	X	X	X		X
7	X	X			X	X	X		X
14e	X	X	X	X	X	X	X		X
	Accessory Minerals								
	Dol	Zrn	St	Hbl	Di	Ap	Rt	Ttn	Opq/Ilm/Po/Ccp
1.1		X	X		X	X			X
3.1		X				X	X		X
7		X						X	X
14e	X	X		X		X			X

Table 7 - Table of main and accessory minerals in the analyzed samples. Dol: Dolomite; Czo: Clinozoisite; Zo: Zoisite; Di: Diopside; Hbl: Hornblende; Opq: Opaque Minerals; Zrn: Zircon; St: Staurolite; Aln: Allanite; Ap: Apatite; Rt: Rutile; Ttn: Titanite; Po: Pyrrhotite; Ccp: Chalcopyrite.

From Figure 48 below, it is clear that the Garnets in samples 1.1 and 14e all show an increase in the endmember Almandine from the cores to the rims, with a decrease in Spessartine plus Grossular. The Garnet from thin section 3.1, however, shows an increase in the Pyrope endmember from its core to its rim. The Garnet composition in sample 7 shows no significant change from core to rim.

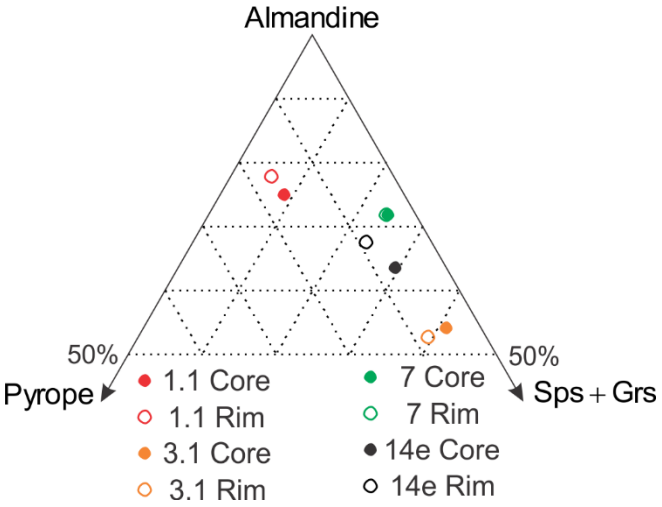

Figure 48 - Ternary diagram showing the composition of the Garnet cores and rims in the selected samples, in terms of the endmember species of Garnet.

In terms of Plagioclase, sample 7 is the exception, and is nearly pure Albite, while the other three samples plot within the Oligoclase range, between 70 and 90% of the Albite endmember (Figure 49).

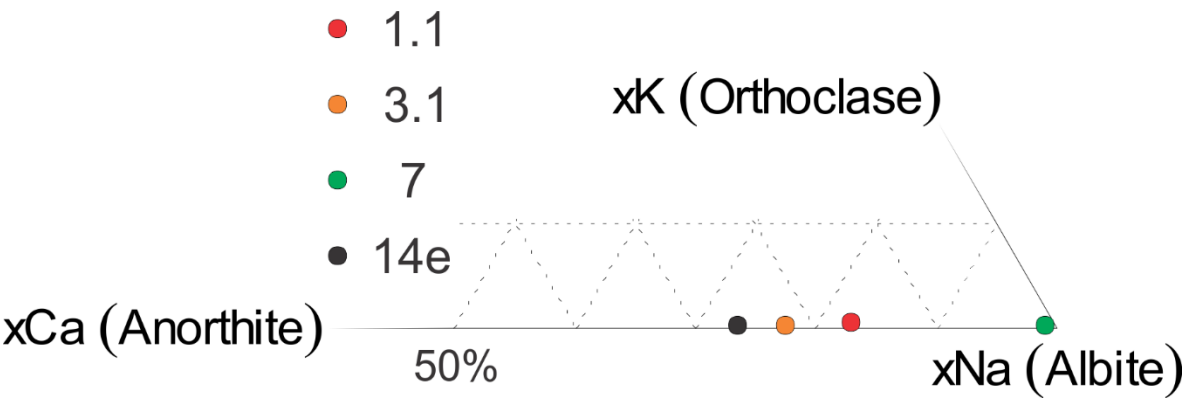

Figure 49 - Ternary diagram showing the composition of the Plagioclase grains from the selected samples, in terms of Plagioclase and Potassium Feldspar end members.

Biotite grains were analyzed in samples 1.1, 3.1, and 14e. From Figure 50 below, an increase in the X_{Mg} values can be seen between samples 1.1 and 3.1. Chlorite was only measured in sample 7, and Staurolite was only identified in sample 1.1.

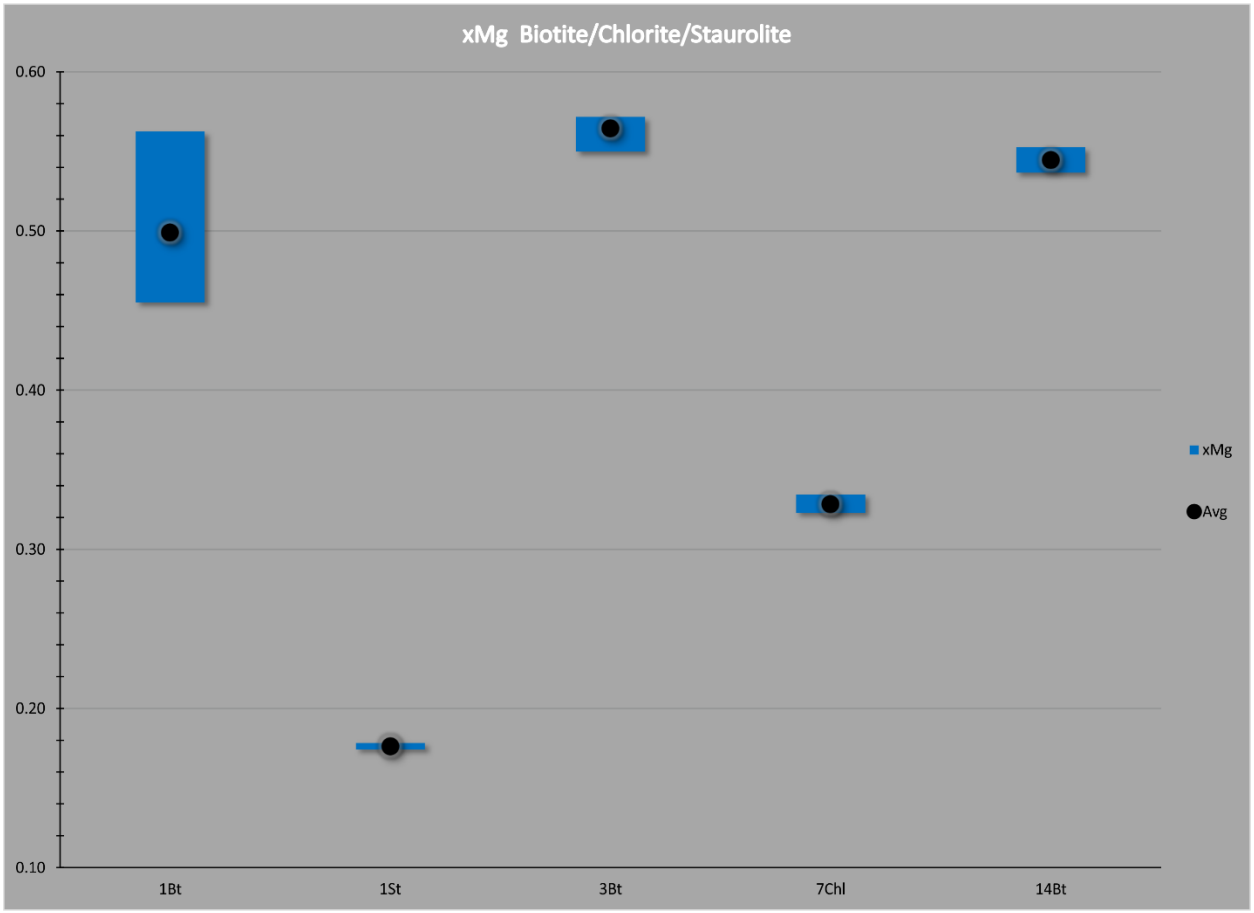

Figure 50 - Graph of X_{Mg} values from Biotite, Chlorite, & Staurolite in the selected thin sections.

Epidote group minerals were analyzed from thin sections 3.1, 7, and 14e. Given the low X_{Fe} values seen in Figure 51, and from the study of these sections under the microscope, these Epidote minerals are predominantly Clinozoisite or Zoisite. The X_{Fe} values in sample 7, however, are greatly increased over samples 3.1 and 14e.

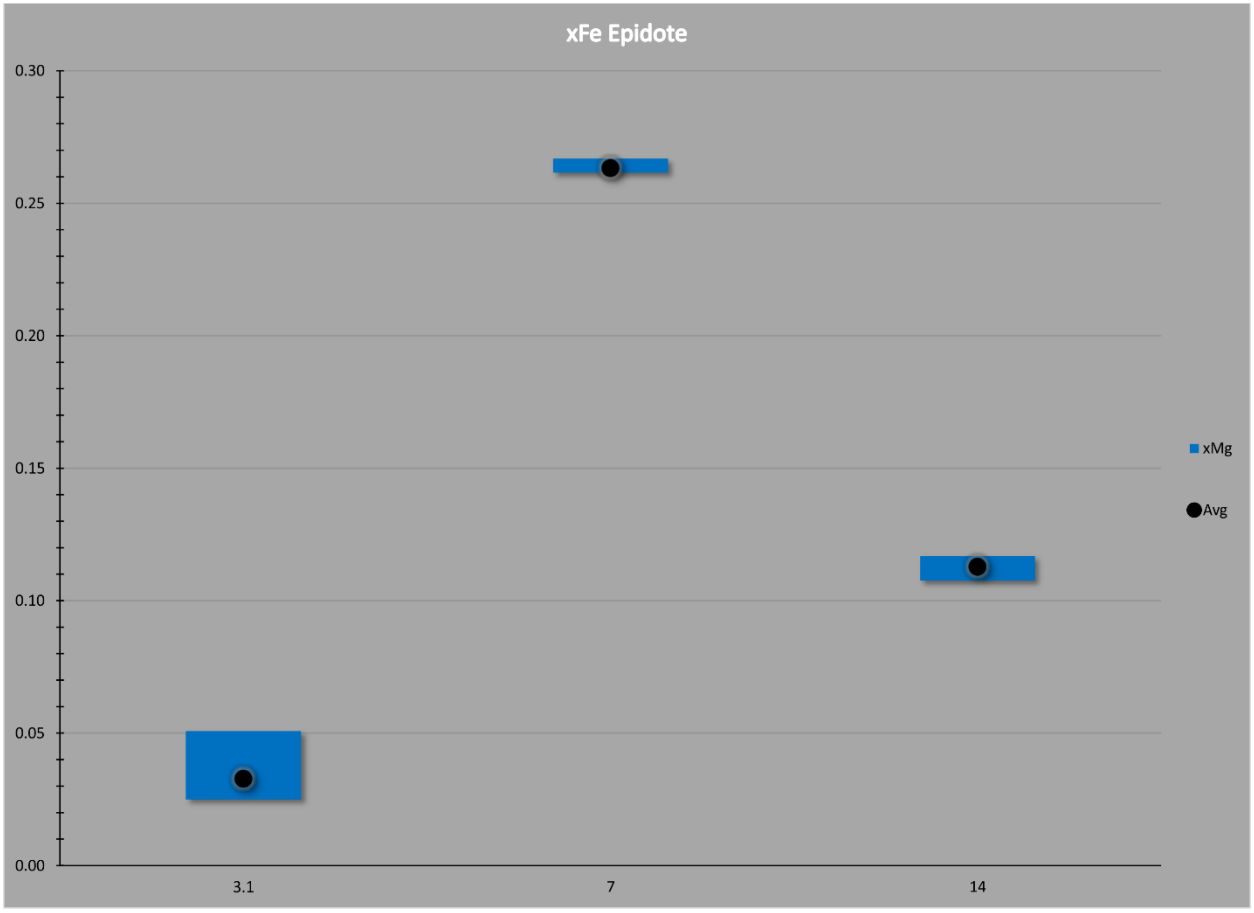

Figure 51 - Graph of X_{Fe} values from Epidote minerals in the selected thin sections.

3.2.2.1 Garnet Mica Gneiss

1.1	Grt Core	Grt Rim	Pl	Bt	Bt in Grt	Ms	St
Wt.%							
SiO_2	37.62	37.73	64.44	35.97	36.12	45.85	27.52
TiO_2	0.01	0.02	0.01	2.55	3.46	0.96	0.59
Al_2O_3	20.99	21.00	21.70	17.47	17.85	32.68	52.19
Cr_2O_3	0.02	0.02	0.01	0.01	0.02	0.01	0.05
MgO	4.13	4.24	0.003	9.82	10.35	0.86	1.55
CaO	1.43	1.42	3.48	0.00	0.00	0.00	0.01
MnO	1.95	0.57	0.01	0.01	0.05	0.004	0.06
FeO	34.07	35.45	0.05	18.58	16.50	2.52	12.94
ZnO	0.00	0.00	0.01	0.06	0.07	0.02	2.07
Na_2O	0.00	0.00	9.42	0.22	0.37	1.09	0.08
K_2O	0.00	0.00	0.09	9.74	9.41	9.77	0.004
F	0.00	0.00	0.00	0.00	0.00	0.003	0.00
Cl	0.00	0.00	0.001	0.03	0.03	0.01	0.00
Total	100.21	100.45	99.20	94.45	94.22	93.78	97.07
Oxygens	12	12	8	11	11	11	22
Normalized Cations							
Si	3.00	3.00	2.87	2.83	2.84	3.11	3.95
Ti	0.001	0.001	0.0004	0.15	0.20	0.05	0.06
Al	1.97	1.97	1.14	1.62	1.65	2.62	8.84
Cr	0.001	0.001	0.0003	0.0007	0.0013	0.0007	0.0051
Fe^{3+}	0.02	0.02	0.00	0.00	0.00	0.05	0.00
Mg	0.49	0.50	0.0002	1.15	1.21	0.09	0.33
Ca	0.12	0.12	0.17	0.00	0.00	0.00	0.001
Mn	0.13	0.04	0.0002	0.001	0.003	0.0002	0.01
Fe^{2+}	2.26	2.34	0.00	1.22	1.08	0.09	1.55
Zn	0.00	0.00	0.0002	0.004	0.004	0.001	0.22
Na	0.00	0.00	0.81	0.03	0.06	0.14	0.02
K	0.00	0.00	0.01	0.98	0.94	0.85	0.001
F	0.00	0.00	0.00	0.00	0.00	0.001	0.00
Cl	0.00	0.00	0.0001	0.004	0.004	0.001	0.00
Total	8	8	5	8	8	7	15
X_{Mg}	0.18	0.18	-	0.48	0.53	0.38	0.18
Alm	0.75	0.77	-	-	-	-	-
Pyr	0.16	0.17	-	-	-	-	-
Sps	0.04	0.01	-	-	-	-	-
Grs	0.04	0.04	-	-	-	-	-
Ab	-	-	0.83	-	-	-	-
An	-	-	0.17	-	-	-	-
Or	-	-	0.01	-	-	-	-

Table 8 - Table of geochemical data from thin section 1.1. Alm: Almandine; Pyr: Pyrope; Sps: Spessartine; Grs: Grossular; Ab: Albite; An: Anorthite; Or: Orthoclase; Al: Aluminium; Mg: Magnesium; Ca: Calcium; Ti: Titanium; Cr: Chromium; Fe^{2+}: Ferrous Iron; Mn: Manganese; Si: Silicon; Na: Sodium; K: Potassium; Zn: Zinc; Fe^{3+}: Ferric Iron. Highlighted values were used during petrological modelling.

The Garnet analyzed and profiled in sample 1.1 was a large, euhedral crystal (Figure 52), and shows only a small amount of zonation between the core and the rim (Figure 53). The Manganese endmember Spessartine shows a clear and steady decrease from the center of the Garnet outwards. Almandine and Pyrope show a minor increase and decrease, respectively, at the very edges of the crystal, while Grossular shows no compositional change. Therefore, no clear indication for a prograde or retrograde history occurs.

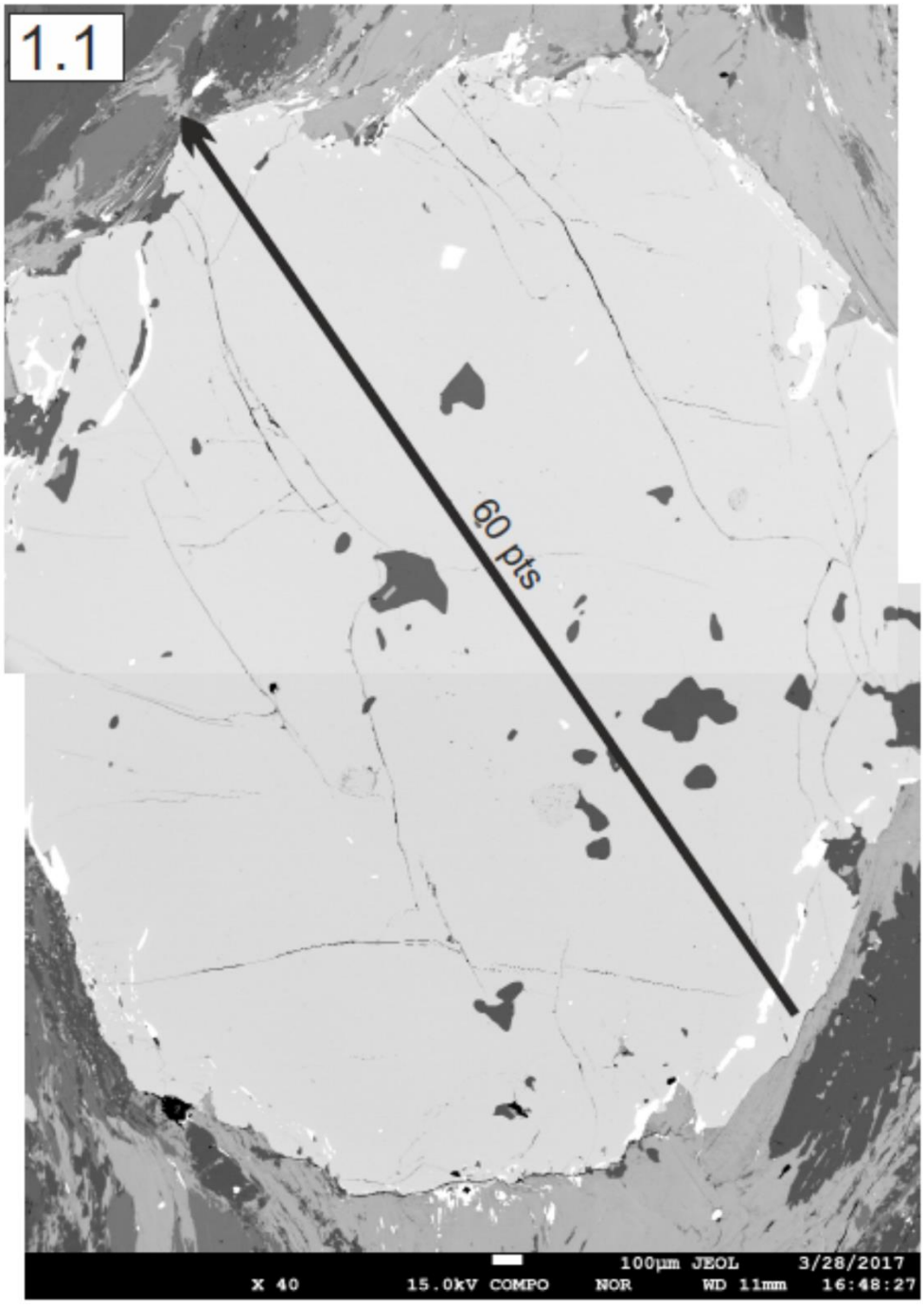

Figure 52 – BSE (Backscattered Electron) image of Garnet from sample 1.1 used for a compositional profile, which is indicated by the black arrow.

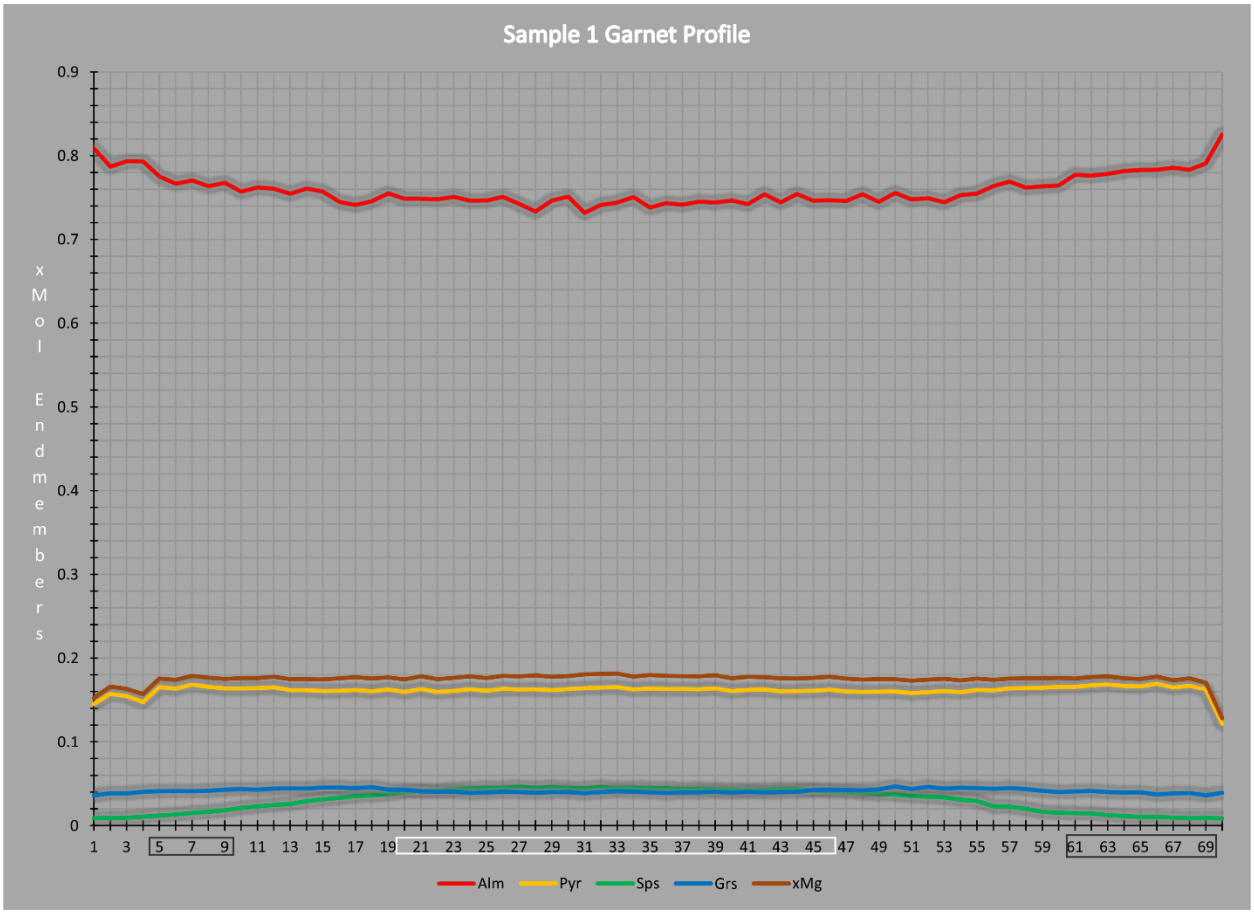

Figure 53 - Graph of compositional Garnet end members along the profile indicated in Figure 52. White and black boxes indicate data used for calculations of core and rim compositions, respectively.

Sample 1.1, representing the Garnet Mica Gneiss of the Nordmannvik Nappe, was modelled to estimate the metamorphic conditions at which the observed assemblage was stable. This section was calculated with an elevated water content (2%) to correspond to near-saturation of the system. The amount of CaO was also adjusted to account for the amount stored in Apatite. From Figure 54 and Figure 55, this section indicates stable conditions of 625-675°C and 8.5-10 kB. These P-T estimates are consistent in both the core and rim/matrix mineral calculations. The stable assemblage predicted includes Bt+Ms+Pl+Grt+Ky+Rt+H2O +/- Pa (Paragonite). The amount of H_2O in these fields is close to the LOI value for this sample. Rutile was not observed in thin section, but the amount predicted in these areas is negligible. Stability fields including melt are nearby, as are fields with Staurolite.

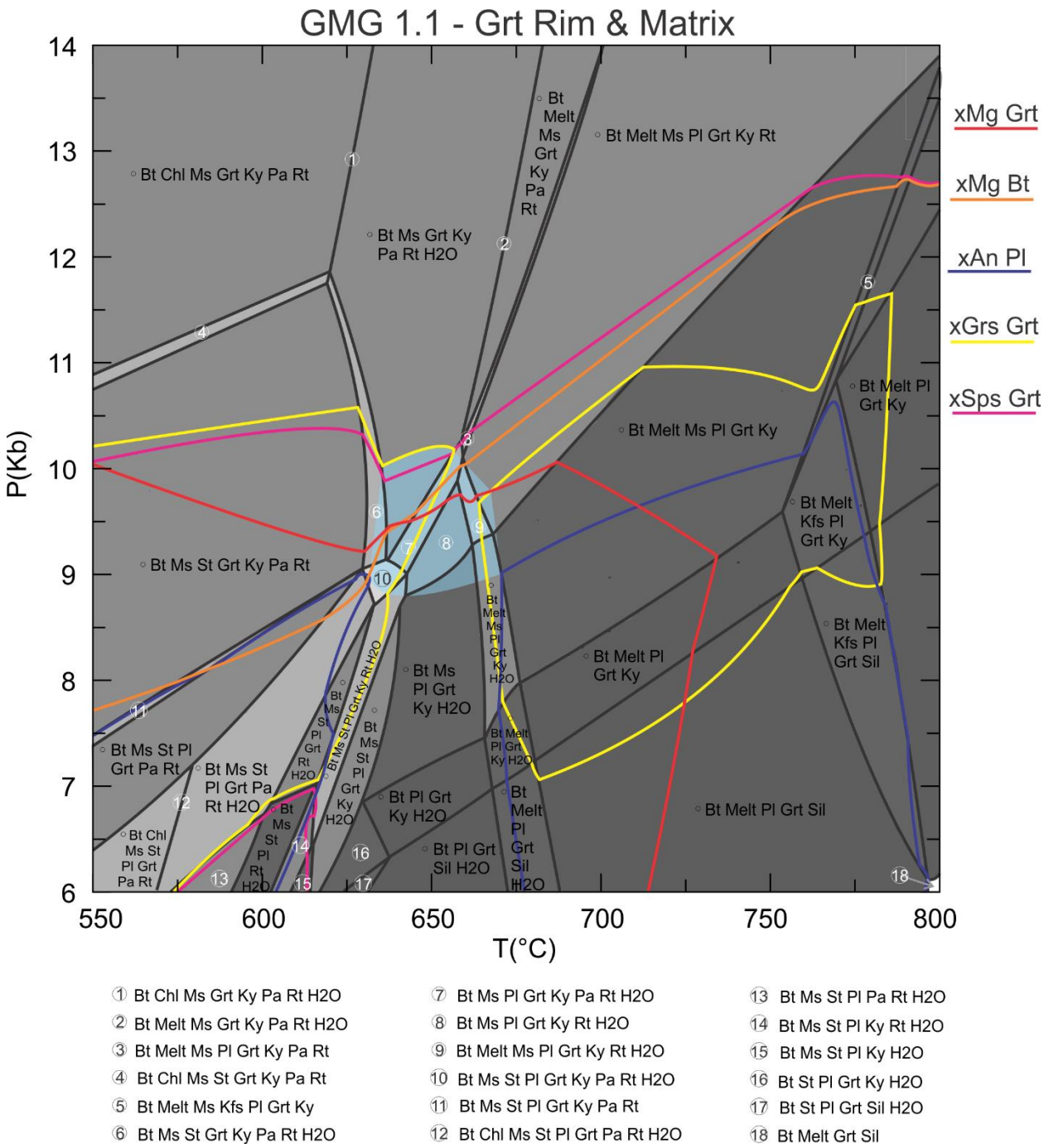

Figure 54 - P-T pseudosection for Garnet Mica Gneiss, with compositional isopleths for the Garnet rim and matrix minerals. Blue highlighted area indicates stable metamorphic conditions indicated from this sample.

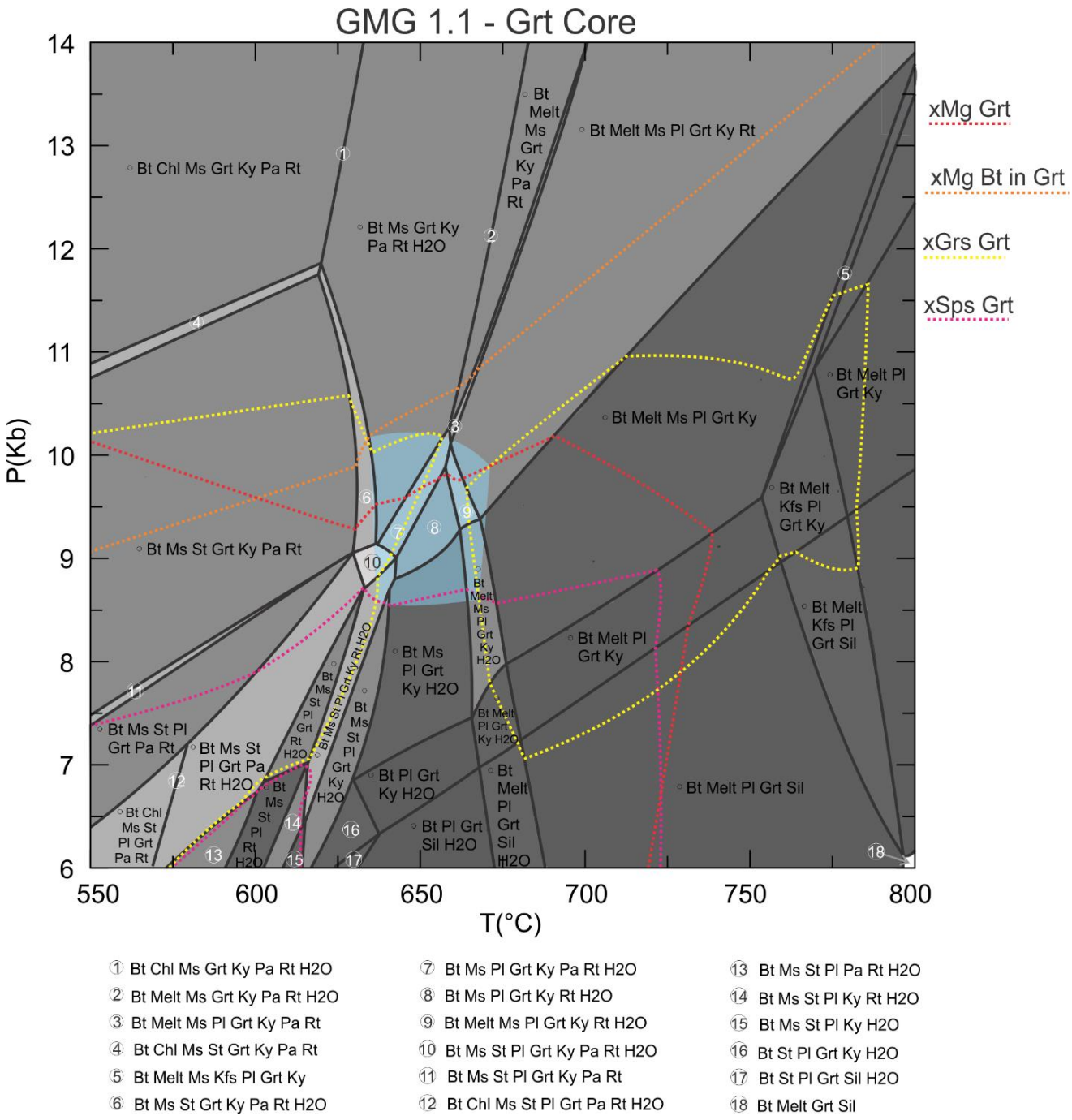

Figure 55 - P-T pseudosection for Garnet Mica Gneiss, with compositional isopleths corresponding to the Garnet core. Blue highlighted area indicates stable metamorphic conditions.

3.2.2.2 Garnet Mica Schist

3.1	Grt Core	Grt Rim	Pl	Bt	Ms	Ep
Wt.%						
SiO_2	37.50	37.95	63.25	37.28	46.96	39.80
TiO_2	0.12	0.05	0.004	1.61	0.46	0.04
Al_2O_3	20.76	21.09	23.40	17.54	34.89	32.37
Cr_2O_3	0.01	0.01	0.005	0.02	0.005	0.002
MgO	1.17	2.02	0.004	12.06	0.95	0.06
CaO	7.35	8.40	4.61	0.00	0.00	24.39
MnO	8.71	6.83	0.01	0.01	0.002	0.20
FeO	24.34	23.94	0.01	16.59	1.09	1.54
Na_2O	0.00	0.00	8.81	0.17	1.80	0.01
K_2O	0.00	0.00	0.06	8.98	8.53	0.002
F	0.00	0.00	0.00	0.05	0.00	0.00
Cl	0.00	0.00	0.004	0.01	0.01	0.01
Total	99.96	100.29	100.18	94.33	94.71	98.41
Oxygens	12	12	8	11	11	12
Normalized Cations						
Si	3.02	3.02	2.80	2.90	3.13	2.69
Ti	0.01	0.003	0.0001	0.09	0.02	0.002
Al	1.97	1.98	1.22	1.61	2.74	2.57
Cr	0.001	0.001	0.0002	0.001	0.0003	0.0001
Fe^{3+}	0.00	0.001	0.00	0.00	0.00	0.09
Mg	0.14	0.24	0.00	1.40	0.09	0.01
Ca	0.63	0.72	0.22	0.00	0.00	1.76
Mn	0.59	0.46	0.0002	0.001	0.0001	0.01
Fe^{2+}	1.64	1.59	0.001	1.08	0.06	0.00
Na	0.00	0.00	0.76	0.03	0.23	0.001
K	0.00	0.00	0.004	0.89	0.72	0.0002
H	0.00	0.00	0.00	0.00	0.00	0.87
F	0.00	0.00	0.00	0.01	0.00	0.00
Cl	0.00	0.00	0.0003	0.002	0.001	0.001
Total	8	8	5	8	7	8
X_{Mg}	0.08	0.13	-	0.56	0.61	0.06
X_{Fe}	-	-	-	-	-	0.03
Alm	0.54	0.53	-	-	-	-
Pyr	0.05	0.08	-	-	-	-
Sps	0.20	0.15	-	-	-	-
Grs	0.21	0.24	-	-	-	-
Ab	-	-	0.77	-	-	-
An	-	-	0.22	-	-	-
Or	-	-	0.004	-	-	-

Table 9 - Table of geochemical data from thin section 3.1. H: Hydrogen. Highlighted values were used during petrological modelling.

The Garnet analyzed in sample 3.1 shows some very interesting characteristics. Similar to the Garnets analyzed in samples 7 and 14e, the grain is sub- to anhedral, intensely poikilitic, and strongly sheared and/or deformed. In Figure 57 below, a compositional core can be seen by the trends of decreasing Pyrope and increasing Spessartine. The edges of this Garnet also show a distinct zonation by each endmember. An interesting note is the appearance of prograde zoning, indicated by the distinct enrichment of Spessartine and depletion of X_{Mg} in the core, and the opposite trends towards the rim.

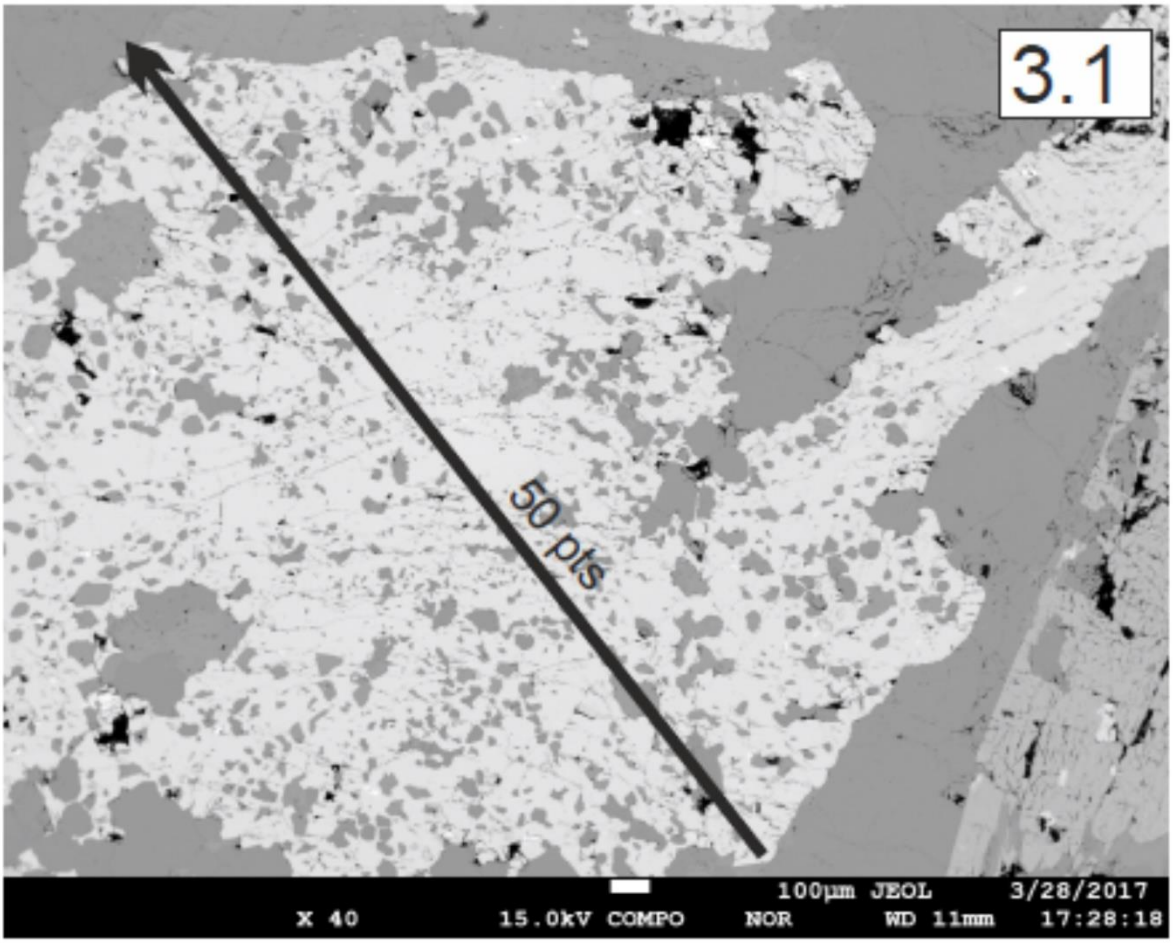

Figure 56 - BSE image of Garnet in thin section 3.1 used for a compositional profile, which is indicated by the black arrow.

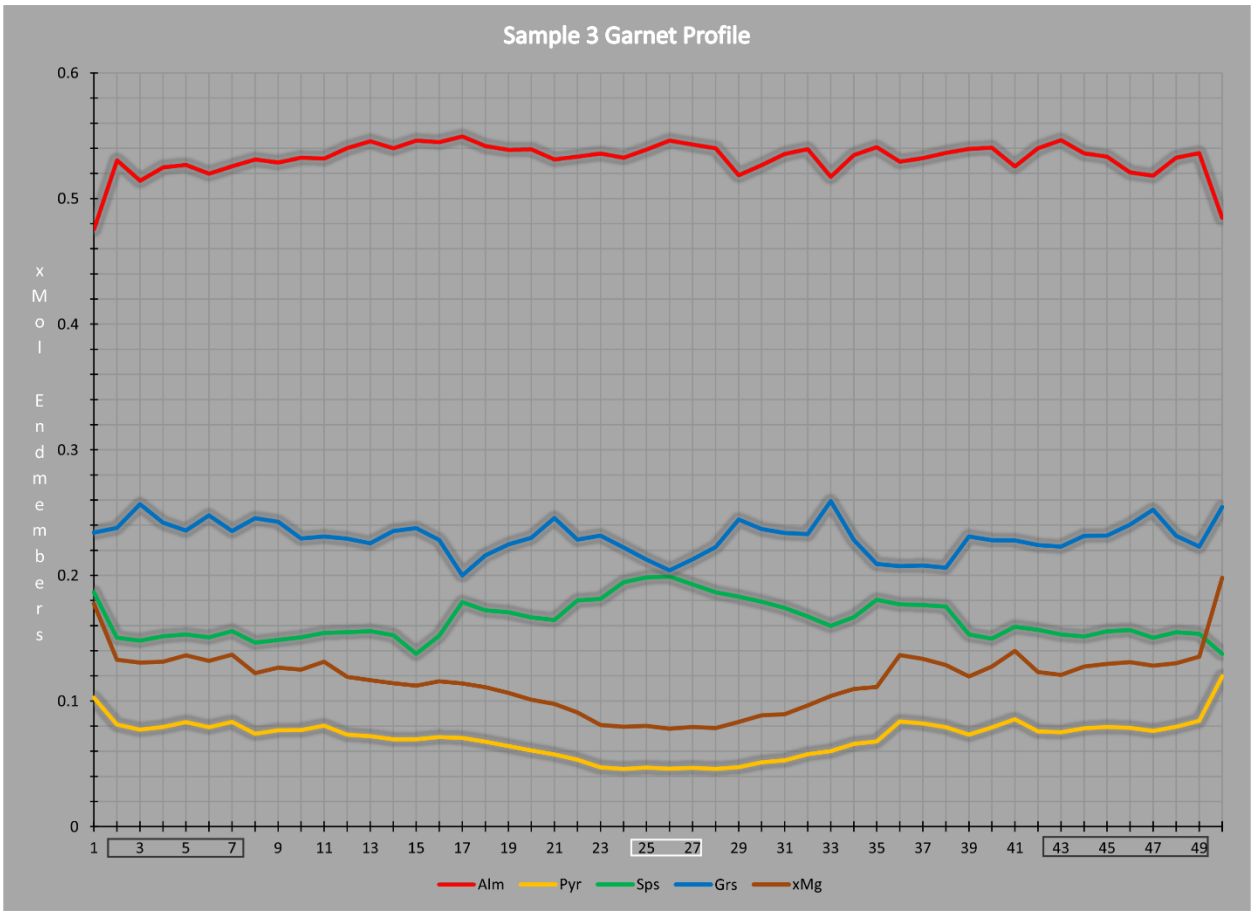

Figure 57 - Graph of Garnet end members along the profile in Figure 56. White and black boxes indicate data used for calculations of core and rim compositions, respectively.

A P-T pseudosection was calculated for the Garnet Mica Schist, represented by sample 3.1. This section was calculated with SiO_2 and H_2O in excess. Compositional isopleths for X_{Mg} of the Garnet rim and Biotite, Grossular in the Garnet rim, and X_{An} (Molar percentage of Anorthosite, An/[Ab+An+Or]) of the Plagioclase agree well and indicate a stable assemblage at P-T conditions of approximately 580-620°C and 10-11 kB (Figure 58). A large discrepancy occurs in the predicted content of Spessartine in the Garnet rim, however, and cannot be explained. The predicted assemblage includes Quartz, Biotite, Muscovite, Plagioclase, Garnet, Paragonite, and Rutile. Zoisite, Chlorite, and Ilmenite were also observed in thin section, but are not included in the calculated peak metamorphic assemblage. From the compositions of X_{Mg}, Grossular, and Spessartine in the Garnet core, there is a field of overlap at conditions of about 515-530°C and 6.25-7.5 kB (Figure 59). These assemblages include these phases and could possibly represent the onset of Garnet crystallization during an earlier metamorphic stage. As the compositional isopleths for the Garnet core are steep, the metamorphic pressure conditions here are more difficult to constrain.

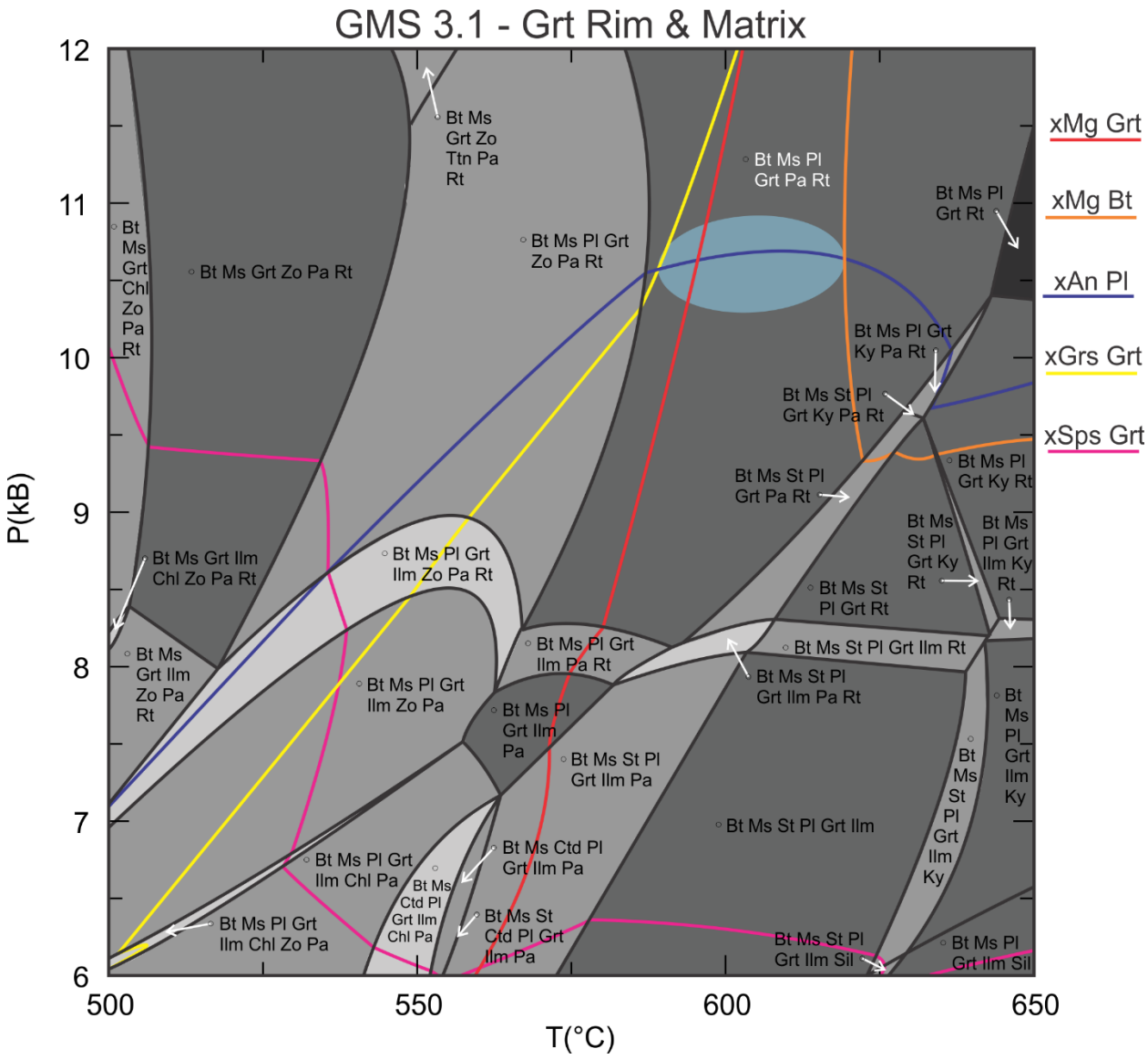

Figure 58 - P-T pseudosection for sample 3.1, with compositional isopleths for the Garnet rim and matrix minerals. The peak metamorphic assemblage is labelled in white. Highlighted blue area indicates stable metamorphic conditions. Ctd: Chloritoid.

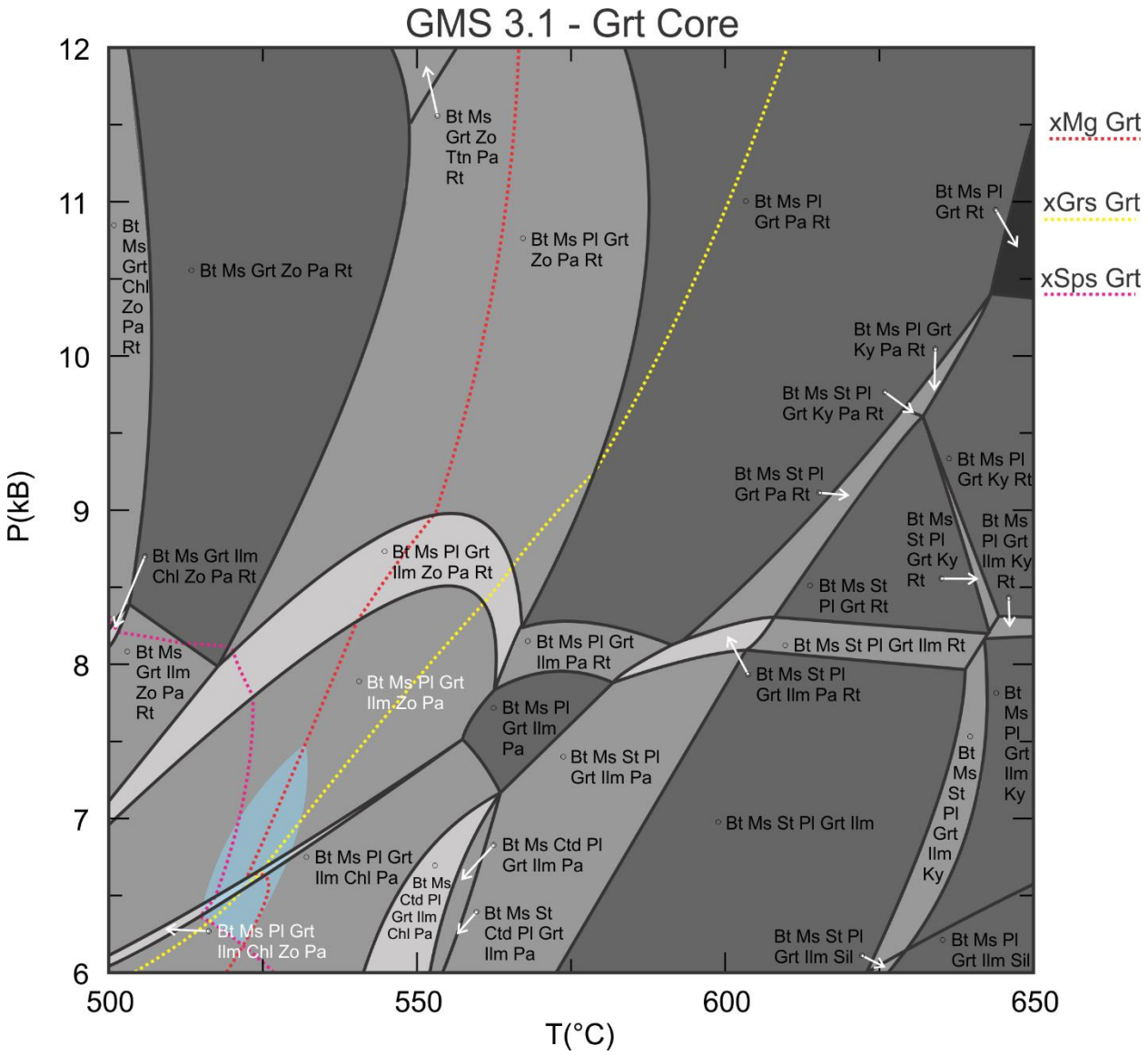

Figure 59 - P-T pseudosection for sample 3.1, showing compositional isopleths for the Garnet cores. Possible early metamorphic assemblages labelled in white. Highlighted blue area indicates stable metamorphic conditions.

3.2.2.3 Chlorite Schist

7	Grt Core	Grt Rim	Pl	Ep	Chl
Wt.%					
SiO_2	36.96	37.08	68.28	37.55	23.97
TiO_2	0.10	0.09	0.01	0.07	0.06
Al_2O_3	20.47	20.64	18.89	23.11	19.67
Cr_2O_3	0.004	0.003	0.001	0.00	0.003
MgO	0.94	0.97	0.01	0.03	9.01
CaO	3.99	4.85	0.18	21.70	0.01
MnO	5.44	4.29	0.01	0.49	0.33
FeO	31.66	32.12	0.10	11.64	32.84
Na_2O	0.00	0.00	11.23	0.02	0.01
K_2O	0.00	0.00	0.06	0.004	0.01
Total	99.55	100.04	98.76	94.61	85.91
Oxygens	12	12	8	12	14
Normalized Cations					
Si	3.02	3.01	3.03	2.70	2.71
Ti	0.01	0.01	0.0003	0.004	0.005
Al	1.97	1.97	0.99	1.96	2.62
Cr	0.0003	0.0002	0.00004	0.00	0.0002
Fe^{3+}	0.002	0.01	0.00	0.70	0.00
Mg	0.11	0.12	0.0004	0.003	1.52
Ca	0.35	0.42	0.01	1.67	0.001
Mn	0.38	0.29	0.0002	0.03	0.03
Fe^{2+}	2.16	2.17	0.004	0.00	3.11
Na	0.00	0.00	0.97	0.003	0.003
K	0.00	0.00	0.003	0.0004	0.001
H	0.00	0.00	0.00	0.93	0.00
Total	8	8	5	8	10
X_{Mg}	0.05	0.05	-	0.005	0.33
X_{Fe}	-	-	-	0.26	-
Alm	0.72	0.72	-	-	-
Pyr	0.04	0.04	-	-	-
Sps	0.12	0.10	-	-	-
Grs	0.12	0.14	-	-	-
Ab	-	-	0.99	-	-
An	-	-	0.01	-	-
Or	-	-	0.003	-	-

Table 10 - Table of geochemical data from thin section 7. Highlighted values were used during petrological modelling.

The Garnets in sample 7 are strongly sheared, and most often are not intact grains, much like the one analyzed in Figure 60 below. Because of this, three separate profiles were used to represent the composition of this grain and were combined in Figure 61. The data point 45 appears to be an error, and its values were omitted from calculations. Pyrope appears to be compositionally level throughout the profile, while Spessartine shows the largest compositional changes. No distinct compositional zoning appears, however.

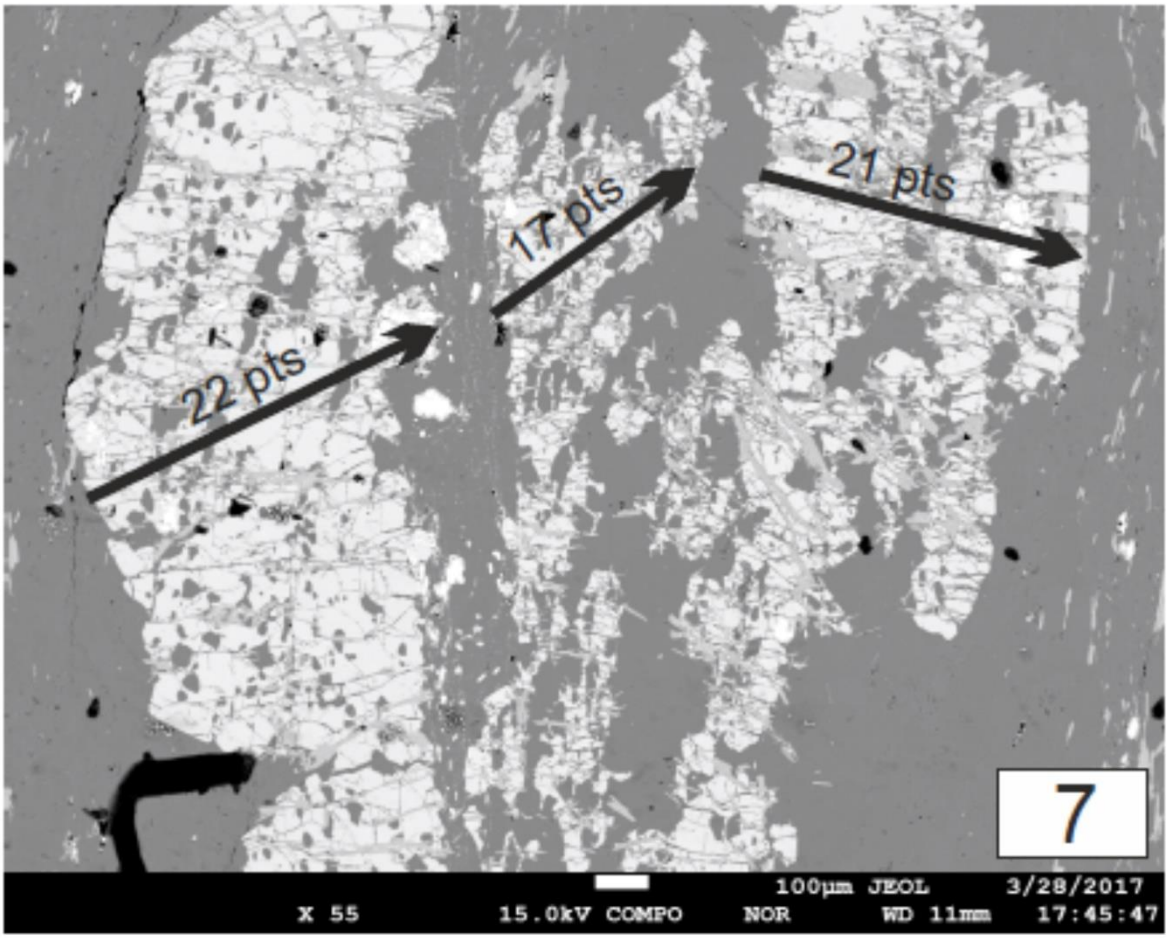

Figure 60 - BSE image of Garnet in thin section 7 used for compositional profiling. Black arrows indicate profile.

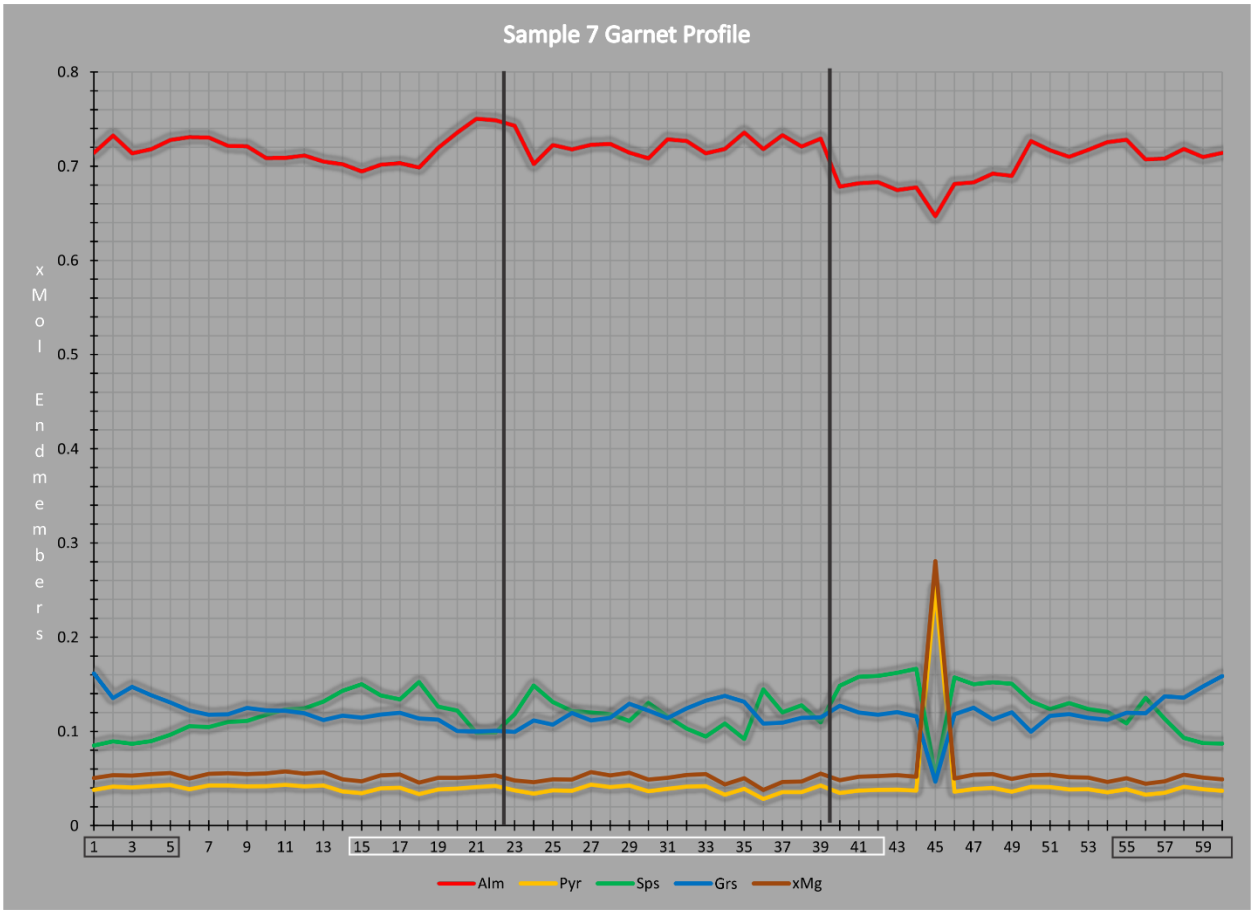

Figure 61 - Graph of Garnet compositional end members in thin section 7 along the profile shown in Figure 60. White and black boxes indicate data used for calculations of core and rim compositions, respectively. Vertical black lines depict connections between profiles.

A P-T pseudosection was created for sample 7, representing the Chlorite Schist. This section was calculated with SiO_2 and H_2O in excess, and with whole-rock compositional data from the XRF analysis run in Tromsø. X_{Mg} of the Chlorite was utilized as the only matrix mineral, as Biotite was not observed, and the Plagioclase occurs as nearly pure Albite. Figure 62 and Figure 63 show good agreement between the cores and rims of the Garnet, with stable metamorphic conditions of roughly 540-550°C and 7-8.25 kB. The predicted assemblage includes Bt-Chl-Pl-Grt-Ab-Ilm, and closely matches that seen in thin section. The amount of Biotite predicted in this assemblage is negligible. These estimated conditions are somewhat dubious, as typical Greenschist facies occurs at lower temperatures and pressures.

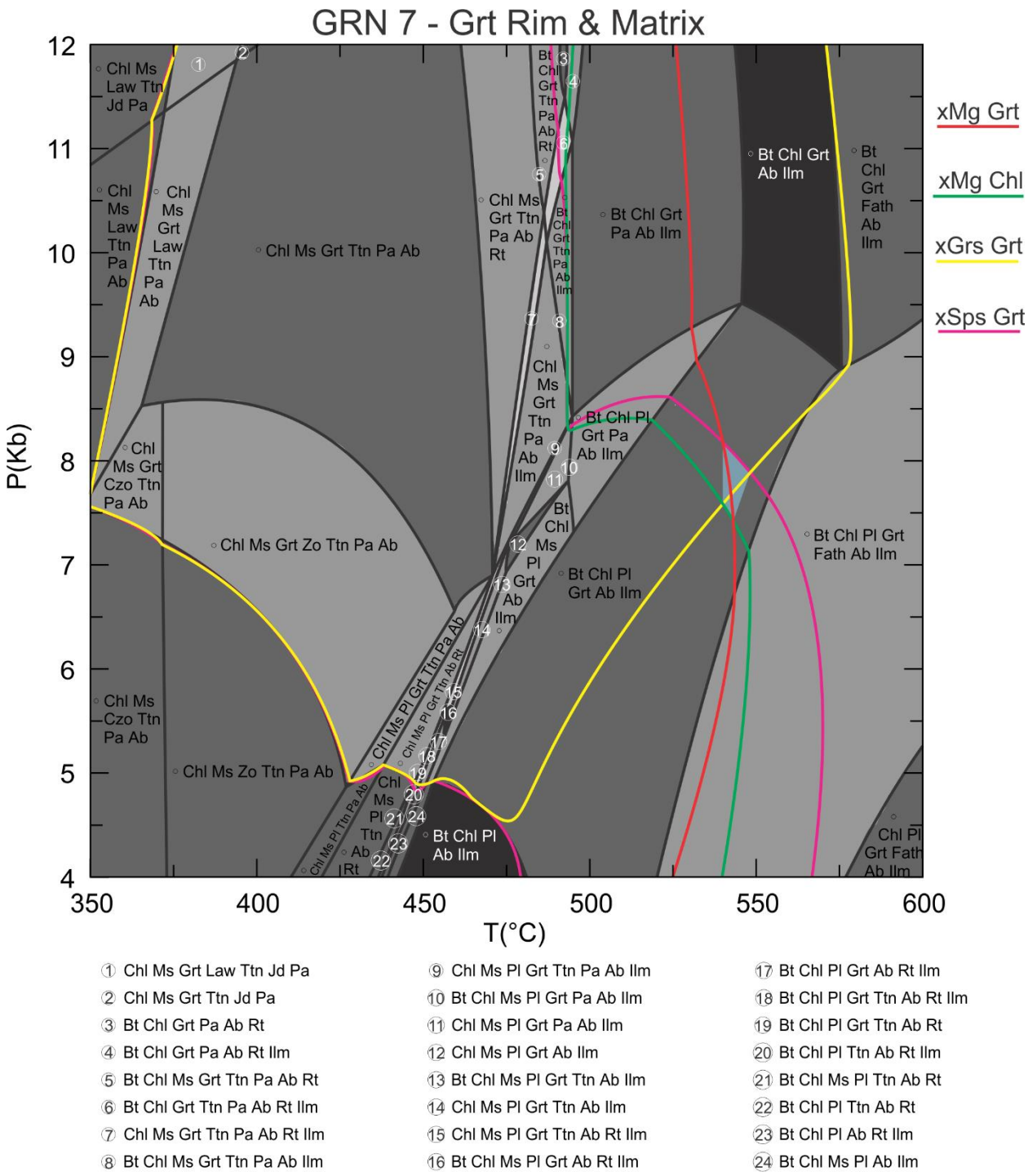

① Chl Ms Grt Law Ttn Jd Pa
② Chl Ms Grt Ttn Jd Pa
③ Bt Chl Grt Pa Ab Rt
④ Bt Chl Grt Pa Ab Rt Ilm
⑤ Bt Chl Ms Grt Ttn Pa Ab Rt
⑥ Bt Chl Grt Ttn Pa Ab Rt Ilm
⑦ Chl Ms Grt Ttn Pa Ab Rt Ilm
⑧ Bt Chl Ms Grt Ttn Pa Ab Ilm
⑨ Chl Ms Pl Grt Ttn Pa Ab Ilm
⑩ Bt Chl Ms Pl Grt Pa Ab Ilm
⑪ Chl Ms Pl Grt Pa Ab Ilm
⑫ Chl Ms Pl Grt Ab Ilm
⑬ Bt Chl Ms Pl Grt Ttn Ab Ilm
⑭ Chl Ms Pl Grt Ttn Ab Ilm
⑮ Chl Ms Pl Grt Ttn Ab Rt Ilm
⑯ Bt Chl Ms Pl Grt Ab Rt Ilm
⑰ Bt Chl Pl Grt Ab Rt Ilm
⑱ Bt Chl Pl Grt Ttn Ab Rt Ilm
⑲ Bt Chl Pl Grt Ttn Ab Rt
⑳ Bt Chl Pl Ttn Ab Rt Ilm
㉑ Bt Chl Ms Pl Ttn Ab Rt
㉒ Bt Chl Pl Ttn Ab Rt
㉓ Bt Chl Pl Ab Rt Ilm
㉔ Bt Chl Ms Pl Ab Ilm

Figure 62 - P-T pseudosection for Chlorite Schist, with compositional isopleths for the Garnet rim and matrix minerals. Blue highlighted field indicates stable metamorphic conditions. Jd: Jadeite; Law: Lawsonite; Fath: Fe-Anthophyllite.

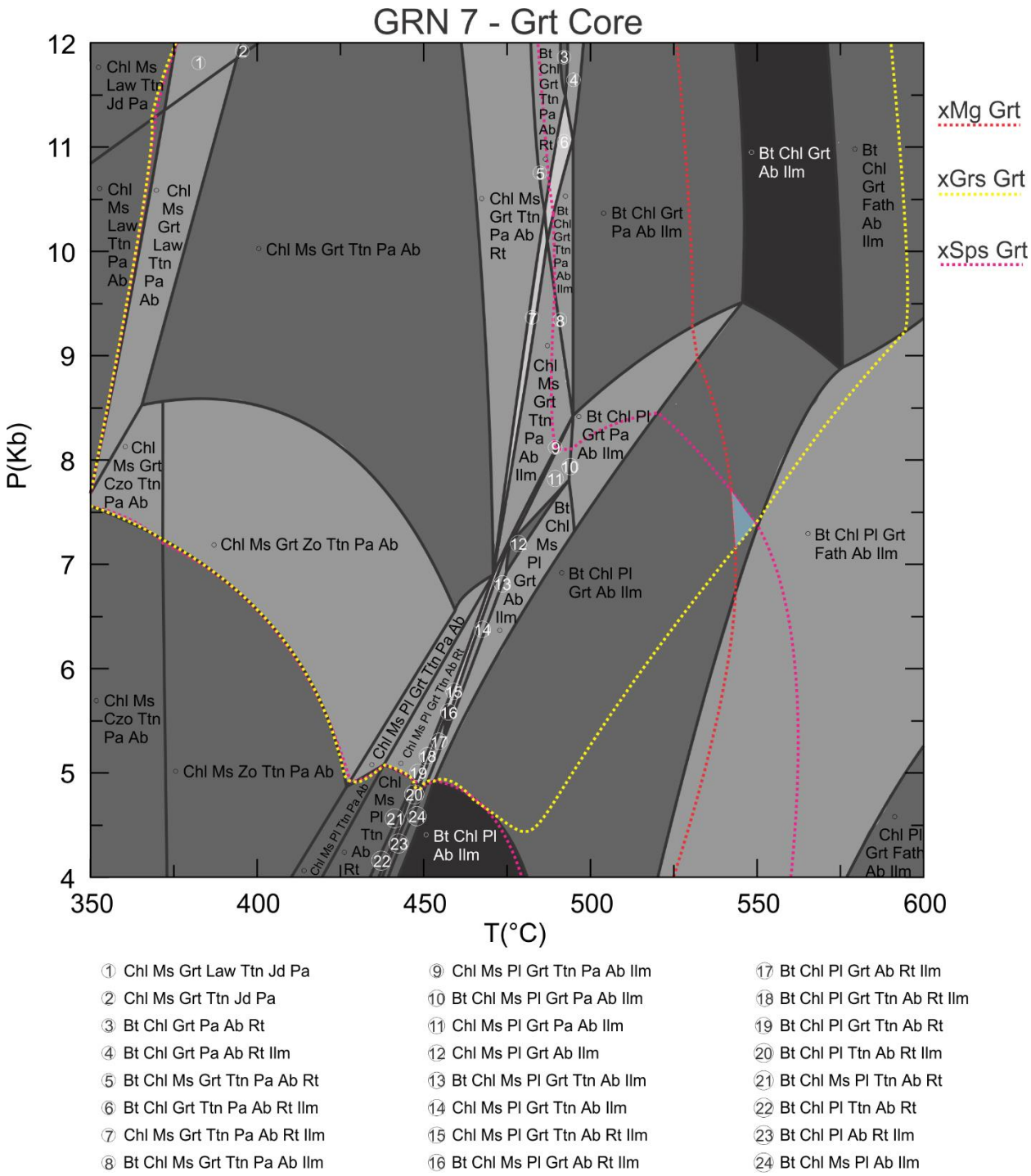

Figure 63 - P-T pseudosection for Chlorite Schist, with compositional isopleths for the Garnet cores. Blue highlighted field indicates stable metamorphic conditions.

3.2.2.4 Amphibolite Schist

14e	Grt Core	Grt Rim	Pl	Bt	Ms	Ep	Ep in Grt
Wt.%							
SiO_2	37.61	37.43	62.15	37.20	46.94	39.16	39.13
TiO_2	0.14	0.06	0.001	1.49	0.39	0.14	0.13
Al_2O_3	20.87	20.82	24.06	17.89	33.97	29.43	29.30
Cr_2O_3	0.01	0.02	0.01	0.02	0.01	0.02	0.02
MgO	1.77	2.22	0.01	11.57	1.16	0.05	0.06
CaO	7.23	6.95	5.42	0.00	0.00	23.73	23.66
MnO	3.86	1.46	0.01	0.03	0.01	0.12	0.12
FeO	28.70	30.44	0.04	17.25	1.52	5.12	5.40
Na_2O	0.00	0.00	8.34	0.21	1.21	0.01	0.18
K_2O	0.00	0.00	0.06	8.74	9.37	0.03	0.03
F	0.00	0.00	0.00	0.003	0.00	0.00	0.00
Cl	0.00	0.00	0.002	0.003	0.001	0.01	0.01
Total	100.20	99.41	100.08	94.39	94.57	97.83	98.04
Oxygens	12	12	8	11	11	12	12
Normalized Cations							
Si	3.01	3.01	2.76	2.90	3.14	2.68	2.67
Ti	0.01	0.004	0.00002	0.09	0.02	0.01	0.01
Al	1.97	1.97	1.26	1.64	2.68	2.38	2.36
Cr	0.001	0.001	0.0002	0.001	0.0003	0.001	0.001
Fe^{3+}	0.004	0.004	0.00	0.00	0.00	0.29	0.31
Mg	0.21	0.27	0.0004	1.34	0.12	0.01	0.01
Ca	0.62	0.60	0.26	0.00	0.00	1.74	1.73
Mn	0.26	0.10	0.0003	0.002	0.0004	0.01	0.01
Fe^{2+}	1.92	2.04	0.001	1.12	0.08	0.00	0.00
Na	0.00	0.00	0.72	0.03	0.16	0.001	0.02
K	0.00	0.00	0.003	0.87	0.80	0.003	0.003
H	0.00	0.00	0.00	0.00	0.00	0.88	0.88
F	0.00	0.00	0.00	0.001	0.00	0.00	0.00
Cl	0.00	0.00	0.0002	0.0004	0.0001	0.001	0.001
Total	8	8	5	8	7	8	8
X_{Mg}	0.10	0.12	-	0.54	0.58	0.02	0.02
X_{Fe}	-	-	-	-	-	0.11	0.12
Alm	0.63	0.68	-	-	-	-	-
Pyr	0.07	0.09	-	-	-	-	-
Sps	0.09	0.03	-	-	-	-	-
Grs	0.20	0.20	-	-	-	-	-
Ab	-	-	0.73	-	-	-	-
An	-	-	0.26	-	-	-	-
Or	-	-	0.004	-	-	-	-

Table 11 - Table of geochemical data from thin section 14e. Highlighted values were used during petrological modelling.

The most recognizable feature of the Garnet sampled in thin section 14e is its shape. It appears to have undergone an intense rotational deformation, as can be seen in Figure 64. Compositionally, end members Almandine, Pyrope, and Spessartine indicate a clear zoning pattern (Figure 65). Most notable is the relationship between the composition of Spessartine in relation to Pyrope and Almandine. Like the Garnet profile in sample 3.1, this sample shows slight prograde characteristics, with enriched Spessartine in the core, and a slight increase of Mg at the rims.

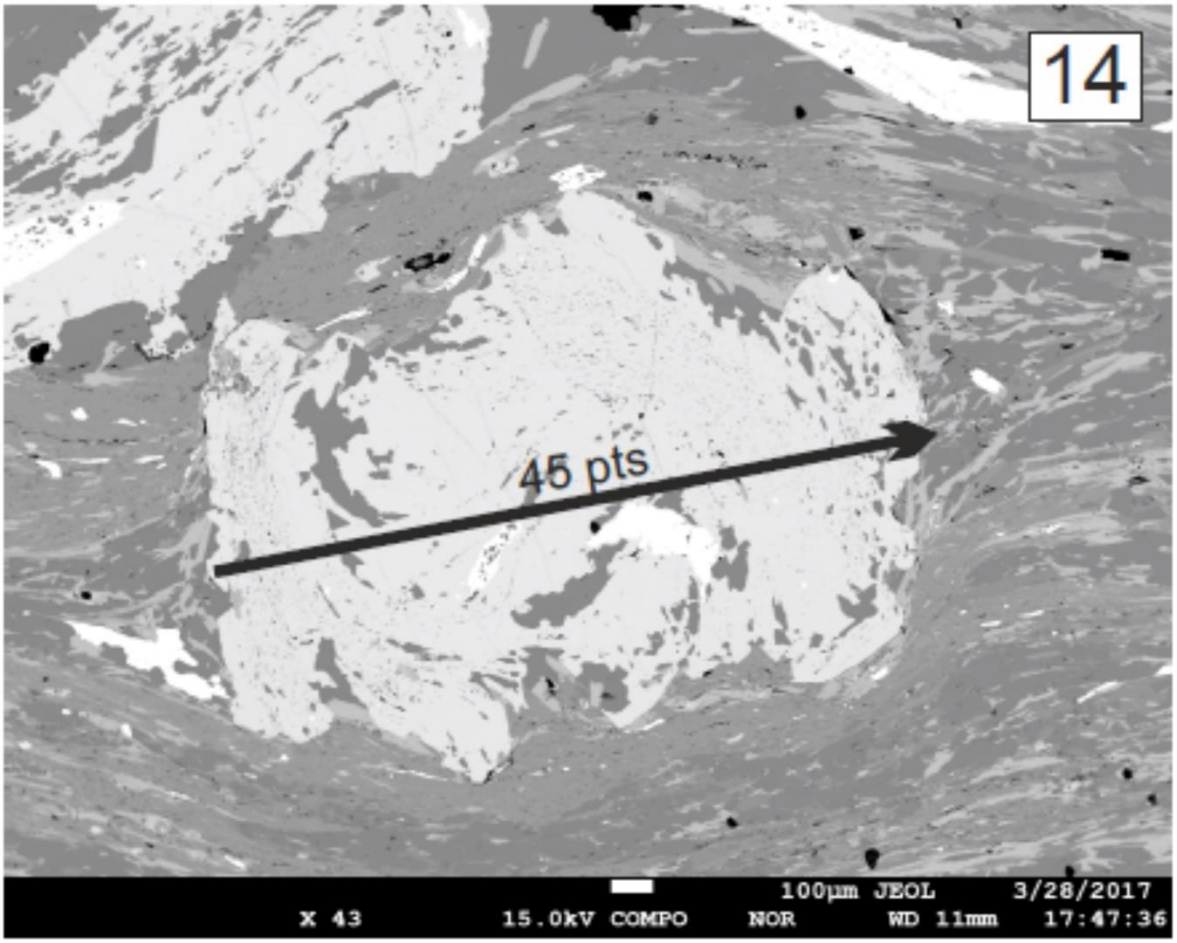

Figure 64 - BSE image of Garnet analyzed in thin section 14e. Black arrow indicates profile.

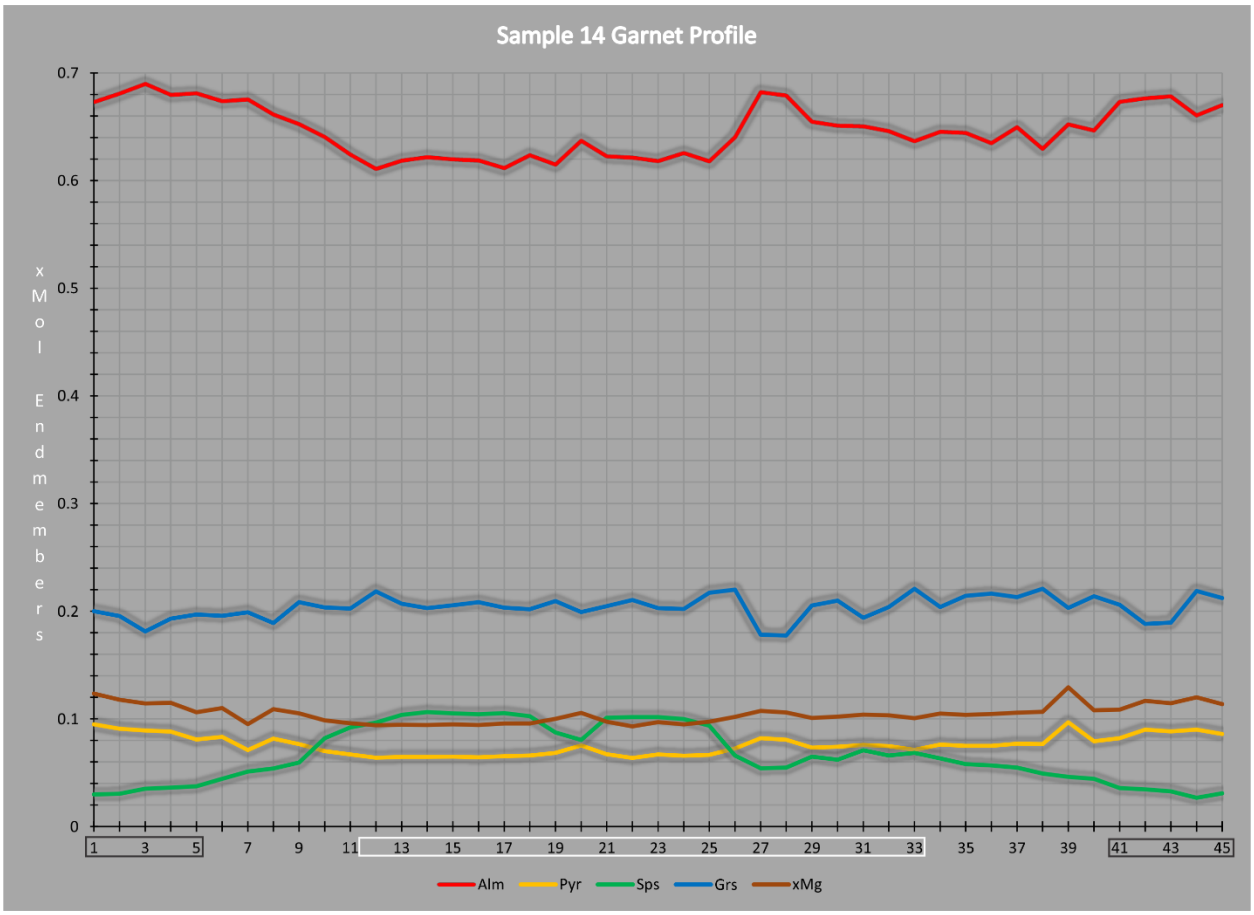

Figure 65 - Graph of compositional end members of Garnet along the profile in thin section 14e. White and black boxes indicate data used for calculations of core and rim compositions, respectively.

A P-T pseudosection was calculated for the Amphibolite Schist of sample 14e, with SiO_2 and H_2O in excess. The compositional isopleths for the Garnet rim and matrix minerals show a good agreement, and indicate a stable assemblage at 575-600°C and 8.5-10.5 kB (Figure 66). This assemblage includes Quartz, Biotite, Muscovite, Plagioclase, Garnet, Zoisite, Paragonite, and Rutile. Two discrepancies arise from this predicted assemblage: an amphibole phase is missing; Rutile is stabilized instead of the Ilmenite observed in thin section, creating a discrepancy in the Titanium-bearing phase. The small field directly above this assemblage (labelled 2) includes the Amphibolite phase, and still contains good agreement from the isopleths. Because the Fe^{3+}/Fe^{2+} ratio of the sample is unknown, the section was calculated with FeO only. However, when a small amount of Fe_2O_3 is added to the system, Ilmenite stabilizes instead of Rutile. Therefore, and due to a lack of other Fe^{3+}-bearing phases, it is assumed that the Fe^{3+}/Fe^{2+} ratio in this sample is very low. Important to note is that when some Fe_2O_3 is added, a slight divergence of the compositional isopleths occurs, most notably in the X_{Mg} of the Garnet. From the compositions within the Garnet core, we see a convergence of the isopleths at around 540-550°C and 8-8.5 kB (Figure 67). This predicted assemblage includes Chlorite, indicating that the Chlorite seen in the thin section could be a relic phase from this earlier metamorphic event.

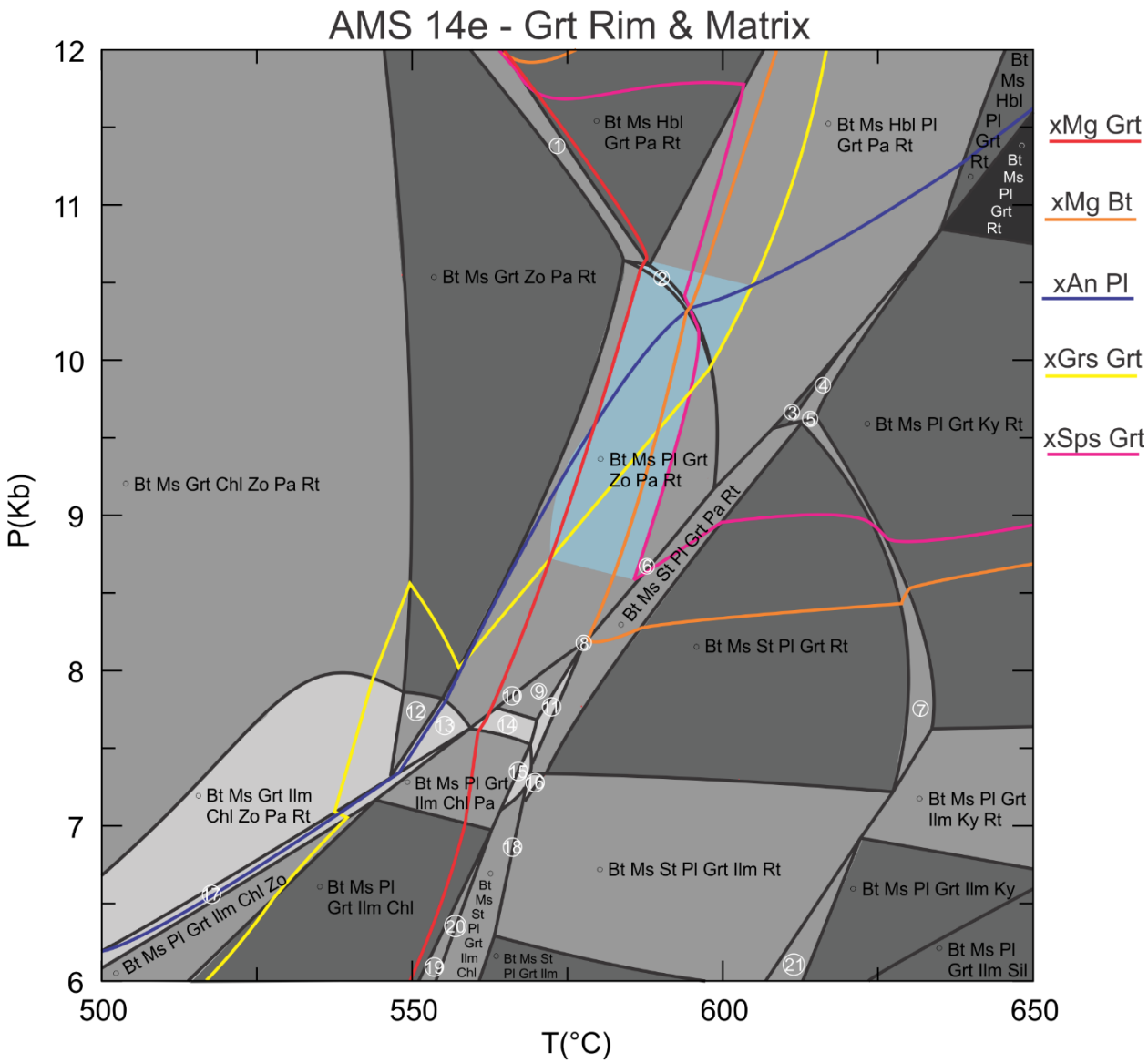

① Bt Ms Hbl Grt Zo Pa Rt
② Bt Ms Hbl Pl Grt Zo Pa Rt
③ Bt Ms Pl Grt Pa Rt
④ Bt Ms Pl Grt Ky Pa Rt
⑤ Bt Ms St Pl Grt Ky Pa Rt
⑥ Bt Ms St Pl Grt Zo Pa Rt
⑦ Bt Ms St Pl Grt Ky Rt
⑧ Bt Ms Pl Grt Pa Ma Rt
Bt Ms St Pl Grt Pa Ma Rt
Bt Ms Pl Grt Chl Pa Ma Rt
⑨ Bt Ms Pl Grt Chl Pa Rt
⑩ Bt Ms Pl Grt Chl Zo Pa Rt
⑪ Bt Ms St Pl Grt Chl Pa Rt
⑫ Bt Ms Grt Ilm Zo Pa Rt
⑬ Bt Ms Pl Grt Ilm Zo Pa Rt
⑭ Bt Ms Pl Grt Ilm Chl Pa Rt
⑮ Bt Ms St Pl Grt Ilm Chl Pa
⑯ Bt Ms St Pl Grt Ilm Pa Rt
⑰ Bt Ms Pl Grt Ilm Chl Zo Pa
⑱ Bt Ms St Pl Grt Ilm Chl Rt
⑲ Bt Ms Ctd Pl Grt Ilm Chl
⑳ Bt Ms St Ctd Pl Grt Ilm Chl
㉑ Bt Ms St Pl Grt Ilm Ky

Figure 66 - P-T pseudosection for Amphibolite Schist, with compositional isopleths for the Garnet rim and matrix minerals. Blue highlighted field indicates stable metamorphic conditions. Ma: Margarite.

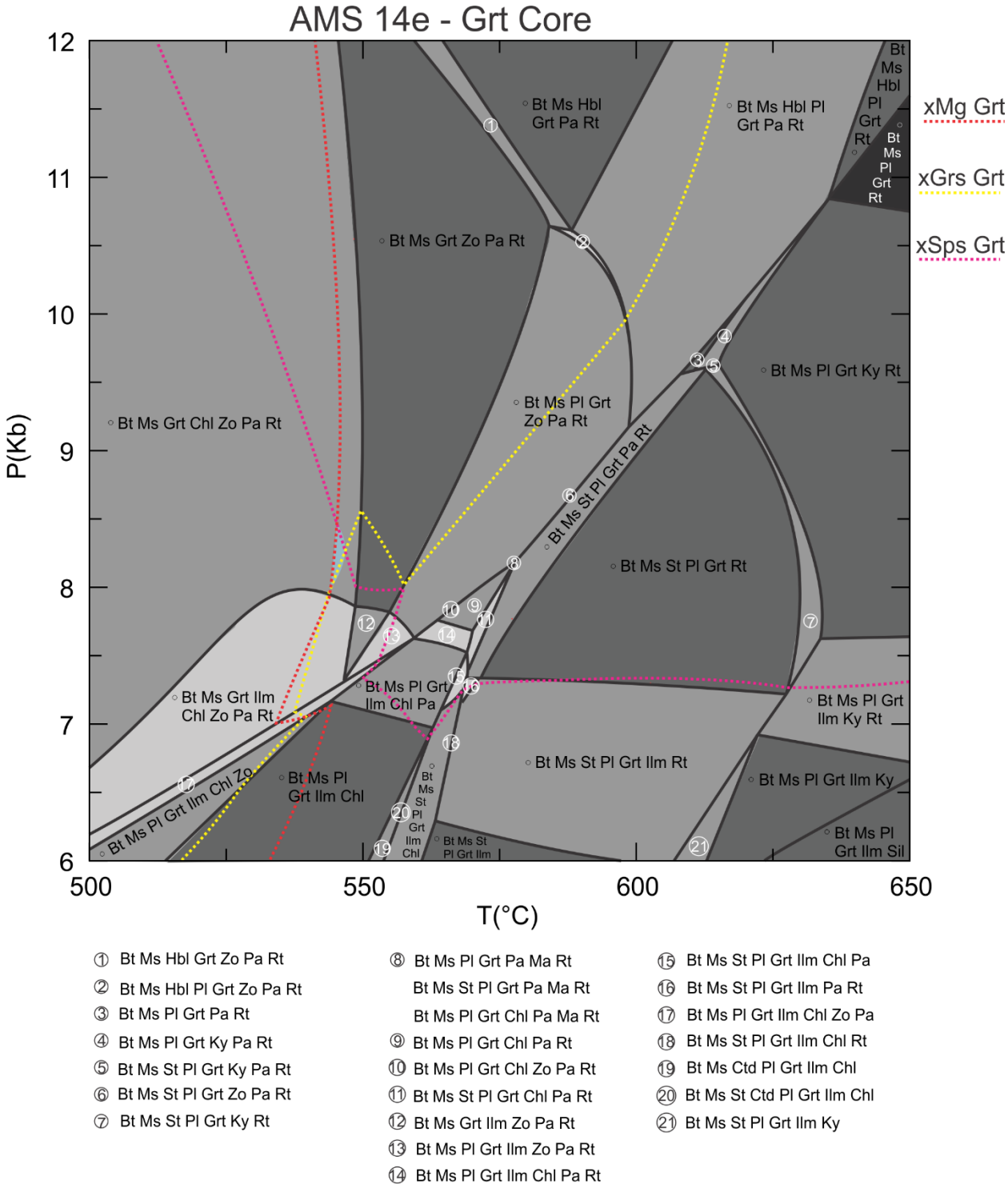

Figure 67 - P-T pseudosection for Amphibolite Schist, with compositional isopleths for the Garnet core. Blue highlighted field indicates stable metamorphic conditions.

3.2.3 Deformation Microstructures

3.2.3.1 Microscopic Shear-Sense Indicators

Many shear sense indicators were observed in the prepared thin sections, and are documented in Table 12 below. In addition to shear bands and sigma clasts (also observed macroscopically in the field), mica fish and S-C' fabrics were also documented. Mica fish are elongate grains of micas, usually Muscovite or Biotite, with their long axis at an angle to the mylonitic foliation (Passchier & Trouw, 2005). S-C and S-C' fabrics are shear band cleavages which develops shear bands that create an overall fabric of S (schistosite, or foliation) and C or C' (cisaillement, or shear) planes.

	Rock	Shear Band	Sigma Clast	Mica Fish	S-C' Fabric	Sense	Hanging Wall Movement
1.1-1	GMG		X	X		Sinistral	WNW; 300
1.1-2	GMG	X		X		Sinistral	WNW; 300
2.1-1	GMG	X				Dextral	WNW; 290
2.1-2	GMG				X	Dextral	WNW; 290
3	GMS		X	X		Dextral	NW; 312
4	FYL	X		X		Sinistral	ESE; 119
6	FYL		X			Sinistral	WNW; 294
7-1	GRN		X			Sinistral	SW; 219
7-2	GRN		X			Sinistral	SW; 219
7-3	GRN		X			Sinistral	SW; 219
14e-1	AMS		X			Dextral	NW; 322
14e-2	AMS			X	X	Dextral	NW; 322

Table 12 - Table listing shear-sense indicators observed in thin section. Bolded and italicized units are illustrated in the figures below.

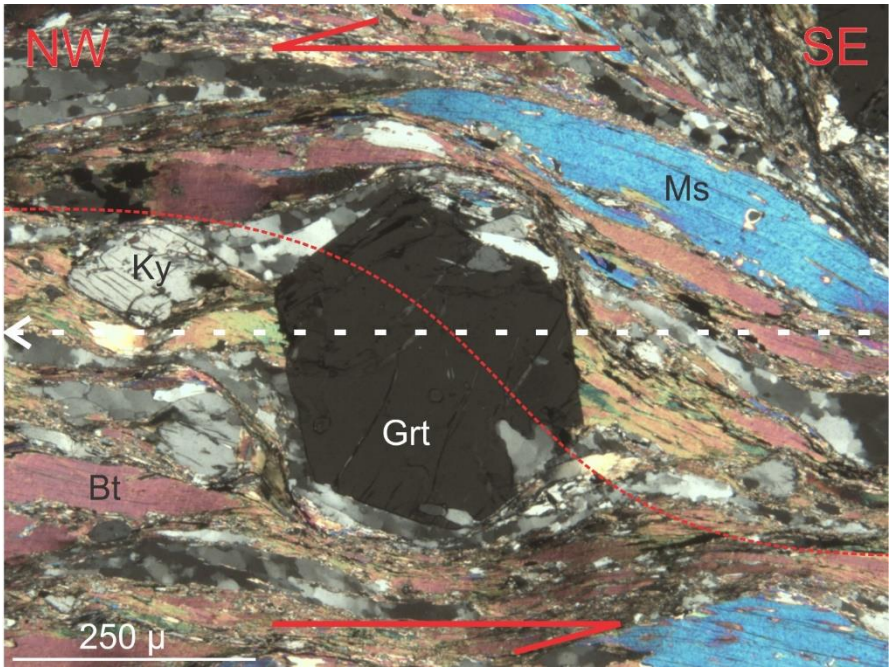

Figure 68 - Microphotograph of Garnet porphyroclast in thin section 1.1, viewed under XPL. Garnet forms a sigma clast with asymmetric tails of Biotite and Quartz, while a large Muscovite grain (upper right) forms a mica fish. Shear sense is sinistral, indicated by red arrows, and the red line details the shear fabric. Foliation plane and lineation trend indicated by white line and arrow. Corresponds to 1.1-1 in Table 12.

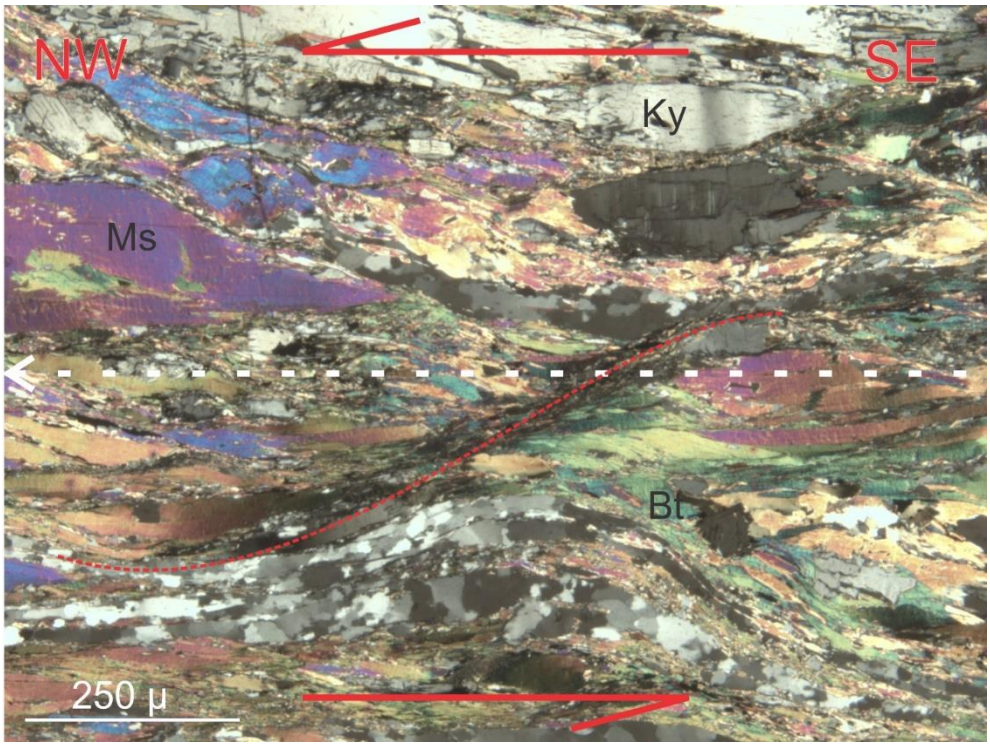

Figure 69 - Microphotograph of a shear band in thin section 1.1, viewed under XPL. Shear band outlined by stippled red curve. Green birefringent Biotite grain above labelled Biotite forms a mica fish. Shear sense is sinistral, indicated by the red arrows. White line and arrow refer to foliation plane and lineation trend, respectively. Corresponds to 1.1-2 in Table 12.

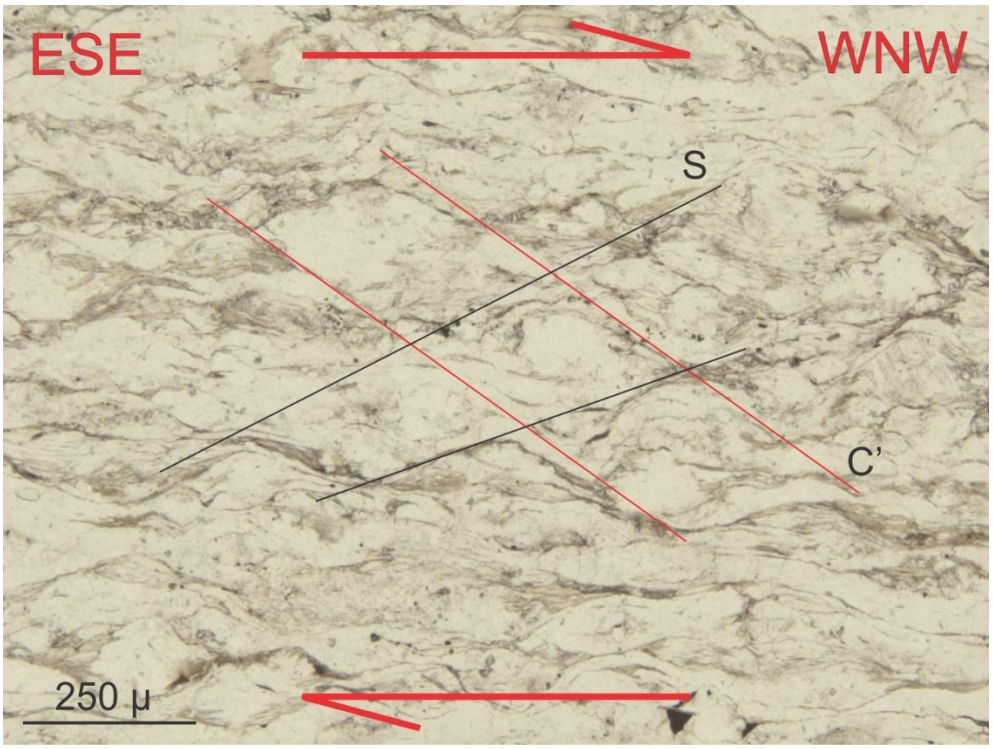

Figure 70 - Microphotograph of S-C' fabric in thin section 2.1, under PPL. Black lines outline the S planes, while red lines detail the C' planes. Shear sense is dextral, as indicated by the red arrows. General rock foliation is horizontal, and the lineation trends West-Northwest. Corresponds to 2.1-2 in Table 12.

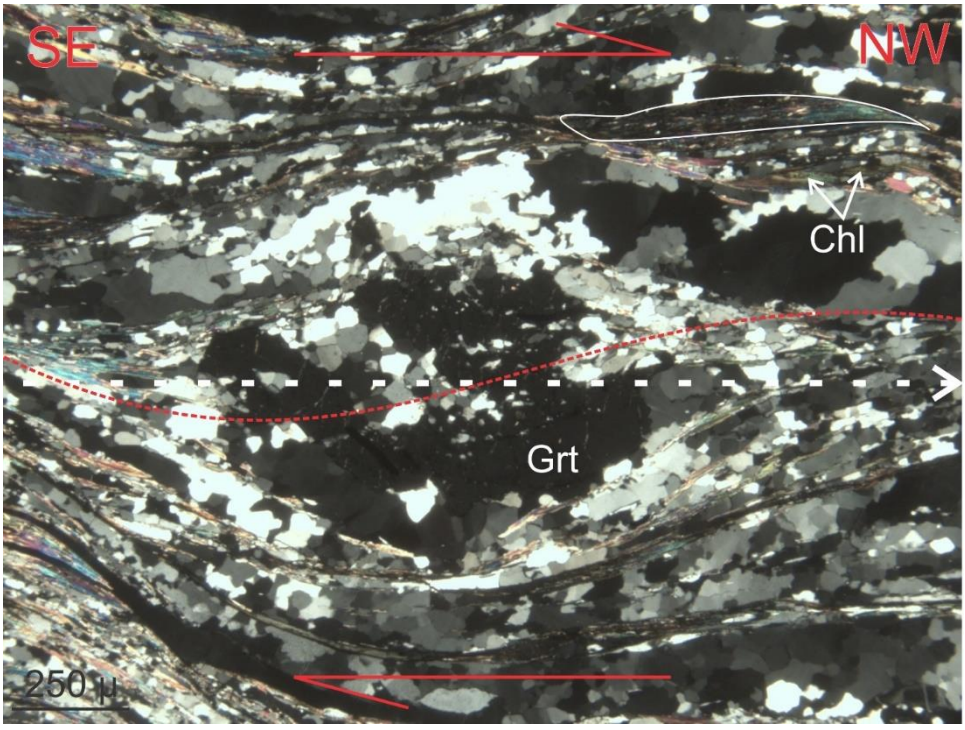

Figure 71 - Microphotograph of a sigma clast and mica fish in thin section 3, under XPL. Strongly sheared Garnet replaced by Quartz forming a sigma clast, Muscovite mica fish outlined in white. Shear sense is dextral, as indicated by red arrows. White stippled line and arrow represent the foliation plane orientation and lineation trend, respectively. Curved red line indicates the shear fabric. Corresponds to 3 in Table 12.

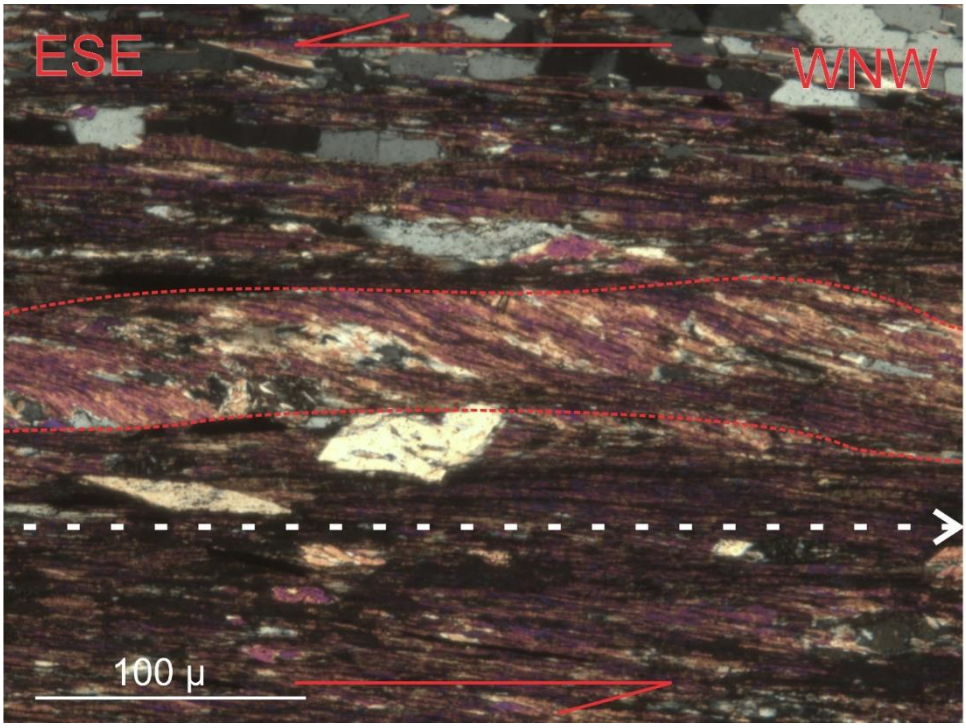

Figure 72 - Microphotograph of Muscovite mica fish ribbon/shear band in thin section 4, viewed under XPL. Shear sense is sinistral, indicated by red arrows. Mica fish ribbon outlined by red lines. White line and arrow indicate foliation plane and lineation trend, respectively. Corresponds to 4 in Table 12.

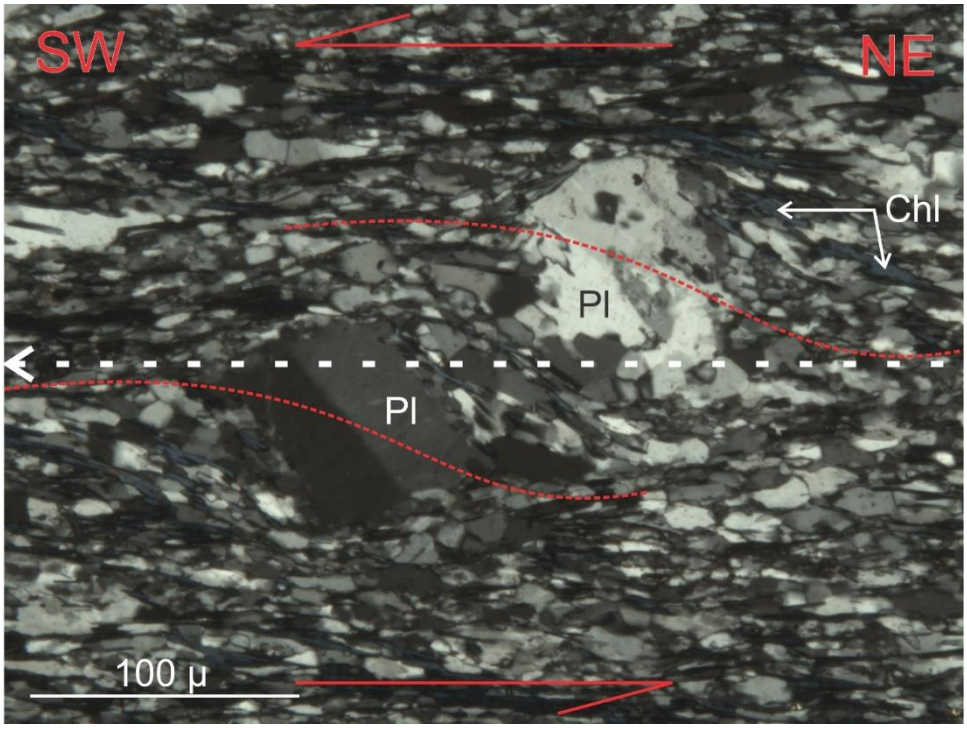

Figure 73 - Microphotograph of sigma clasts in thin section 7, viewed under XPL. Plagioclase porphyroclasts in a matrix of Quartz and Chlorite form sigma clasts. Shear sense is sinistral, as indicated by red arrows. Stippled red lines outline the shear fabric, and the white line and arrow detail the foliation plane and lineation trend, respectively. Corresponds to 7-1 in Table 12.

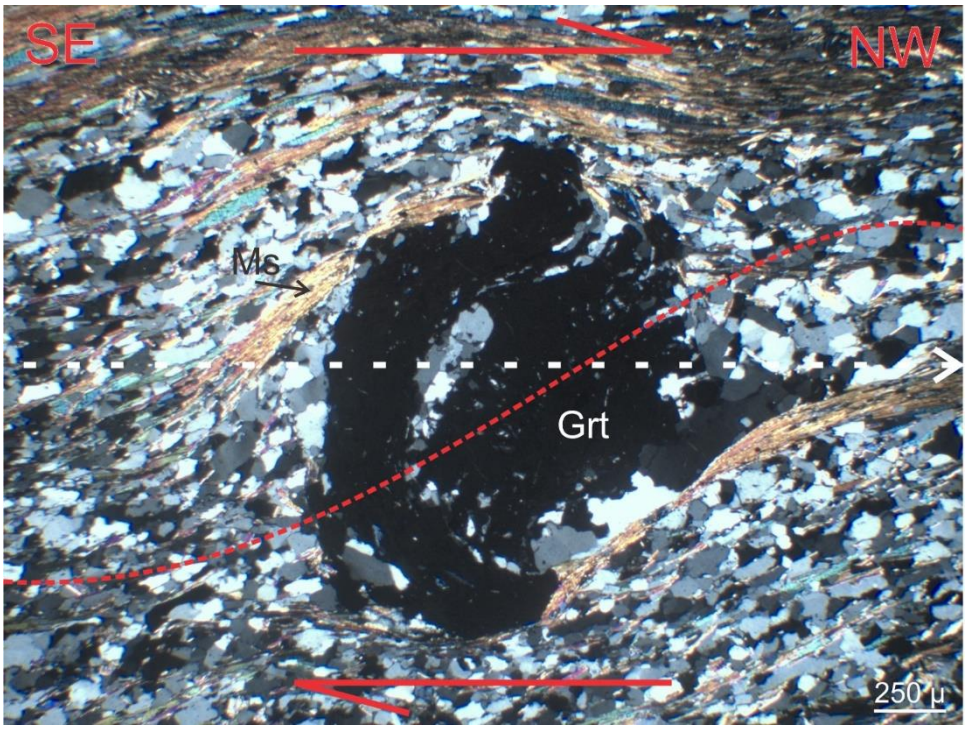

Figure 74 - Microphotograph of a deformed Garnet in thin section 14e, viewed under XPL. A delta clast is formed by wings of Muscovite, and helical inclusion trails can be seen in the Garnet. Dextral shear sense is indicated by red arrows, while stipled line and arrow indicate foliation plane and lineation direction, respectively. Red stipled line represents the shear fabric. Corresponds to 14e-1 in Table 12.

3.2.3.2 Quartz Recrystallization Mechanisms

Three samples were taken in the field from Quartz veins in the host rock (thin sections 1.2, 2.2, and 3.2), for the purpose of detailed investigations of recrystallization mechanisms and CPOs of Quartz through the contact. Three main types of recrystallization in Quartz are studied here: BLG (bulging), SGR (subgrain rotation), and GBM (grain boundary migration). These mechanisms, when observed, can give an indication of both temperature and strain rate. Bulging occurs when grain boundaries bulge into adjacent crystals with a high dislocation density, and sometimes also forms new small crystals, which is commonly observed as core-mantle structures (Passchier & Trouw, 2005). Undulose extinction is also common in old, non-recrystallized grains. Subgrain rotation is carried out through the addition of dislocations to subgrain boundaries, and occurs at a higher temperature than BLG (Passchier & Trouw, 2005). Old grains are commonly elongate with visible subgrains, and core-mantle structures are also possible. At higher temperatures, grain boundaries can mobilize through dislocations and subgrain boundaries, producing lobate crystal boundaries (Passchier & Trouw, 2005). SGR processes can also be active, but there is generally a decrease of subgrains and undulose extinction with lower strain rates (and higher temperatures).

Thin Section	**BLG**	**SGR**	**GBM**
1.1			X
1.2			X
2.1		X	XX
2.2			X
3.1		X	X
3.2		XX	X
4	X	X	
5	X	X	
6	X	X	
7	X	X	
14e	X	X	
8		X	X

Table 13 - Table of observed Quartz recrystallization mechanisms in thin section. Bold and italicized sections are illustrated in the figures below. Xs indicated observed mechanisms, XXs express the dominant recrystallization mechanism.

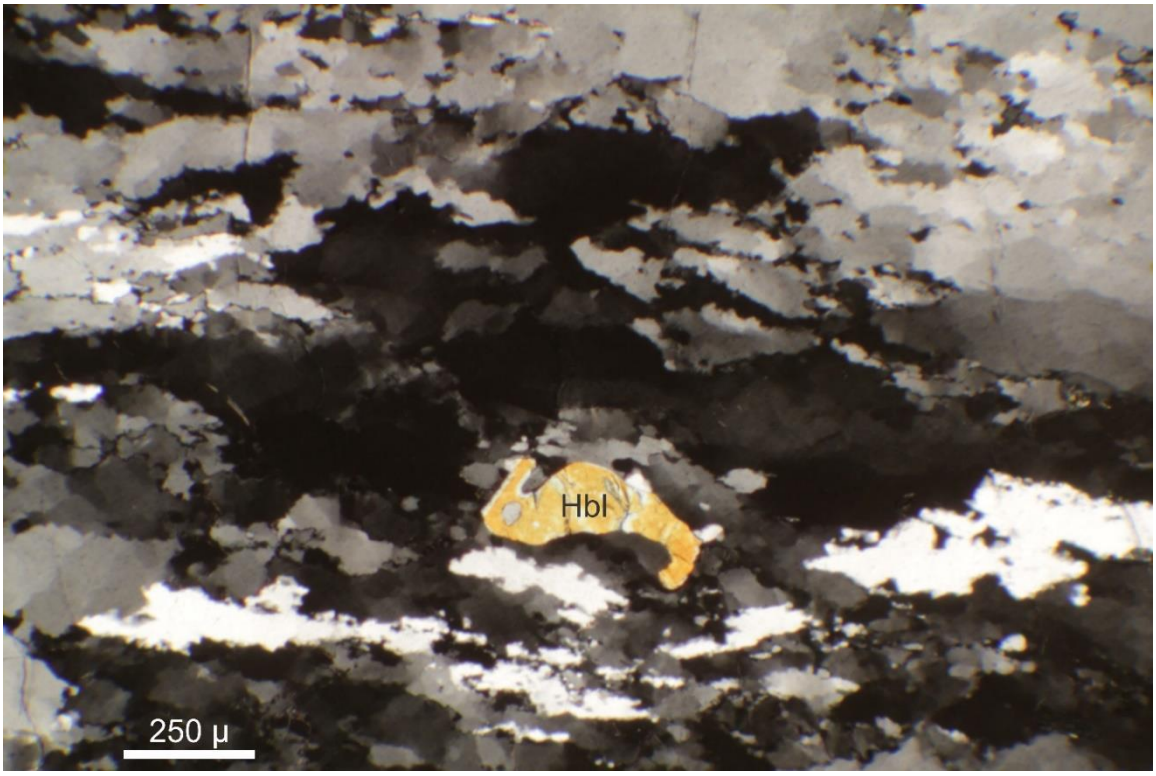

Figure 75 - Microphotograph of thin section 1.2, viewed under XPL. Hornblende grain in Quartz vein. Quartz crystals exhibiting lobate grain boundaries and core-mantle structures.

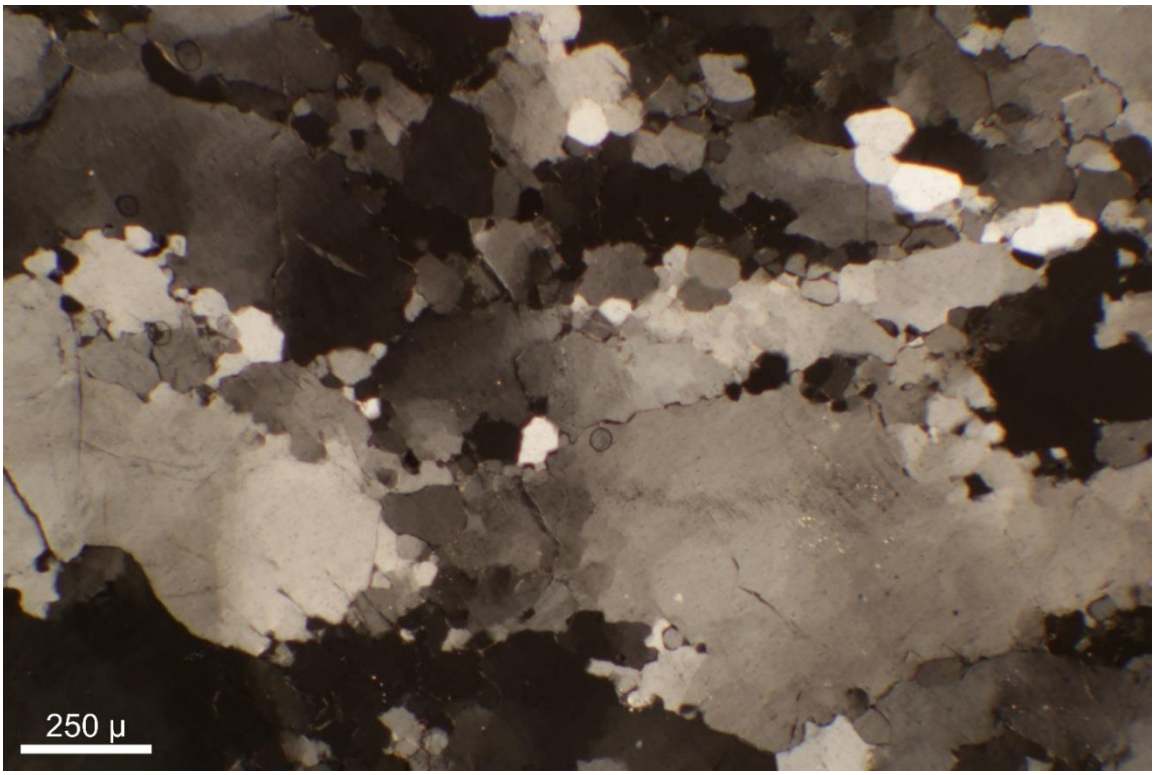

Figure 76 - Microphotograph of thin section 2.2, viewed under XPL. Quartz vein with GBM characteristic lobate grain boundaries, undulose extinction, and core-mantle structures.

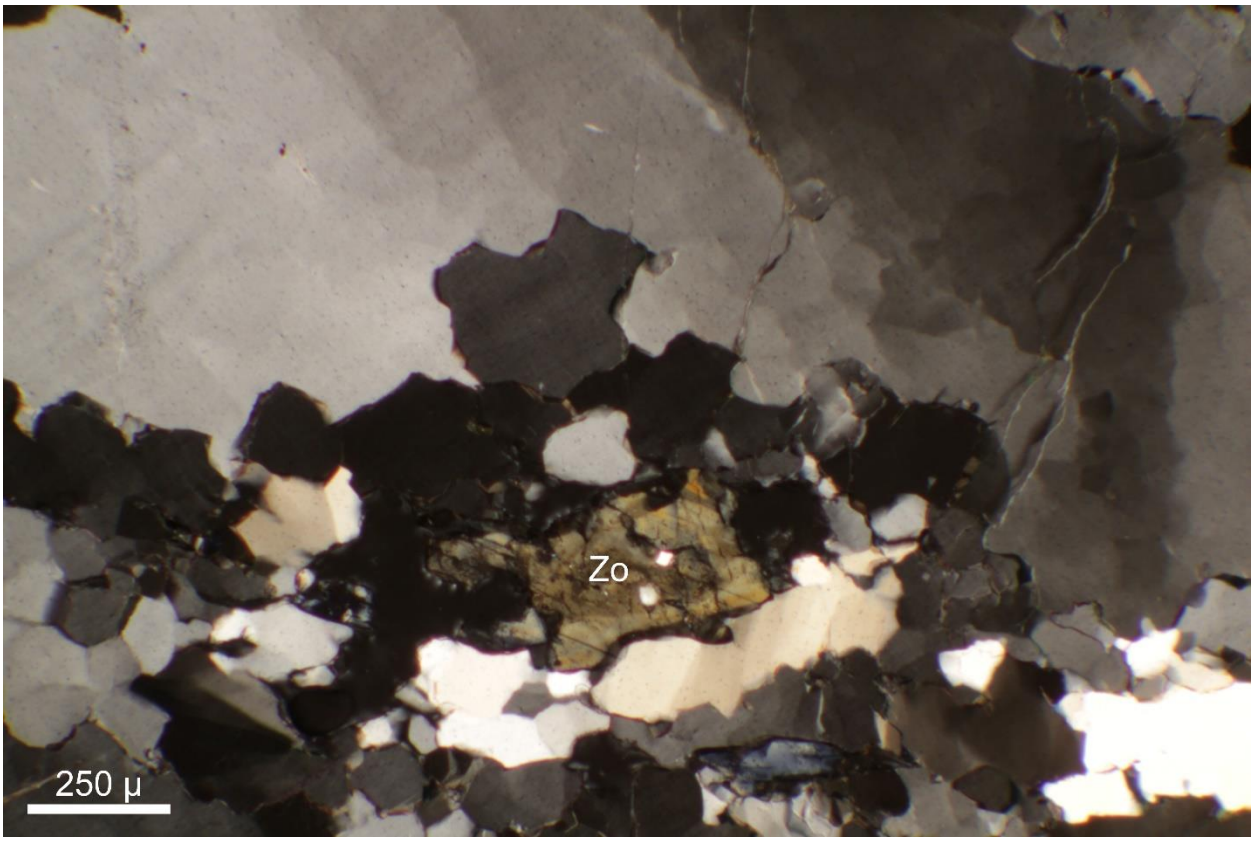

Figure 77 - Microphotograph of thin section 3.2, viewed under XPL. Subhedral Zoisite crystals in Quartz vein. Large Quartz grain in upper image displays typical undulose extinction.

3.3 Nappe Kinematics From Shear Sense Indicators

From the shear sense indicators observed both in the field and in thin section, a map was created to show the sense of movement in those locations, seen in Figure 78 below.

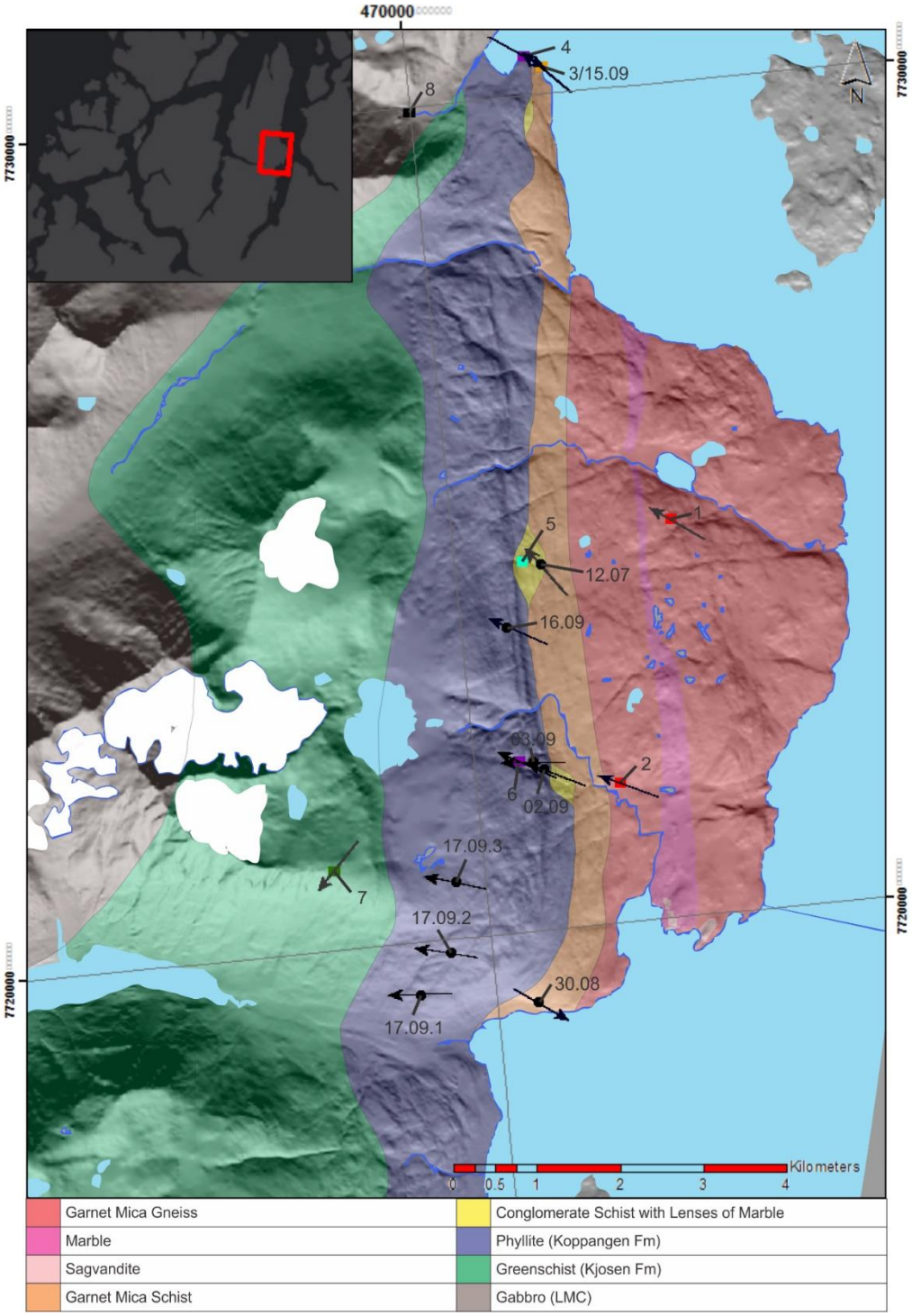

Figure 78 - Map of shear sense indicator and sample/station locations. Arrows indicate sense of hanging wall movement. Colored squares represent sample locations of prepared thin sections. Black circles are field station locations where shear sense indicators were observed.

4 DISCUSSION

4.1 LITHOLOGIES

The rocks of the Nordmannvik Nappe and the LMC are particularly well-studied (Munday, 1970; Chroston, 1972; Munday, 1974; Furnes et al., 1979; Andresen & Bergh, 1985; Andresen et al., 1985; Gayer et al., 1985; Minsaas & Sturt, 1985; Anderson et al., 1992; Lindstrom & Andresen, 1992; Furnes & Pedersen, 1995; Oliver & Krogh, 1995; Slagstad, 1995; Kvassnes et al., 2004; Hibelot, 2013; Augland et al., 2014; Kraus, 2016) (Faber, pers. comm., 2017), and evidence from the field and the lab generally agree with the previous literature. The units between those rocks (the phyllites, for example) are the more crucial ones to this particular study, and are critically under-studied and not very well understood.

4.1.1 Garnet Mica Gneiss

The Nordmannvik gneisses studied in this paper are not considered to be typical Nordmannvik rocks, such as those described in the previous literature (Andresen & Bergh, 1985; Andresen et al., 1985; Lindstrom & Andresen, 1992; Hibelot, 2013; Augland et al., 2014; Kraus, 2016) (Faber, pers. comm., 2017), as they generally contain some level of late retrograde metamorphic overprinting, which is more pronounced in the overlying units. In the area between Koppangen and Lyngseidet, only the rocks at the very Eastern edge of the peninsula displayed characteristics similar to those previously described. Further West, towards the center of the peninsula where these rocks are heavily mylonitized, it was assumed that this fabric was created from the Caledonian nappe-stacking event. Microstructural and petrological analysis, however, indicates that the deformation associated with the final emplacement of the Lyngen Nappe may have penetrated farther down into the upper crust than previously thought, and some of the overprinting seen in these units could be a consequence of that later event.

4.1.2 Garnet Mica Schist

These rocks, occurring between the Nordmannvik gneisses and the Koppangen FM phyllites, are not considered as a separate entity in the previous literature (Andresen & Bergh, 1985; Andresen et al., 1985; Lindstrom & Andresen, 1992; Hibelot, 2013; Augland et al., 2014; Kraus, 2016). While compositionally nearly identical to the underlying gneisses, there is a distinct structural and microstructural difference in these rocks, and it is suggested that there should be a distinction between these units. While they are clearly related to the Garnet Mica Gneiss in petrologic terms, these schists are more structurally similar to the overlying phyllites.

4.1.3 Conglomerate Schist

The carbonate-rich lenses described here are separated from the other rock units, but it is not intended to distinguish them as a separate lithological unit. Only a few relatively small lenses and zones of this rock were observed and were found to occur along the studied contact between the Nordmannvik schists and the overlying phyllites. The source of these calc-silicate rocks is unclear, as carbonate clasts were observed in both schist and phyllitic host rocks. Large carbonate-rich areas were not recognized Westward of the contact zone, but an adjacent marble unit trending North-South is known in the Nordmannvik Nappe, just to the East of the studied boundary.

4.1.4 Phyllite (Koppangen FM)

Mentions of this unit in previous literature are sparse and brief (Andresen & Bergh, 1985; Andresen et al., 1985; Oliver & Krogh, 1995; Hibelot, 2013; Augland et al., 2014), and no clear resolution to its origin is defined. Its fine-grained nature, both in the field and in thin section, make it difficult to positively constrain mineral assemblages. Gradational contact zones at its base and top also contribute to a complex tectonometamorphic evolution. Various changes in field appearance were observed both along and across strike, including mineralogy, texture, and structure. What is clear, however, is that this unit played a major role in the tectonic history regarding the Nordmannvik and Lyngen nappes.

4.1.5 Greenschist (Kjosen FM)/Chlorite Schist

The Kjosen FM is briefly detailed in previous literature (Munday, 1970; Randall, 1971; Chroston, 1972; Munday, 1974; Andresen et al., 1985; Gayer et al., 1985; Furnes & Pedersen, 1995; Augland et al., 2014), and is simply described as dominantly greenschists and amphibolites. They are inferred to have derived from the overlying LMC, based on compositional similarities (Munday, 1970; Randall, 1971; Munday, 1974; Gayer et al., 1985; Furnes & Pedersen, 1995). Since investigations of these rocks in the field were limited, and only one sample was taken, it is difficult to provide a solid solution to their origin. Based on the mineralogy and petrology, this sample is now interpreted to be an upper extension of the Phyllite, instead of the Kjosen FM described in the literature. This is primarily due to a lack of Amphibolite phases in the selected sample. However, there is a clear mineralogical and grain size difference in comparison to the Phyllite when viewed in thin section.

4.1.6 Amphibolite Schist

While not occurring in the primary study area of this paper (between Koppangen and Lyngseidet), this unit was included for analysis due to its key stratigraphic placement, in the hope that it could help provide a better petrological understanding of this contact. These rocks are unique, because they occur above the phyllites, but seem to be more similar in composition to the Nordmannvik rocks below. As there is no Greenschist unit in this area (near Nordkjosbotn), the Amphibolite schists are bounded above and below by the LMC and the phyllites, respectively. South of Nordkjosbotn, where the phyllites pinch out, this unit is bounded below by the Nordmannvik gneisses.

4.1.7 Gabbro (LMC)

Because the mafic rocks of the LMC are particularly well-studied (Munday, 1970; Chroston, 1972; Munday, 1974; Furnes et al., 1979; Andresen & Bergh, 1985; Andresen et al., 1985; Gayer et al., 1985; Minsaas & Sturt, 1985; Anderson et al., 1992; Furnes & Pedersen, 1995; Oliver & Krogh, 1995; Slagstad, 1995; Kvassnes et al., 2004; Augland et al., 2014), a thorough evaluation of these rocks was not prioritized. Quality outcrops were especially difficult to reach, and each one possessed significant differences in the structure and appearance of the rocks. For example, the location from which sample number 9 was produced yielded a thin section that agreed well with the previous literature's description of the Metagabbro (Munday, 1974). From studying thin section 8 under the microscope, however, a fair amount of Quartz was noted, indicating that this might instead be classified as a calc-silicate rock, or possibly closer in composition to a Diorite. Field observations between the two sample locations were very similar, and were interpreted to be the same rock. The occurrence of a calc-silicate rock or Diorite within the mapped Gabbro unit is an interesting note. It could possibly infer the interaction between the LMC and an adjacent pelitic unit (Einaudi & Burt, 1982).

4.2 Structure & Kinematics

An emphasis was placed on retrieving structural and kinematic data during field work, and the results have been outlined in the section above. Further studies of the microscopic structures from the prepared thin sections have also produced relevant data. This section will explore the possible explanations and implications of these results.

4.2.1 Macroscale

11 field locations yielded interpreted shear sense indicators, and were documented. A few are fairly ambiguous, however most cases are clear in their sense of shear. Shear bands were fairly common in the Garnet Mica Schist and the Phyllite, while sigma clasts were observed in most units. The majority of observed shear sense indicators showed a top-to-the-West hanging wall movement. From the field data alone, the Nordmannvik gneisses displayed top-East senses, while the Nordmannvik schists showed both top-West and top-East movement senses. Field-observed indicators in the phyllites were top-to-the-West only. This could imply that the structurally lower gneisses were not affected by normal faulting of the overlying Lyngen Nappe, while the transitional Garnet Mica Schist was overprinted by this event, but still retained some relic fabrics. With the absence of a Caledonian-related top-to-the-East nappe-stacking fabric in the Phyllite, it is still unclear whether these rocks could have originated from the Nordmannvik units. However, it could also be possible that any relict fabrics in the Phyllite would have been completely destroyed by this event.

The structural orientations of the studied units also have some interesting characteristics. A sharp increase in dip angles is observed between the Nordmannvik Gneiss and the overlying schists and phyllites, with another increase seen in the Kjosen FM Greenschist. The lineation trend in the Greenschist also shows a distinct difference, with a more Southwesterly orientation than the predominant West to Northwest trend of the lower units. Because normal faults generally occur at steep angles (~60°), while thrust faults are typically low-angle (less than 45°) (Twiss & Moores, 1992), it is conceivable that this increase in dip angle is due to the overprinting of a higher angle normal faulting of the Lyngen Nappe, as opposed to the generally low-angle thrust faulting of the Nordmannvik Nappe. The differing lineation trend in the greenschists could also indicate evidence of an origin separate from the phyllites.

4.2.2 Microscale

Studies of these rocks in thin section also provided several kinematic indicators. Much like in the outcrops, shear bands and sigma clasts were also common on the micro scale. At this level, mica fish and S-C' fabrics could also be observed. Nearly all of the documented shear sense indicators in thin section produced top-to-the-West shear sense, with the exception of one top-East indicator. What is interesting to note is that one of the Phyllite samples, thin section number 4, produced the top-East shear sense, while the Garnet Mica Gneiss samples displayed clear top-to-the-West kinematics. For the gneisses, this could indicate that a normal faulting episode penetrated further down into the Nordmannvik Nappe than previously thought. For the phyllites, it presents possible evidence of a Caledonian nappe-stacking fabric.

4.3 Deformation Microstructures

4.3.1 Quartz Recrystallization

The recrystallization of Quartz grains was analyzed in the prepared thin sections, especially in samples 1.2, 2.2, and 3.2, as these were sampled from veins of Quartz in their respective host rocks. None of these three samples indicated a distinct shear sense when viewed through the accessory Gypsum plate. Thin section 2.2 showed a possible preference of blue, which would indicate a dextral (and thus top-West) shear sense in that case, but was deemed too ambiguous to draw any conclusions from. Recrystallization mechanisms, however, were generally clear and easily identified. A trend was noted through all of the samples, as the Quartz in the Nordmannvik gneisses were predominantly recrystallized through GBM with some SGR, the Garnet Mica Schist was mostly recrystallized through SGR with some GBM, and the rest of the overlying units (with the exception of samples 8 and 9) displaying characteristics of both BLG and SGR. The Quartz observed in sample 8, which was sampled as a Gabbro, displayed both SGR and GBM features. This trend would indicate a decrease in metamorphic temperature conditions stratigraphically upwards (Figure 79). This again implies a lower temperature event (e.g. Normal faulting) overprinting the higher temperature fabrics of the Nordmannvik Nappe.

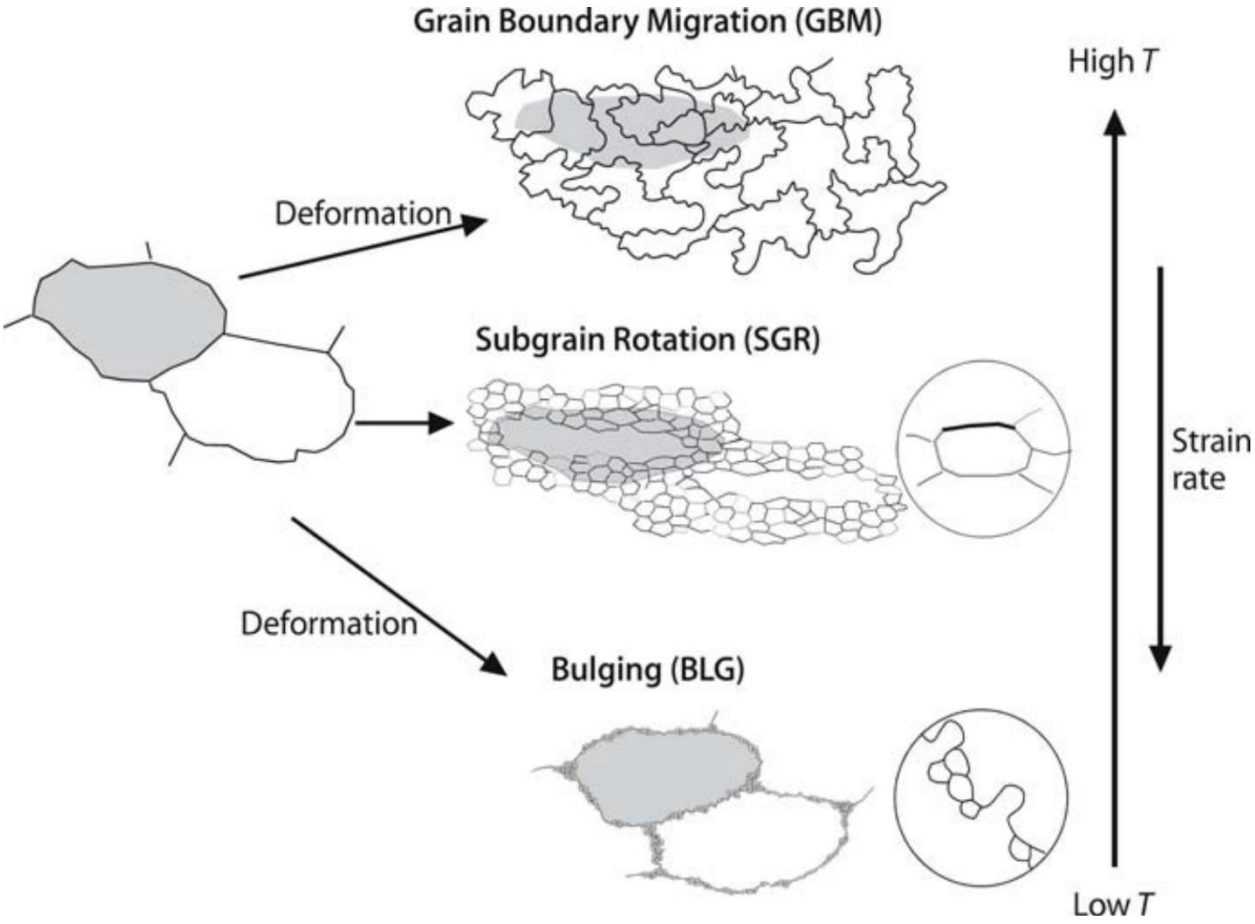

Figure 79 - Illustration of the three primary methods of Quartz recrystallization, after Passchier and Trouw (2005).

4.4 Metamorphic Pathways

All four of the samples that were included in the petrological investigation yielded results that plot within the Amphibolite facies metamorphic grade (Figure 80). This is somewhat surprising, in particular for the Chlorite Schist sample, although it does provide a lower metamorphic grade than the other three samples. The Garnet Mica Gneiss sample of the Nordmannvik Nappe yielded the highest P-T conditions. However, this value was lower than expected, and is interpreted to represent the minimum P-T conditions in the Nordmannvik Nappe. Previous studies of this unit have shown that these rocks underwent partial melting (Hibelot, 2013; Kraus, 2016) (Faber, pers. comm., 2017), and so the P-T estimate from this sample probably represents an assemblage that re-equilibrated during cooling. The Garnet Mica Schist and the Amphibolite Schist indicate comparatively similar conditions, and both also show a significant jump in P-T conditions from the cores of the garnets to the rims. These jumps in metamorphic grade, combined with the prograde characteristics observed in the Garnet profiles, could be a result of either two separate metamorphic events, or an extended event with increasing P-T conditions. It is curious that the Chlorite Schist sample plots well within the Amphibolite facies field, while the mineralogy clearly represents a Greenschist facies assemblage.

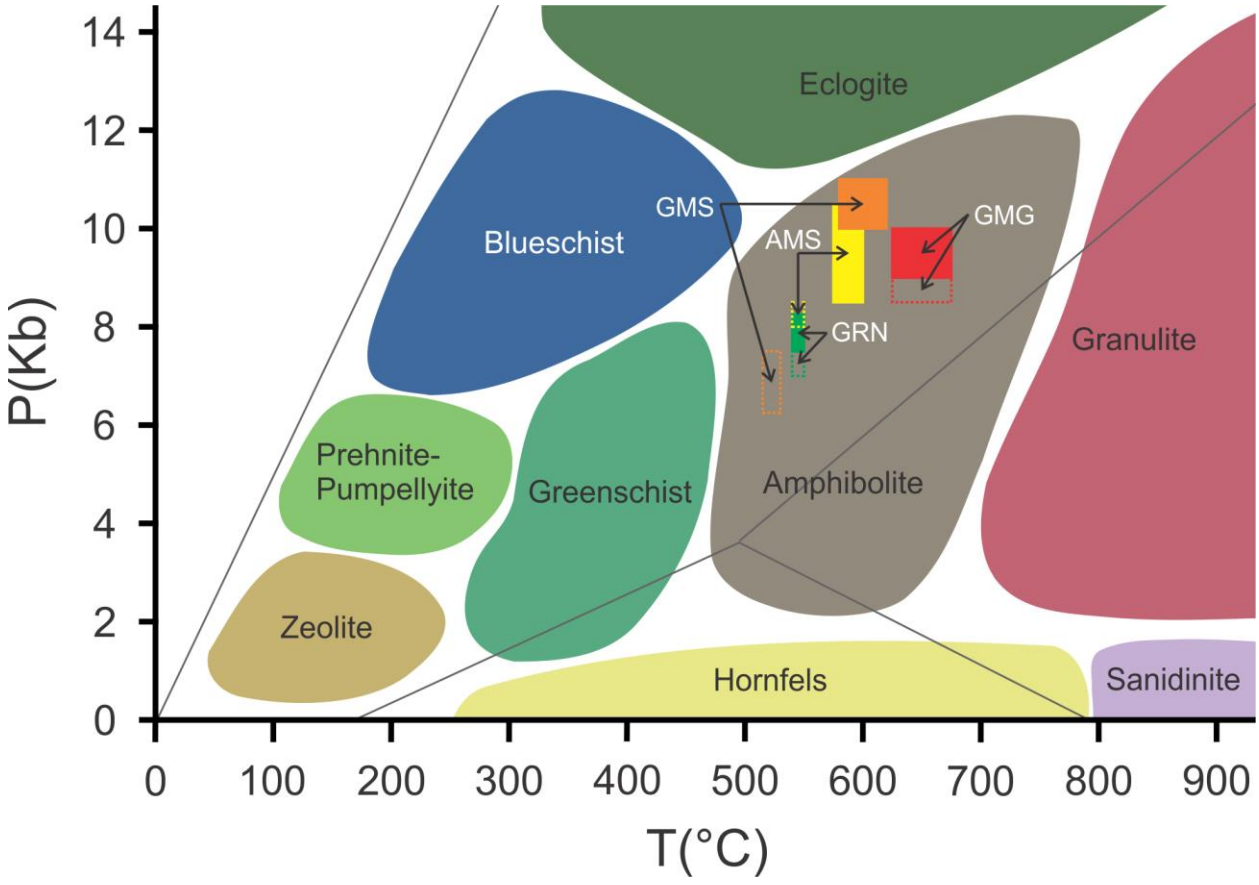

Figure 80 - P-T diagram indicating the conditions for the various metamorphic faces, with estimated conditions plotted for the four investigated samples. Solid boxes represent conditions estimated from the Garnet rim and matrix minerals, dotted boxes indicate conditions estimated from the Garnet cores.

4.5 Mineralogical Relationships

4.5.1 Main Minerals

Distinct mineralogical phase changes could be observed between many of the samples. For example, in a succession of samples 1.1, 2.1, and 3.1, a sharp decrease in the abundance of Biotite was noted. This trend was accompanied by an increase in Potassium Feldspar and Chlorite, and can be explained by the retrograde reaction Chl+Kfs=Bt+Ms+Qz+H_2O, with Biotite being consumed. In the amphibole-bearing Schist, the garnets appear to be syn-tectonic, with reaction tails of Muscovite and Chlorite. From the reaction Bt+Chl=Grt+Ms+H_2O, this can be inferred as a prograde event. The garnets in sample 1.1 are strongly euhedral, compared to the poikilitic garnets of samples 3.1 and 7. This could indicate late growth of these grains, possibly occurring through the St+Ms+Qz=Grt+Bt+Ky/Sil+H_2O reaction.

4.5.2 Accessory Minerals

Zoisite and Epidote minerals were commonly noted in small proportions in many of the observed samples. Other important accessory minerals noted from petrologic investigations include Ilmenite, Rutile, and Titanite. Accessories noted in the high-temperature Nordmannvik Gneiss include Ilmenite, Sillimanite, and Staurolite. While Kyanite was the dominant Aluminium Silicate mineral, the presence of Sillimanite suggests a higher-temperature relict phase, probably in association with some melt in the rock. Staurolite, on the other hand, probably grew later during either an exhumation/cooling event, or a lower-grade overprinting event. In the Garnet Mica Schist, important accessory minerals observed were Zoisite, Ilmenite, Chlorite, and Rutile. From the petrologic modelling, this sample appears to show a prograde evolution, with Ilmenite, Chlorite, and Zoisite stable at the onset of Garnet growth, and a stability of Rutile during peak metamorphism. However, Ilmenite was observed with inclusions of Rutile, and could contradict this interpretation, if the Ilmenite formed later around the Rutile. Rutile is commonly a detrital mineral, however, and so may have just been part of the original Nordmannvik sedimentary assemblage, and not of metamorphic origin in these rocks. Similar to this sample is the Amphibolite Schist, with accessories of Zoisite, Ilmenite, Chlorite, and Hornblende. In this sample, however, the Zoisite appears to have been stable throughout the rock's metamorphic evolution, while Chlorite is clearly derived from the interpreted earlier, lower-temperature conditions. Finally, in the Chlorite Schist sample, Ilmenite, Epidote, and Titanite were the noted accessories. These minerals were commonly in association, with Ilmenite typically surrounded by Titanite. However, from the P-T pseudosections calculated for this rock, the predicted assemblage includes only Ilmenite. As the Titanite is probably a later phase growing around the Ilmenite, this could indicate a Greenschist facies overprint of the modelled peak assemblage.

4.6 Origin Of Phyllites & Greenschists

One of the primary objectives of this paper is to provide a clearer picture into the origin of the low-grade rocks comprising the contact zone between the LMC and the underlying high-grade Nordmannvik Nappe. This is a complex geologic issue, and several possibilities exist. It was proposed earlier that an origin of both the Kjosen FM greenschists and the Koppangen FM phyllites should be investigated. However, the Chlorite Schist sample studied here more likely represents an extension of the Koppangen FM, and so one should defer to the previous conclusions for the Kjosen FM and its origin from the Lyngen mafic rocks (Munday, 1970; Randall, 1971; Munday, 1974; Gayer et al., 1985; Furnes & Pedersen, 1995). For the phyllites, a strong argument exists for their common origin with the metapelites of the Nordmannvik Nappe. When observing these units along the profile, the mineralogic and structural similarities between these rocks are best explained by a common protolith. Microstructural studies, such as the observed Quartz recrystallization mechanisms, have also provided a correlative trend between these units. A common origin of these rocks would naturally imply that the Phyllites are retrograded from the Nordmannvik Nappe.

4.7 Tectonometamorphic Evolution

Based on the results of this study, and on the data from previous literature, an absolute determination of the processes and mechanisms involved with the final emplacement of the Lyngen Nappe is quite difficult to attain. The issue is complex, and future studies of this contact may be able to provide further evidence for a stronger conclusion. Nonetheless, it was the goal of this study to provide important data to a critically understudied area of the Norwegian Caledonides. The biggest question of this contact arises dominantly from the significant decrease in metamorphic grade from the Nordmannvik Nappe to the overlying Lyngen Nappe, as the trend below the Nordmannvik rocks is one of increasing metamorphic grade with each successively higher nappe (Kraus, 2016). The Nakkedal and Tromsø nappes above the Lyngen Nappe then mark a return to high metamorphic conditions (Indrevær, 2011). This anomaly formed the basis of the primary question of an out-of-sequence thrust versus a low-angle normal fault mechanism for the emplacement of the Lyngen Nappe. Possible tectonic models are presented and discussed herein.

4.7.1 Low-Angle Normal Faulting

In a question of an out-of-sequence thrust versus a low-angle normal fault, the structural data and observations of this study provide a strong argument for the latter. In the non-overprinted rocks of the Nordmannvik Nappe, shear-sense indicators were very clear in their top-to-the-East movement sense, which is related to the Caledonian nappe-stacking event. The majority of top-to-the-West shear-sense indicators in the rocks comprising the contact zone (and the uppermost gneisses of the Nordmannvik Nappe), however, provide ample suggestion for a normal movement sense of the hanging wall. Some ambiguity exists at a few locations, especially within the lower-Phyllite/Garnet Mica Schist/upper-Garnet Mica Gneiss domain, but this could be caused by structural overprinting. Foliation data may also argue for a normal-faulting event, given by the increase in dip angles stratigraphically upwards. However, petrologic modelling has estimated that the units involved in this contact zone have undergone lower-Amphibolite facies metamorphism, higher than the previous Greenschist facies assessments in previous literature (Andresen & Bergh, 1985; Andresen et al., 1985; Gayer et al., 1985; Furnes & Pedersen, 1995; Oliver & Krogh, 1995; Augland et al., 2014).

4.7.2 Channel Flow

One possible model that could help resolve the observed structures and modelled metamorphic conditions is the Channel Flow model, recently postulated for the Himalayan orogenic belt (Godin et al., 2006). In this scenario, tectonic slices of the underthrusting Baltica basement would be detached at successively lower levels and higher grades, creating a thrust fault at the base of this 'channel', and normal fault kinematics at the top (Figure 81). This model could account for the observed progradational characteristics of the Amphibolite and Garnet Mica schists overlying the Nordmannvik gneisses, and the subsequently lower temperature Phyllite and Chlorite Schist. As each imbricate slice is detached, it effectively 'records' the P-T conditions at its respective level. In this model, it would be difficult to ascertain whether the overlying LMC was actively moving, or if the movement sense was caused strictly by the underthrusting Baltica margin, or vice versa. Many of the proposed Channel Flow models (for the Himalayas, in particular) describe the channel as a weak and viscous layer influenced by partial melting (Godin et al., 2006). This presents a problem with the application of this model to the studied area, as the sheared contact zone rocks do not indicate temperatures high enough for any melt in the rock. Therefore, the Channel Flow model presented in this section is proposed primarily for its structural implications.

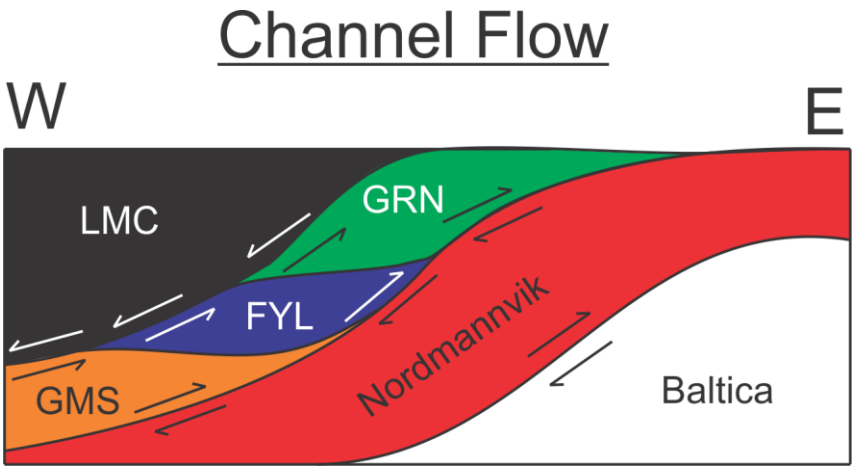

Figure 81 - Schematic diagram of Channel Flow tectonic model, with underthrusting of the Baltica margin/Nordmannvik Nappe beneath the Lyngen ophiolite, with detachments comprising the channel between.

4.7.3 Wedge Extrusion

Another possibility is the occurrence of the sheared rocks of the contact zone acting as an extruded wedge. This model would produce similar structures and kinematic indicators, however the tectonic wedge would act as one unit between the lower Baltica margin and the upper ophiolitic Lyngen Gabbro (Figure 82). This scenario could possibly reconcile the gradational contacts at the base and top of the Phyllite, but may not explain the fine-grained and intensely sheared nature of this unit. As with the Channel Flow model, it would be difficult to know the absolute movements of each interacting unit. A key point in this model is that crustal extension is not required for the exhumation of the rocks in this setting, and can happen during horizontal shortening (Ring & Glodny, 2010).

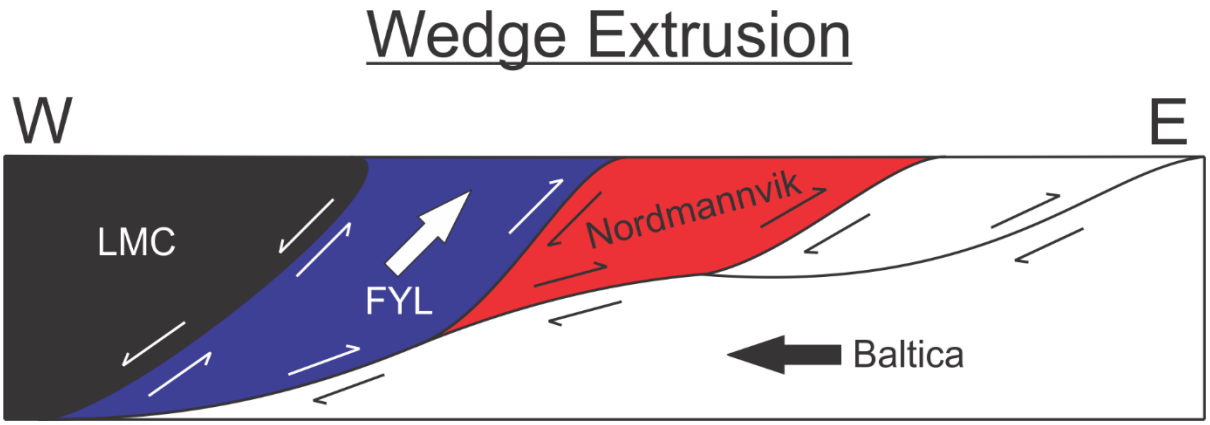

Figure 82 - Schematic diagram of the Wedge Extrusion tectonic model, with the sheared phyllites and adjacent units comprising the tectonic wedge between the LMC and the Baltica margin.

5 CONCLUSIONS

Based on the results and interpretations of this study, several conclusions can be made:

- The uppermost mylonitic gneisses of the Nordmannvik Nappe have been subjected to a period of lower-temperature cooling and/or exhumation that allowed for the growth of some lower temperature phases (e.g. Staurolite). They have also been overprinted structurally by a top-to-the-West kinematic event, possibly creating this low-temperature environment.
- The units referred to in this paper as the Garnet Mica Schist and the Amphibolite Schist share a common origin and evolution as meta-sedimentary rocks of the Nordmannvik Nappe. Their prograde character, however, differentiates their tectonometamorphic history from the high-temperature gneisses.
- Uncertainties still exist as to whether the Phyllite is Nordmannvik-derived, although structural and mineralogical similarities favor this interpretation.
- No clear consensus can be reached regarding a suitable tectonic model that properly addresses every complexity of this study, as each have strong arguments as well as ambiguities. What does seem to be clear, however, is the lack of supporting evidence for an out-of-sequence thrust event as the final emplacement of the Lyngen Nappe. Therefore, it is proposed that some form of an extensional detachment, by way of one of the above models or otherwise, is the driving force for the observed structures through this contact.

6 REFERENCES

Andersen, T. B., Jamtveit, B., Dewey, J. F., & Swensson, E. (1991). Subduction and eduction of continental crust: major mechanisms during continent-continent collision and orogenic extensional collapse, a model based on the south Norwegian Caledonides. *Terra Nova, 3*(3), 303-310.

Anderson, M., Barker, A., Bennett, D., & Dallmeyer, R. (1992). A tectonic model for Scandian terrane accretion in the northern Scandinavian Caledonides. *Journal of the Geological Society, 149*(5), 727-741.

Andréasson, P. (1994). The Baltoscandian margin in Neoproterozoic-early Palaeozoic times. Some constraints on terrane derivation and accretion in the Arctic Scandinavian Caledonides. *Tectonophysics, 231*(1-3), 1-32.

Andresen, A., & Bergh, S. (1981). Stratigraphy and tectonometamorphic evolution of the Ordovician-Silurian Ullsfjord Group, Lyngen Nappe Complex, North Norwegian Caledonides. *Terra cognita*(1), 32-33.

Andresen, A., & Bergh, S. (1985). Stratigraphy and tectonometamorphic evolution of the Ordovician-Silurian Balsfjord Group, Lyngen Nappe, north Norwegian Caledonides. *The Caledonide Orogen-Scandinavia and related areas, John Wiley and Sons, London*, 579-591.

Andresen, A., Fareth, E., Bergh, S., Kristensen, S., & Krogh, E. (1985). Review of Caledonian lithotectonic units in Troms, north Norway. *The Caledonide Orogen-Scandinavia and related areas. John Wiley, New York*, 569-578.

Andresen, A., & Steltenpohl, M. G. (1994). Evidence for ophiolite obduction, terrane accretion and polyorogenic evolution of the north Scandinavian Caledonides. *Tectonophysics, 231*(1), 59-70. doi:10.1016/0040-1951(94)90121-X

Augland, L. E., Andresen, A., Corfu, F., Simonsen, S. L., & Andersen, T. (2012). The Beiarn nappe complex: a record of Laurentian Early Silurian arc magmatism in the Uppermost Allochthon, Scandinavian Caledonides. *Lithos, 146*, 233-252.

Augland, L. E., Andresen, A., Gasser, D., & Steltenpohl, M. G. (2014). Early Ordovician to Silurian evolution of exotic terranes in the scandinavian caledonides of the Ofoten-Troms area-terrane characterization and correlation based on new U-Pb zircon ages and Lu-Hf isotopic data. *Geological Society Special Publication, 390*(1), 655-678. doi:10.1144/SP390.19

Barker, A. (1986). The geology between Salangsdalen and Gratangenfjord, Troms, Norway. *Norges Geologiske Undersokelse Bulletin, 405*, 41-56.

Barnes, C. G., Frost, C. D., Yoshinobu, A. S., McArthur, K., Barnes, M. A., Allen, C. M., . . . Prestvik, T. (2007). Timing of sedimentation, metamorphism, and plutonism in the Helgeland Nappe Complex, north-central Norwegian Caledonides. *Geosphere, 3*(6), 683-703.

Bergh, S. G. (1980). Stratigrafiske, strukturgeologiske og metamorfe undersøkelser av kaledonske bergarter vest for Balsfjord i Troms. Tromsø: S. G. Bergh.

Bjørlykke, A., & Olaussen, S. (1981). *Sibirian Sediments, Volcanics and Mineral Deposits in the Sagelvvatn Area, Troms, North Norway*: Universitetsforlaget.

Braathen, A., Nordgulen, O., Osmundsen, P. T., Andersen, T. B., Solli, A., & Roberts, D. (2000). Devonian, orogen-parallel, opposed extension in the central Norwegian Caledonides. *Geology (Boulder), 28*(7), 615-618. doi:10.1130/0091-7613(2000)028<0615:DOPOEI>2.3.CO;2

Chapman, T., Gayer, R., & Williams, G. (1985). Structural cross-sections through the Finnmark Caledonides and timing of the Finnmarkian event. *The Caledonide orogen–Scandinavia and related areas. John Wiley & Sons, Chichester*, 593-610.

Chroston, P. N. (1972). A gravity profile across Lyngenhalvoeya, Troms, northern Norway. *Norsk Geologisk Tidsskrift. Supplement, 52*(3), 295-303.
Cocks, L. (2001). Ordovician and Silurian global geography. *J. Geol. Soc., 158*, 197-210.
Cocks, L. R. M., & Torsvik, T. H. (2002). Earth geography from 500 to 400 million years ago; a faunal and palaeomagnetic review. *Journal of the Geological Society of London, 159*, 631-644. doi:10.1144/0016-764901-118
Coker, J., Steltenpohl, M. G., Andresen, A., & Kunk, M. (1995). An Ar-40/Ar-39 thermochronology of the Ofoten-Troms region: Implications for terrane amalgamation and extensional collapse of the northern Scandinavian Caledonides. *Tectonics, 14*(2), 435-447.
Connolly, J. (2009). The geodynamic equation of state: what and how. *Geochemistry, Geophysics, Geosystems, 10*(10).
Corfu, F., Roberts, R., Torsvik, T., Andersen, T., Ramsay, D., & Ashwal, L. (2004). *Crustal processing: the Finnmarkian orogen reassessed.* Paper presented at the Geochimica et Cosmochimica Acta.
Dale, J., Powell, R., White, R., Elmer, F., & Holland, T. (2005). A thermodynamic model for Ca–Na clinoamphiboles in Na2O–CaO–FeO–MgO–Al2O3–SiO2–H2O–O for petrological calculations. *Journal of Metamorphic Geology, 23*(8), 771-791.
Dallmeyer, R., & Andresen, A. (1992). Polyphase tectonothermal evolution of exotic caledonian nappes in Troms, Norway: Evidence from 40Ar39Ar mineral ages. *Lithos, 29*(1-2), 19-42.
Eide, E. A., & Torsvik, T. H. (1996). Paleozoic supercontinental assembly, mantle flushing, and genesis of the Kiaman Superchron. *Earth and Planetary Science Letters, 144*(3-4), 389-402. doi:10.1016/S0012-821X(96)00176-8
Einaudi, M. T., & Burt, D. M. (1982). Introduction; terminology, classification, and composition of skarn deposits. *Economic Geology, 77*(4), 745-754. doi:10.2113/gsecongeo.77.4.745
Fortey, R. A., & Cocks, L. R. M. (2003). Palaeontological evidence bearing on global Ordovician–Silurian continental reconstructions. *Earth Science Reviews, 61*(3), 245-307. doi:10.1016/S0012-8252(02)00115-0
Fossen, H. (2000). Extensional tectonics in the Caledonides: Synorogenic or postorogenic? *Tectonics, 19*(2), 213-224.
Fossen, H., & Dunlap, W. J. (1998). Timing and kinematics of Caledonian thrusting and extensional collapse, southern Norway: evidence from 40Ar/ 39Ar thermochronology. *Journal of Structural Geology, 20*(6), 765-781. doi:10.1016/S0191-8141(98)00007-8
Fuhrman, M. L., & Lindsley, D. H. (1988). Ternary-feldspar modeling and thermometry. *American Mineralogist, 73*(3-4), 201-215.
Furnes, H., & Pedersen, R. (1995). The Lyngen magmatic complex: Geology and geochemistry. *Geonytt, 22*, 30.
Furnes, H., Roberts, D., Sturt, B., Thon, A., & Gale, G. (1979). *Ophiolite fragments in the Scandinavian Caledonides.* Paper presented at the Ophiolites—Proceedings of the International Ophiolite Symposium, Cyprus.
Gale, G. H., & Roberts, D. (1974). Trace element geochemistry of Norwegian Lower Palaeozoic basic volcanics and its tectonic implications. *Earth and Planetary Science Letters, 22*(4), 380-390. doi:10.1016/0012-821X(74)90148-4
Gayer, R., Humphreys, R., Binns, R., & Chapman, T. (1985). Tectonic modelling of the Finnmark and Troms Caledonides based on high level igneous rock geochemistry. *The Caledonide Orogen–Scandinavia and Related Areas*, 931-952.
Gee, D. (1975). A tectonic model for the central part of the Scandinavian Caledonides. *American Journal of Science, 275*(A), 468-515.

Gee, D. G., Fossen, H., Henriksen, N., & Higgins, A. K. (2008). From the early Paleozoic platforms of Baltica and Laurentia to the Caledonide Orogen of Scandinavia and Greenland. *Episodes, 31*(1), 44-51.

Godin, L., Grujic, D., Law, R., & Searle, M. (2006). Channel flow, ductile extrusion and exhumation in continental collision zones: an introduction: Geological Society of London.

Grenne, T., Ihlen, P. M., & Vokes, F. M. (1999). Scandinavian Caledonide Metallogeny in a plate tectonic perspective. *International Journal of Geology, Mineralogy and Geochemistry of Mineral Deposits, 34*(5), 422-471. doi:10.1007/s001260050215

Harland, W., & Gayer, R. (1972). The Arctic Caledonides and earlier oceans. *Geological Magazine, 109*(04), 289-314.

Hibelot, T. (2013). Relationships Between Metamorphism And Deformation In The Nordmannvik Nappe, South Of Lyngseidet: A Focus On High Grade Relics.

Hodges, K. (1985). Tectonic stratigraphy and structural evolution of the Efjord-Sitasjaure area, northern Scandinavian Caledonides *Norges Geologiske Undersokelse Bulletin*.

Holland, T., Babu, E., & Waters, D. (1996). Phase relations of osumilite and dehydration melting in pelitic rocks: a simple thermodynamic model for the KFMASH system. *Contributions to Mineralogy and Petrology, 124*(3-4), 383-394.

Holland, T., Baker, J., & Powell, R. (1998). Mixing properties and activity-composition relationships of chlorites in the system MgO-FeO-Al2O3-SiO2-H2O. *European Journal of Mineralogy*, 395-406.

Holland, T., & Powell, R. (1991). A Compensated-Redlich-Kwong (CORK) equation for volumes and fugacities of CO2 and H2O in the range 1 bar to 50 kbar and 100–1600°C. *Contributions to Mineralogy and Petrology, 109*(2), 265-273. doi:10.1007/bf00306484

Holland, T., & Powell, R. (2001). Calculation of phase relations involving haplogranitic melts using an internally consistent thermodynamic dataset. *Journal of Petrology, 42*(4), 673-683.

Holland, T. J. B., & Powell, R. (1998). An internally consistent thermodynamic data set for phases of petrological interest. *Journal of Metamorphic Geology, 16*(3), 309-343. doi:10.1111/j.1525-1314.1998.00140.x

Hossack, J. R. (1984). The geometry of listric growth faults in the Devonian basins of Sunnfjord, W Norway. *Journal of the Geological Society, 141*(4), 629-637. doi:10.1144/gsjgs.141.4.0629

Indrevær, K. (2011). The Tromsø Nappe Contact with the Nakkedal Nappe Complex NE of Tromsdalstind: Shear kinematics and relationship with metamorphism.

Irvine, T., & Baragar, W. (1971). A guide to the chemical classification of the common volcanic rocks. *Canadian journal of earth sciences, 8*(5), 523-548.

Kraus, K. (2016). *Caledonian nappe emplacement: an example from Uløya, Northern Norway.* UiT Norges arktiske universitet.

Kvassnes, A., Strand, A., Moen-Eikeland, H., & Pedersen, R. (2004). The Lyngen Gabbro: the lower crust of an Ordovician Incipient Arc. *Contributions to Mineralogy and Petrology, 148*(3), 358-379. doi:10.1007/s00410-004-0609-8

Lindstrom, M., & Andresen, A. (1992). Early Caledonian high-grade metamorphism within exotic terranes of the Troms Caledonides? *Norsk Geologisk Tidsskrift, 72*(4), 375-379.

Minsaas, O., & Sturt, B. A. (1985). The Ordovician-Silurian clastic sequence overlying the Lyngen Gabbro Complex, and its environmental significance./n Gee, DG & Sturt, BA. *The Caledonide Orogen-Scandinavia and related areas*, 379-393.

Munday, R. J. C. (1970). *The geology of the Northern part of the Lyngen Peninsula, Troms, Norway.* University of Newcastle upon Tyne.

Munday, R. J. C. (1974). The geology of the northern half of the Lyngen Peninsula, Troms, Norway. *Norsk Geologisk Tidsskrift. Supplement, 54*(1), 49-62.

Norton, M. G. (1987). The Nordfjord-Sogn Detachment, W. Norway. *Norsk Geologisk Tidsskrift, 67*(2), 93-106.

Oliver, G., & Krogh, T. E. (1995). U-Pb zircon age of 469 5 Ma for a metatonalite from the Kjosen Unit of the Lyngen Magmatic Complex northern Norway. *NORGES GEOLOGISKE UNDERSOKELSE, 428*, 27-32.

Olsen, R. (1982). *Petrografiske, sedimentologiske og strukturgeologiske undersøkelser av metasedimentære bergarter øst for Balsfjord i Troms.* University of Tromsø.

Osmundsen, Andersen, Markussen, & Svendby. (1998). Tectonics and sedimentation in the hangingwall of a major extensional detachment: the Devonian Kvamshesten Basin, western Norway. *Basin Research, 10*(2), 213-234. doi:10.1046/j.1365-2117.1998.00064.x

Osmundsen, P. T., Braathen, A., Nordgulen, Ø., Roberts, D., Meyer, G., & Eide, E. (2003). The Devonian Nesna Shear Zone, north-central Norwegian Caledonides, and its regional implications. *J. Geol. Soc. Lond., 160*, 137-150.

Osmundsen, P. T., Redfield, T. F., Hendriks, B. H. W., Bergh, S., Hansen, J., Henderson, I. H. C., . . . Davidsen, B. (2010). Fault-controlled alpine topography in Norway. *Journal of the Geological Society of London, 167*(1), 83-98. doi:10.1144/0016-76492009-019

Passchier, C., & Trouw, R. (2005). *Microtectonics*. Berlin: Springer.

Pedersen, R.-B., Furnes, H., & Dunning, G. (1991). AU/Pb age for the Sulitjelma Gabbro, North Norway: further evidence for the development of a Caledonian. *Geol. Mag, 128*(2), 141-153.

Pedersen, R., Furnes, H., & Dunning, G. (1988). Some Norwegian ophiolite complexes reconsidered. *Norges Geologiske Undersokelse Special Publication, 3*, 80-85.

Ramsay, D., Sturt, B., Zwaan, K., & Roberts, D. (1985). Caledonides of northern Norway. *The Caledonian Orogen: Scandinavia and related areas. Edited by DG Gee and BA Sturt. Wiley, Chichester, UK*, 163-184.

Randall, B. (1971). An outline of the geology of the Lyngen peninsula, Troms, Norway. *Norges Geologiske Undersölkelse, 269*, 68-71.

Ring, U., & Glodny, J. (2010). No need for lithospheric extension for exhuming (U) HP rocks by normal faulting. *Journal of the Geological Society, 167*(2), 225-228.

Roberts, D. (1990). Geochemistry of mafic dykes in the Corrovarre nappe, Troms, North Norway. *Nor. geol. unders, 419*, 45-54.

Roberts, D. (2003). The Scandinavian Caledonides: event chronology, palaeogeographic settings and likely modern analogues. *Tectonophysics, 365*(1), 283-299. doi:10.1016/S0040-1951(03)00026-X

Roberts, D., & Gee, D. G. (1985). An introduction to the structure of the Scandinavian Caledonides. *The Caledonide Orogen–Scandinavia and Related Areas, 1*, 55-68.

Roberts, D., Melezhik, V., & Heidal, T. (2002). Carbonate formations and early NW-directed thrusting in the highest allochthons of the Norwegian Caledonides: evidence of a Laurentian ancestry. *J. Geol. Soc., 159*, 117-120.

Roberts, D., Nordgulen, Ø., & Melezhik, V. (2007). The Uppermost Allochthon in the Scandinavian Caledonides: From a Laurentian ancestry through Taconian orogeny to Scandian crustal growth on Baltica. *Geological Society of America Memoirs, 200*, 357-377.

Rykkelid, E., & Andresen, A. (1991). *Late Caledonian crustal extension and backsliding in the Rombak Area.* Paper presented at the Terra Abstr.

Seranne, M. (1992). Late Paleozoic kinematics of the Møre-Trøndelag Fault Zone and adjacent areas, central Norway. *Nord. Geol. Tidsskr., 72*(2), 141-158.

Slagstad, D. (1995). Lyngen Magmatic Complex Rypdalen Shear Zone: magmatic and structural evolution. *Geonytt, 22*, 67.

Stephens, M. B. (1988). The Scandinavian Caledonides: a complexity of collisions. *Geology Today, 4*(1), 20-26.

Stephens, M. B., & Gee, D. G. (1985). A tectonic model for the evolution of the eugeoclinal terranes in the central Scandinavian Caledonides. *The Caledonide Orogen–Scandinavia and Related Areas*, 953-970.

Stephens, M. B., & Gee, D. G. (1989). Terranes and polyphase accretionary history in the Scandinavian Caledonides. *Geological Society of America Special Papers, 230*, 17-30.

Stephens, M. P., Gustavson, M., Ramberg, I. B., & Zachrisson, E. (1985). The Caledonides of central-north Scandinavia - a tectonostratigraphic overview. *The Caledonide Orogen–Scandinavia and Related Areas*, 135-162.

Stern, R. J. (2004). Subduction initiation: spontaneous and induced. *Earth and Planetary Science Letters, 226*(3-4), 275-292. doi:10.1016/s0012-821x(04)00498-4

Sturt, B. A., Pringle, I. R., & Ramsay, D. M. (1978). The Finnmarkian phase of the Caledonian Orogeny. *Journal of the Geological Society, 135*(6), 597-610. doi:10.1144/gsjgs.135.6.0597

Tajcmanová, L., Connolly, J. A. D., & Cesare, B. (2009). A thermodynamic model for titanium and ferric iron solution in biotite. *Journal of Metamorphic Geology, 27*(2), 153-165. doi:10.1111/j.1525-1314.2009.00812.x

Torsvik, T., Rehnstroem, E., & Torsvik, T. (2001). Cambrian palaeomagnetic data from Baltica: implications for true polar wander and Cambrian palaeogeography. *Journal of the Geological Society, 158*(2), 321-329.

Torsvik, T. H., & Cocks, L. R. M. (2005). Norway in space and time; a centennial cavalcade. *Norsk Geologisk Tidsskrift, 85*(1), 73-86.

Torsvik, T. H., Smethurst, M. A., Meert, J. G., Van der Voo, R., McKerrow, W. S., Brasier, M. D., . . . Walderhaug, H. J. (1996). Continental break-up and collision in the Neoproterozoic and Palaeozoic — A tale of Baltica and Laurentia. *Earth Science Reviews, 40*(3), 229-258. doi:10.1016/0012-8252(96)00008-6

Twiss, R. J., & Moores, E. M. (1992). *Structural geology*: Macmillan.

White, Powell, Holland, & Worley. (2000). The effect of TiO2 and Fe2O3 on metapelitic assemblages at greenschist and amphibolite facies conditions: mineral equilibria calculations in the system K2O–FeO–MgO–Al2O3–SiO2–H2O–TiO2–Fe2O3. *Journal of Metamorphic Geology, 18*(5), 497-511. doi:10.1046/j.1525-1314.2000.00269.x

White, R., Powell, R., & Holland, T. (2001). Calculation of partial melting equilibria in the system Na2O–CaO–K2O–FeO–MgO–Al2O3–SiO2–H2O (NCKFMASH). *Journal of Metamorphic Geology, 19*(2), 139-153.

White, R., Powell, R., & Holland, T. (2007). Progress relating to calculation of partial melting equilibria for metapelites. *Journal of Metamorphic Geology, 25*(5), 511-527.

White, R. W., Powell, R., Holland, T. J. B., Johnson, T. E., & Green, E. C. R. (2014). New mineral activity–composition relations for thermodynamic calculations in metapelitic systems. *Journal of Metamorphic Geology, 32*(3), 261-286. doi:10.1111/jmg.12071

Xu, W., Lithgow-Bertelloni, C., Stixrude, L., & Ritsema, J. (2008). The effect of bulk composition and temperature on mantle seismic structure. *Earth and Planetary Science Letters, 275*(1), 70-79.

Zwaan, K., Fareth, E., & Grogan, P. (1998). Geologisk kart over Norge, berggrunnskart Tromsø, M 1: 250.000. *Norges geologiske undersøkelse*.

Zwaan, K., & van Roermund, H. (1990). A riftrelated mafic dyke swarm in the Correvarre Nappe of the Caledonian Middle Allochthon, Troms, North Norway, and its tectonostratigraphic significance. *Nor. Geol. Unders. Bull, 419*, 4490-4500.